CRITICAL K-EIGENVALUE PREDICTION FOR THE FAMILY OF BOILING WATER REACTORS AT OFF-RATED POWER CONDITIONS

By

BRETT DAVID RAMPAL

A THESIS PRESENTED TO THE GRADUATE SCHOOL
OF THE UNIVERSITY OF FLORIDA IN PARTIAL FULFILLMENT
OF THE REQUIREMENTS FOR THE DEGREE OF
MASTER OF SCIENCE

UNIVERSITY OF FLORIDA

2009

To my Family and Friends, for putting up with my nonsense

ACKNOWLEDGMENTS

I would like to acknowledge all those who were integral to the completion of this analysis and thesis. The advice and help offered by my thesis committee, composed of Dr. Edward Dugan and Dr. James Baciak, as well as certain professors, Dr. Samim Anghaie in particular, has been essential to my success on this analysis. The help offered by Angelo Chopelas and Xavier Mouney, my mentors at General Electric-Hitachi, ensured successful completion of my thesis as well as allowing me to gain useful experience that could be used later in my career. Furthermore, the work done by Ugur Mertyurek was instrumental as a starting point in this analysis. Without the help of these individuals, my thesis would never have become a reality.

TABLE OF CONTENTS

page

LIST OF TABLES

LIST OF FIGURES

LIST OF ABBREVIATIONS

3DWINR	3D MONICORE windowed interface new rapport
ABWR	Advanced Boiling Water Reactor
AEC	Atomic Energy Commission
ANL	Argonne National Laboratory
BOC	Beginning of cycle
BORAX-N	The N^{th} boiling water reactor experiment
BWR	Boiling water reactor
BWR/N	Boiling water reactor of generation N
ECCS	Emergency core cooling system
EOC	End of cycle
ESBWR	The most advanced boiling water reactor currently in development, previously stood for economically simplified boiling water reactor
INL	Idaho National Laboratory
GE	General Electric
GEH	General Electric-Hitachi
pcm	Percent mil, equal to one percent of a thousand or $1x10^{-5}$
LOCA	Loss of coolant accident
LWR	Light water reactor
MPa	Megapascal
MWD	Megawatt-day of electrical power production
MWe	Megawatt of electrical power production
MWth	Megawatt of thermal power production
NRC	Nuclear Regulatory Commission
PCIOMR	Pre-conditioning interim operating management recommendations
psi	Pounds per square inch

PWR	Pressurized water reactor
SBWR	Simplified Boiling Water Reactor
ST	Short ton
US	United States of America

Abstract of Thesis Presented to the Graduate School
of the University of Florida in Partial Fulfillment of the
Requirements for the Degree of Master of Science

CRITICAL K-EIGENVALUE PREDICTION FOR
THE FAMILY OF BOILING WATER REACTORS
AT OFF-RATED POWER CONDITIONS

By

Brett Rampal

May 2009

Chair: Edward Dugan
Major: Nuclear Engineering Sciences

The k-eigenvalue, or k-effective, represents the ratio of neutron gain to loss in a nuclear reactor. With the establishment of a self-sustaining nuclear chain reaction in the reactor, referred to as equilibrium or steady state, the k-eigenvalue is equal to one. Because of the negative reactivity inherent to BWRs stemming from the burnable poisons and control rods necessary for reactor control, as well as uncertainties in parameters used to calculate the k-eigenvalue, the steady state value is not constant and actually greater than one. The steady state k-eigenvalue, which fluctuates above the critical value of one, is known as the critical k-eigenvalue. In order to plan power maneuvers and operations over the course of a reactor cycle, an estimate of the critical k-eigenvalue, known as the design k-eigenvalue, is utilized to determine important reactor parameters, the most important of which is the coolant flow rate. Unfortunately, the design k-eigenvalue represents a linear estimation of the change over the course of the cycle and does not take into account power maneuvers or rod exchanges. The design k-eigenvalue takes into account the 600 pcm change due to fuel depletion over the course of a cycle but misses the 700 pcm change that can be introduced due to off-rated conditions. Utilizing the design k-

eigenvalue at off-rated power conditions in order to calculate the coolant flow rate can result in up to 25% error, and subsequently result in the inability to achieve full reactor power.

The main purpose of this research was to determine a methodology for predicting the actual critical k-eigenvalue at off-rated conditions using reactivity data to forecast the change in k-eigenvalue. Moreover, data from several different BWRs were examined in order to determine if the same methodology could be used for all reactors, or if critical k-eigenvalue predication needs to be done on a plant-by-plant basis. Additionally, the methodology created was examined to determine whether it could be used for all off-rated conditions, power maneuvers and startups, or if specific methodologies were needed for each situation. Furthermore, the developed methodologies were compared to what has been done previously, in order to characterize which approach, that developed previously by GEH, the plant-specific, or universal, best characterized changes in the critical k-eigenvalue.

This analysis found that a correlation using reactivity data, xenon and gadolinium worth, Doppler worth, and control rod worth could be used to accurately predict the critical k-eigenvalue within 100 pcm at off-rated power conditions. It was further found that the previously developed methodology failed to live up to its principles and designs and the methodologies developed in this analysis generated better results, with the best coming from the universal approach.

CHAPTER 1
INTRODUCTION

General Introduction

Following the destructive demonstrations of nuclear energy at the end of the Second World War, focus around the world began to expand on the potential beneficial uses of nuclear energy. In the 1950s, this new focus was proven commercially viable with the development of two distinct and competing LWR technologies in the US. The first of these technologies, the PWR, is characterized by an operating pressure high enough to prevent bulk boiling and two-phase flow, while the second technology, the BWR is distinguished by a lower operating pressure and the presence of bulk boiling. PWR technology mostly grew out of technology developed for naval nuclear submarines, while BWR technology stemmed from work done by GE and ANL.

Currently, there are 104 operating nuclear power reactors in the US, including both PWRs and BWRs. Many of these reactors have been in operation for at least thirty years and others for more than fifty years. Originally designed for forty years of operation, many reactors in the US have undergone power uprates and have continued operating beyond their planned lifetimes. While extremely beneficial from a standpoint of profitability and power generation, power uprates can have the unintended consequence of reducing a reactor's margin for operation; of particular significance is the reduction in operating margin for flow control. By lengthening the cycle in some cases and improving fuel utilization, the window for flow control has shrunk and the middle ground comfort zone that was previously desired no longer exists, or has minimized to a point where it is meaningless. An important parameter that is utilized in flow rate prediction is the critical k-eigenvalue and can affect the final flow rate forecast drastically. The k-eigenvalue, or k-effective, represents the ratio of neutron gain to loss in a nuclear reactor. With the establishment of a self-sustaining nuclear chain reaction in the reactor, referred to as

equilibrium or steady state, the k-eigenvalue is equal to one. Because of the negative reactivity inherent to BWRs stemming from the burnable poisons and control rods necessary for reactor control, as well as uncertainties in parameters used to calculate the k-eigenvalue, the steady state value is not constant and actually greater than one. The steady state k-eigenvalue, which fluctuates above the critical value of one, is known as the critical k-eigenvalue. Flow rate prediction requires an accurate estimate of the critical k-eigenvalue at that point in the cycle; and prior to power uprates, estimates of the critical k-eigenvalues could be off 100 pcm from actual. Following uprates, and with the shrinkage of the flow rate window, more accurate predictions of the critical k-eigenvalue will ensure a more accurate calculation for flow rate control.

Boiling Water Reactor Description

The major factor that distinguishes the BWR from all other LWR technologies currently in operation in the US is the presence of bulk boiling within the core. Bulk boiling occurs in a BWR due to the reduced pressure versus a PWR, where the pressure is almost double that in a BWR and usually around 2200 psi or 16 MPa. Even though extra complexity is introduced into reactor operations by the presence of boiling and two-phase flow, there are certain important advantages to a BWR. In a BWR, steam is produced in the reactor itself and goes directly to the turbine; hence a direct cycle, rather than requiring separate heat transfer loops with steam generators as in the PWR where an indirect cycle is utilized. Moreover, water can absorb less heat in the form of sensible heat, or the heat to change temperature of a liquid than as latent heat, or the heat necessary to vaporize a fluid. Because vaporization occurs in BWRs, more total water would be need to be pumped through a PWR per unit time than in a BWR for the same amount of heat absorption, or the same power output. On the other hand, because steam is produced directly in the reactor, the steam is radioactive and requires the shielding of the power production side of the plant (turbines, condenser, pumps, piping, etc.). The radioactivity stems

from the activation of nitrogen, creating Nitrogen-16, a short-lived isotope with a seven second half-life, dictating only a concern from a radioactivity standpoint during power operations before decay has eliminated the concern (Lamarsh, 2001).

A cross-sectional view of the reactor pressure vessel and associated important components can be seen in Figure 1-1. The coolant flow paths are shown within Figure 1-1 by arrows and track the path of liquid water through the reactor vessel. Examining Figure 1-1, Feedwater enters about two-thirds of the way up the vessel wall. The fully liquid coolant enters above the active height of reactor fuel and travels down outside the core shroud and within the reactor vessel, through the area known as the downcomer before reaching the lower plenum. While in the downcomer, the jet pumps and recirculation pumps are utilized to control and alter coolant flow velocity and distribution. The pumps in the downcomer provide enough pressure to force the coolant back up through the center of the reactor core. The jet pumps are unique to BWRs and add to the inherent safety of the BWR in that jet pumps utilize no moving parts and allow for the generation of about one-third of full reactor power without operating the recirculation pumps. The static jet pumps are responsible for around two-thirds of the full recirculation flow within the system (BWR/6, 1980). Figure 1-2 shows a schematic drawing of a jet pump. The recirculation flow generated by the jet pumps and variable speed recirculation pumps become very important for operators in controlling and monitoring power plants.

After entering the lower plenum, water coolant is forced up through the active length of the reactor core where it is acted upon by the fuel. Sensible heat and latent heat are both added to the coolant and a portion of coolant is vaporized and turned to steam before rising above the active height of the fuel. The mixture of steam and water then enters a series of turning vanes and static vanes known as steam dryers and separators, respectively. The liquid level within the

reactor vessel is about half way up the steam separators, the first assembly that the coolant encounters after leaving the reactor core. The separators remove most of the water before the steam enters the dryer assemblies, where the remaining water is removed. The steam then exits the vessel via a steam line at the top of the reactor on its way to the turbine. The residual water from the separators and dryers mixes with the feedwater entering the vessel, before traveling through the downcomer and reaching the lower plenum and beginning the process anew.

Figure 1-3 shows a more detailed schematic of the BWR pressure vessel and the components contained within. Figure 1-3 illustrates a noteworthy fact in that the reactor fuel assemblies are but one small part of the entire vessel, taking up about a third of the space in the vessel. BWR fuel is composed of UO_2 with the amount of the isotope Uranium-235 increased versus natural Uranium in order to increase the probability of fission. Uranium with a higher ratio of Uranium-235 to other isotopes than natural Uranium is known as enriched Uranium, while a lower ratio indicates depleted Uranium. In a BWR, reactor fuel assemblies are square lattices of fuel rods arranged in either 7 x 7, 8 x 8, or 10 x 10 formations. Several hundred fuel assemblies are then arranged in a roughly cylindrical shape and form the reactor core. The remaining room in the pressure vessel is mostly taken up by the static steam separators and dryers, which are shown in more detail, control rod guide tubes, and the recirculation and jet pumps. A unique feature of the BWR that can also be seen is the fact that BWR control rods enter from the bottom of the reactor. Control rods are placed on the bottom of the reactor versus the top, as is common in other LWRs, in order to avoid the steam separators and dryers as well as to avoid the steam voids at the top of the reactor which impair control rod function. Used for power shaping and reactor control, control rods for a BWR are cruciform in shape when viewed from above and contain B_4C, a neutron absorber. The cruciform shape of the control rods allow

for the rods to be inserted in the space between four separate fuel assemblies and hydraulic locking piston systems are utilized to force the rods up.

The remaining major components of the direct cycle BWR power system are shown in Figure 1-4. The steam produced in the reactor vessel is routed directly to the turbine, which as previously stated, must be shielded due to the radioactivity within the steam. The majority of BWRs utilize multi-stage turbines, three stages being the most common, which allow for the extraction of power from the steam at both high and low pressure. Steam leaving each stage of the turbine travels through reheaters and moisture seperators as liquid in the turbine could cause significant damage to the blades. Steam leaving the turbine is turned back into liquid water in the condenser before being demineralized, reheated again and pumped back into the reactor, beginning the cycle all over again. A typical BWR produces saturated steam at about 900 psi or 7 MPa and 290^{o}C or 554^{o}F with an overall thermal efficiency around 33% (Lamarsh, 2001).

Boiling Water Reactor Evolution

During the 1950s, boiling water was thought to result in dangerous instabilities within a nuclear reactor. The BORAX-1 test, which was performed at INL from 1953 to 1954, demonstrated that instabilities would occur if the reactor were operated at a low pressure, but also found the reactor was controllable and stable if the pressure was raised. BORAX-1 was intentionally destroyed in 1954 in order to determine safe limits for the operation of a nuclear reactor utilizing boiling water. BORAX-2 through BORAX-5 were performed throughout the rest of the decade and demonstrated the ability for a boiling water generate commercial power as well as testing fuel materials. The BORAX experiments generated from 1.4 to around 60 megawatts over the five iterations and were used to power the city of Arco, utilizing 500 kilowatts, as well as the BORAX test facility (Stacy, 2000).

Following BORAX-1 through BORAX-3, which demonstrated the ability to generate electricity for the grid, and other experiments performed at INL in conjunction with GE, GE moved forward with plans for commercial BWRs. The introduction of BWR product line by GE occurred in 1957 when Vallecitos 1 came online in California and was issued the first reactor license by the AEC, the precursor to today's NRC. Vallecitos 1 operated at 1000 psi and produced 5 MWe directly to the Pacific Gas & Electric Company grid until the shutdown of the coupled power production facility in 1963. Vallecitos 1 served as a test bed for technologies, fuel and core components, control, and personnel that would later be utilized in the first truly commercial BWRs. The Vallecitos BWR tested the feasibility of both the direct cycle and dual cycle power generation systems and also tested stability concerns for forced and natural circulation systems. Following the introduction of Vallecitos 1, the GE company released a product line of nuclear reactors that were continually refined and modified over the next fifty years. BWR technology evolved along two separate paths, focusing on improvement of the reactor and associated components on one hand and on the containment building and structure on the other.

The first truly commercial BWR was the Dresden 1 plant located near Morris, Illinois, which produced 180 MWe when power operations began in 1961. Dresden 1 and its sister plants were introduced by GE in 1955 and are known collectively as the BWR/1 product line. BWR/1 plants were utilized as prototypes for technologies and systems that would later be utilized in the more advanced BWRs that would come online in later years. Unlike later BWRs, Dresden 1 utilized a dual cycle as it was thought that it combined the best aspects of reliability, stability, power density, and reactor control. Dresden 1 and its sister dual cycle plants, most of which were built outside the US, proved the overall viability of the BWR concept and many are still

producing electricity to this day. Unfortunately, dual-cycle plants had increased capital and maintenance costs due to the need for steam generators and a larger containment building. Other BWR/1 plants built following Dresden 1 were direct-cycle starting with Big Rock Point and Humboldt Bay (Lahey, 1993).

The BWR/1 plants served as demonstrations to prove important reactor and operational concepts and were tailored to the requests of individual utilities' requests. The GE company used the lessons and experience gained from the operation of BWR/1 plants in order to establish a standard BWR product line, with the introduction of the BWR/2 in 1963. The BWR/2 was the first modern LWR and Oyster Creek, which produced 500 MWe when it began operation in 1969, was the first of these plants. The BWR/2 plants were the first domestic turnkey plants and incorporated internal steam separation systems pioneered in one of the final BWR/1 plants built, KRB. BWR/2 plants utilized 7 x 7 fuel bundles and incorporated two important features that would remain in all later BWRS, forced circulation and variable speed recirculation. As Vallecitos 1 proved, a direct cycle utilizing forced circulation served to eliminate as much reactor instability as possible, and BWR/2 plants achieved forced circulation through five external recirculation loops. The variable speed pumps within the external recirculation loops added the ability to control reactor power through flow rate in addition to just utilizing the control rods. This load following capability through recirculation flow rate plays a major role in all modern BWRs and in this analysis and is later discussed in more depth.

In 1965, the BWR product line was further refined with the introduction BWR/3 at the twin Dresden 2 and 3 units. The major improvement in the BWR/3 was the inclusion of the first internal jet pumps, which allowed for a reduction in the total number of external recirculation loops. BWR/3 style plants had power levels around 800 MWe and first began power operations

in 1970. The GE product line was further improved with the BWR/4 introduction when construction began on the Brown's Ferry nuclear power station in 1966. The BWR/4 incorporated improvements to fuel and core loading that allowed for a 20% increase in power density, resulting in power levels around 1100 MWe. Advancement of BWR technology continued when the ground was broken for the first BWR/5 at the Zimmer power station in 1969. The BWR/5 incorporated improved reactor safeguards in order to reduce the likelihood of certain accident events as well as incorporating variable speed recirculation flow through variable valve control. By adjusting flow rate through valve control, rather than controlling the speed of the recirculation pumps, the BWR/5 series of plants had reduced capital costs for the overall control system and were able to follow more rapid load variations (Lahey, 1993).

BWR development has continued since the introduction of the first plants in the 1950s and 1960s and presently, the most advanced BWR built in the US is the BWR/6, of which the Cofrentes plant is a prime example. The major change from BWR/5 to BWR/6 involved improvements in fuel and fuel bundle design. Improved power shaping and flattening was accomplished by the inclusion of Gadolinium as a burnable poison and improved coolant distributions. Gadolinium serves to absorb neutrons produced in the reactor and helps control the reactor while playing a major role in this analysis, which will be examined fully. The most visible change for the BWR/6 involved the shift from a 7 x 7 fuel rod bundle to an 8 x 8 square-lattice. By utilizing smaller-diameter, longer-length fuel rods, within the same external outline as the previous bundle, power density was increased and fuel duty reduced, both beneficial consequences. Increased power density versus BWR/5 has allowed for up to a 20% power increase in power production while the reduction in fuel duty allows for longer fuel lifetimes in the reactor. Evolution of the BWR reactor vessel can be seen in Figure 1-5, and clearly depicts

the simplification of the system at each iteration. Certain more advanced BWR concepts are shown in Figure 1-5, notably the ABWR and ESBWR, but BWR/6 is the most advanced plant in operation in the US, and represents the most advanced plant that will be examined in this analysis. On the other hand, Figure 1-5 illustrates that advancement of BWR technology has not ended with the introduction of the BWR/6. Table 1-1 lists examples of each subsequent BWR generation, the date of introduction and operation, and key improvements made for each subsequent evolution.

Changes and modifications to the reactor containment building have been the major other improvement to the GE BWR product line. Figure 1-6 shows the changes that have occurred to the containment building over the course of the evolution of the BWR. Initial containment buildings were spherical, dry, and had to be large enough to accommodate steam generators and the prototype external recirculation loops. The Mark I containment building was the first new containment building for BWRs and was shaped like an inverted light bulb with a steel torus storing a water pressure suppression pool. The next iteration, the Mark II, utilized a conical design and a large drywell for ECCS and steam piping. BWR/6 plants all utilize the most advanced containment design, the Mark III, which include improved access for maintenance and horizontal vents to reduce the possible consequences of a LOCA. Figure 1-6 shows the simplification of the containment building through Mark III and beyond, for the more advanced reactor designs currently in development in the US and production outside the US.

Boiling Water Reactor Operation and Control

Neutrons are the lifeblood of a nuclear reactor and control as well as perpetuate the fission chain reaction within the fuel. A single fission event within Uranium fuel produces about two and a half neutrons and one of these fission-produced neutrons is required to stimulate the chain reaction and keep the reactor critical. However, even though two and a half neutrons should be

more than enough to sustain the fission process, neutrons are often lost to competing processes in effect during reactor operations in the form of absorption or leakage. This concept of balancing neutron production to neutron loss is known as neutron economy and is the governing principle behind all reactor operations. Operators and designers of nuclear reactors must ensure that each neutron produced in a given generation produces one in the next generation and the critical k-eigenvalue is an important factor for monitoring the trends in neutron production and loss.

Critical k-Eigenvalue

The k-Eigenvalue, also known as the effective multiplication constant or k_{eff}, is closely tracked during operations in order to understand the status of the fission chain reaction within the reactor. Equation 1-1 illustrates the mathematics behind the k-eigenvalue as well as its significance for reactor operations and can also be known as the neutron balance.

$$\text{k - eigenvalue} = \frac{\text{neutrons produced in a generation}}{\text{neutrons absorbed and leaked in a generation}} \tag{1-1}$$

A value of the k-eigenvalue less than one indicates a decreasing number of chain reactions and the reactor is said to be subcritical, while a value greater than one indicates an increasing number of chain reactions with the reactor being consider in supercritical operation. The nuclear chain reaction is considered self-sustaining and the reactor is deemed critical when the value of the k-eigenvalue is equal to one. A self-sustaining chain reaction is integral to reactor power production and must be maintained for normal operations.

In order to accurately calculate the current k-eigenvalue as well as predict future changes to the eigenvalue, two major sources play an important factor, the core configuration and feedback from the thermal hydraulics of the reactor. The overall reactor power and coolant flow rate affect the steam to liquid water ratio in the reactor and in turn effects both neutron moderation as well as production and loss. The thermal hydraulic concerns of reactor power and

coolant flow rate are coupled with the core configuration, specifically, the control rod mass in the core, in order to accurately determine the neutron balance and in turn the k-eigenvalue. Figure 1-7 illustrates the factors that are taken into account when calculating the k-eigenvalue during reactor operations. Due to uncertainties in the modeling process used to determine the neutron balance in the reactor as well as the absorption and leakage effects of burnable poisons, control rods, and other forces, the true reactor eigenvalue for critical operation is greater than one and referred to as the critical k-eigenvalue.

Reactivity

In a nuclear reactor, anything that serves to either reduce or increase the k-eigenvalue is known as reactivity, or ρ. This departure from criticality serves an important function in a reactor as the major source of reactor control and power shaping. Equation 1-2 shows how reactivity is calculated is often expressed as a percent of change in k-eigenvalue or %Δk/k.

$$\rho = \frac{\text{neutrons produced in generation 1 - neutrons produced in generation 2}}{\text{neutrons produced in generation 1}} \qquad (1\text{-}2)$$

The format of %Δk/k becomes convenient for examination purposes, as expected values of reactivity are extremely small, on the order of 10^{-3} or 10^{-4}. An example of a source of negative reactivity in the reactor could result from any process serving to increase the absorption or leakage of neutrons. Because the enrichment of the Uranium fuel is slowly reduced as fission events occur over the course of a reactor cycle, the reactor core is loaded in such a way that enough excess reactivity will be present at the beginning of fuel usage to ensure criticality throughout the cycle. Sources of negative reactivity are then paramount to reactor operation to ensure that the excess reactivity incorporated into the fuel is consistently reduced to the point of criticality. On the other hand, some sources of negative reactivity are inherent to BWR operation, such as increased leakage from voiding of coolant as temperature rises, also dictating

excess positive reactivity be incorporated into reactor fuel. The sources of negative reactivity and excess initial positive reactivity both contribute to why the critical k-eigenvalue is greater one. Several sources of negative reactivity that play an important part in this analysis are discussed further in this section. The sources of reactivity discussed here are the major factors affecting changes in the critical k-eigenvalue and are utilized as data for predicting said changes.

Control rod reactivity worth

In order to ensure that the neutron balance within the reactor and the value of the critical k-eigenvalue is as close to unity as possible, control rods utilizing negative reactivity are employed. The controlling effects of the rods are achieved through absorption of mostly thermal but also epithermal neutrons, effectively removing them from the chain reaction. Additionally, the control rods play a major role in shutting down the reactor, as they are the only force able to make the reactor subcritical enough for shutdown and maintain that condition. Two major factors affecting the absorptivity of a control rod within the reactor core, the thermal neutron flux reaching the rod and the thermal neutron diffusion length affect and alter the performance of the rods. Control rods are considered essentially "black" to all neutrons and the neutron flux reaching that rod is the major contribution to differences in the reactivity between rods. Should an area within the reactor have a slightly higher neutron flux than the average, the control rods in the higher flux field would have more negative reactivity available to them than the average rod. The thermal diffusion length also plays a major role in the effectiveness of control rods and describes the distance away from a control rod that a neutron can be produced and still be captured by a control rod before being able to cause fission. The Fermi age, which describes the time it takes for a neutron to slow down from fast to thermal, also affects the absorption of control rods. In the presence of voids, the Fermi age increases, and the control rods, which predominantly absorb thermal neutrons, are less likely to absorb the fast moving neutrons which

haven't had enough time to slow down. Moderator temperature contributes to the magnitude of the thermal diffusion length in that hotter coolant would be less dense and therefore result in an increased thermal diffusion length. Additionally, because two phases of flow are present in BWRs, the occurrence of voids in the reactor serves to increase the thermal diffusion length in that fission is less likely to occur in steam than in liquid water. The change in thermal diffusion length due to coolant voiding is a major factor in the decision to have control rods enter the core from the bottom, as voiding will be reduced at the bottom of the core, versus the top. The increased thermal diffusion length means that neutrons produced farther from the rod will still be captured, increasing the negative reactivity effects of the individual rod (BWR, 1971).

Control rods within the BWR core are cruciform rods, consisting of two crossed blades as shown in Figure 1-8. The cruciform shape allows for rods to fit closely into the corners and along the sides of a fuel assembly as depicted in Figure 1-9. BWR cruciform control rods are composed of stainless steel tubes filled with B_4C powder, a neutron absorber, arranged in a cruciform array and surrounded by a stainless-steel sheath. Each individual tube is sealed at the bottom and top and serves as a pressure vessel to contain the helium gas that is released during the boron-neutron capture process.

Xenon reactivity worth

In a nuclear reactor, fission is achieved by allowing small and quickly moving neutrons to slam into a big, "overweight" nucleus, uranium, in the case of a modern LWR, and expect the heavy nucleus to split. A fission reaction of the type utilized in a nuclear reactor would result in the production of two fission products of differing mass and extra neutrons all having high kinetic energy. These quickly moving reaction products slow down through collisions with other atoms in the reactor fuel, releasing their energy in the form of heat. The heat produced in the fission process is utilized to heat reactor coolant and in turn generate electrical power, the point

of a nuclear power station. However, the two different mass fission products produced in the fission reaction are not stable on their own, and will undergo radioactive decay. Certain progeny resulting from this radioactive decay process have an extremely large absorption cross section, which significantly affects the reactivity of the core. Xenon-135 can result from the fission process as shown in Figure 1-10, which also depicts the parents of xenon-135 and their associated half-lives, or the average time before half of the examined isotopes undergo a radioactive decay process. Certain parent isotopes resulting in xenon-135 are very short-lived and are assumed to decay to daughter products almost as soon as they are created. However, xenon-135 and its direct precursor, iodine-135, have half-lives on the order of several hours, versus several seconds for their ancestor isotopes. The longer-lived aspect of xenon versus its progenitors means that xenon content in the reactor will accumulate over the course of steady-state reactor operations. Unfortunately, the thermal neutron absorption cross section for xenon-135 is around 2.7×10^{6} barns or 2.7×10^{-18} cm^2, and this high cross section implies that a very small amount of the xenon-135 fission product in the reactor could "poison" the reactor as xenon-135 leeches neutrons from the chain reaction. The negative and poisoning reactivity effects of xenon-135 within the reactor affect the transient operation of the reactor as well as the critical condition of the reactor as xenon is produced through fission and lost due to thermal absorption and radioactive decay (Duderstadt, 1976).

Doppler broadening reactivity worth

Materials utilized in nuclear reactors have been studied in-depth for many years, and the role that temperature can play on said materials has important consequences for reactor operations. Uranium-238, utilized in reactor fuel in large quantities, and its neutron capture cross section is affected drastically by the temperature of reactor fuel. The neutron absorption, or capture, cross-section for uranium-238 obeys the 1/v law that affects most common materials.

The 1/v law implies that the capture cross section of uranium-238 is a function of neutron speed with the cross section increasing as neutron speed decreases. Unfortunately uranium-238 and many other materials exhibit a narrow energy band where the 1/v law ceases to apply and the energy band is known as the resonance absorption band. Figure 1-11 illustrates a typical capture cross-section for a material as a function of neutron energy, with the resonance peak and energy band depicted. In this narrow energy band, the likelihood of neutron capture vastly increases and it can be assumed, for all practical purposes, that any neutron slowing down and rebounding with an energy within the resonance absorption band will be captured and lost from the chain reaction.

Doppler broadening and the effects that fuel temperature can have on it within a reactor are tracked by monitoring the change in the Doppler coefficient of reactivity versus a change in fuel temperature. At ambient temperatures, the Doppler coefficient operates on the order of 10^{-5} $\Delta k/k/^{o}F$ and an increase or decrease in fuel temperature can affect the shape and size of the resonance absorption band. At high temperatures, the resonance peak is short and wide while taller and narrow at low temperatures. The trend in Doppler coefficient versus fuel temperature is illustrated in Figure 1-12, which also shows trending versus void content and water temperature. Figure 1-12 shows the void composition and coolant temperature above each curve and illustrates the increased reactivity effects of increasing void content and coolant temperature. As illustrated, the presence of increased voiding allows neutrons to travel further before slowing down, in turn increasing the probability of uranium-238 capture. The hardening of the flux spectrum, which occurs in the presence of voids and results in more fast neutrons, also serves to increase resonance absorption and the negative reactivity effects of Doppler broadening

Gadolinium reactivity worth

Burnable poisons or absorbers are materials with a high probability of neutron capture that are incorporated into reactor designs in order to achieve better fuel utilization and efficient

reactivity control. A certain amount of these materials are placed in the core to account for the initial supercritical fuel loading and the amount of the burnable absorber decreases as it absorbs neutrons and is effectively "burned," or utilized. LWRs utilize burnable absorbers in many different ways, ranging from fuel coatings to poison rods placed in the reactor for power flattening or shaping. Even though a reactor always includes adequate excess reactivity in order to increase reactor power, the net reactivity of the core must remain at zero to ensure a critical chain reaction and ensure constant power production. In a lot of LWRs, this reduction in reactivity, or reactivity control, has typically been achieved through the use of control rods and a burnable chemical shim, a poison material mixed in the coolant for neutron absorption. The boric acid that is usually used in LWRs as a chemical shim fails to operate as intended in the presence of two-phase flow and steam voids in BWRs. To counter for the absence of chemical shim, BWR designers turned to mixing a burnable poison material directly in with the reactor fuel and a gadolinium oxide, Gd_2O_3, is the absorber that was developed for this purpose. By mixing the gadolinium directly into the reactor fuel, burnable poison concentration can be monitored and controlled very accurately within the core as well as not displacing fuel, as burnable poison rods would. Natural gadolinium is composed of almost thirty percent gadolinium-155 and gadolinium-157, and have large thermal neutron absorption cross sections, 58,000 and 240,000 barns, respectively. These high cross sections and the moderately high cross sections of the daughters of gadolinium produced through neutron capture, contribute to the negative reactivity effects of this blended burnable poison (Cochran, 1999).

Critical k-Eigenvalue, Flow Control, and Reactor Power

In addition to control rods, variable recirculation flow control in BWRs is employed in order to vary reactor power output. In contrast to control rods, the use of variable speed recirculation flow as the control device has the added benefit of maintaining radial neutron flux

and power distribution. As previously described, voids and the density of reactor coolant can significantly affect the neutron balance and variable flow control takes advantage of this in order to adjust reactor power. Void, or steam concentration in the coolant channels has a net negative reactivity effect on the reactor in that voids increase the thermal diffusion length and allow for increased neutron absorption through a lack of slowing down neutrons past the uranium-238 resonance region. Recirculation flow rate has a direct effect on reactor power in that an increase in the flow rate will increase the speed at which steam is removed from the reactor, increasing reactor power. Steam generation will then balance the increased removal from the core and a new equilibrium steam volume and power level can be achieved. Reactor power can be altered over a range of about 35 percent of the operational power level; and in BWRs, normal operations use flow rate as the dominant control device and control rods for shaping, ensuring safe operation, compensating for uneven burnup, and emergencies.

During the planning and startup stages of a reactor cycle, control rod patterns, anticipated power levels, and the predicted critical k-eigenvalue trending are utilized to create an operational map for flow control in what is almost the exact opposite of the process in Figure 1-7. The operational map will then be used for control purposes, as it will predict the necessary recirculation flow rate to maintain safe operations during both off-rated power events and normal operations. Accuracy of the flow rate predictions then becomes extremely important during the reactor cycle in order to ensure the targeted power level is reached as quickly as possible while still remaining within the regulated thermal limits. An inaccurate flow rate prediction could also mean that a given power plant might not reach rated power over the entire course of a fuel cycle as flow margin is lost during off-rated power events.

With power uprates and the process for extending the life of a nuclear power plant beyond its original forty-year planned lifetime, the margin in the operational flow control power range has decreased and more accuracy in both the flow rate prediction and the critical k-eigenvalue has become necessary. In the years prior to power uprates, a piecewise linear function that varied over the course of the reactor cycle, known as the design k-eigenvalue, has been utilized in order to make the proper predictions and calculations for flow control. Unfortunately, this design k-eigenvalue only takes into account the original design considerations and expected burnup of the reactor core and omits any fluctuations that may occur during the cycle due to operational control. The off-rated power conditions where critical -eigenvalue fluctuations occur represents the least exact region of flow control and predicted k-eigenvalue, dictating more accurate predictions for both parameters to ensure proper reactor operation.

Over the course of a reactor fuel cycle, operators must adjust the control rod pattern to ensure an even and consistent burn of the nuclear fuel in addition to maintaining or altering the power shape and distribution. These rod exchanges and power maneuvers must be planned before the fuel cycle has even begun and the critical k-eigenvalue is employed to calculate the correct coolant flow rate, and in turn return the reactor to operational power following a power maneuver. Figure 1-13 depicts a fuel cycle from 2004 for one of the nuclear power plants analyzed over the course of this analysis. In many ways, the fuel cycle shown in Figure 1-13 is typical of many nuclear power plants; however, in other ways, it illustrates the need and purpose for this analysis. The data in Figure 1-13 came from a nuclear power plant that will be known as Plant C, for the rest of this analysis. The Plant C fuel cycle demonstrates how the critical k-eigenvalue can fluctuate several hundred pcm over the course of the length of the fuel cycle, in addition to fluctuating several hundred pcm over the duration of a power maneuver or rod

exchange. The final few months of the Plant C fuel cycle shown in Figure 1-13, on the far right of the graph, depict a reactor cycle where poor critical k-eigenvalue prediction led to the worst possible outcome for power operations, reduced operational power. Plant C lost several million dollars over the course of the 2004 fuel cycle, and an inaccurate design k-eigenvalue, poorly predicting the critical k-eigenvalue, has been determined to be the culprit.

Purpose and Objectives of Analysis

Power uprates and the ensuing reduction in operational margin for certain reactor parameters and control concerns has led to the increased focus on accurately predicting the critical k-eigenvalue. The design k-eigenvalue does a good job of predicting the change in the critical k-eigenvalue due to exposure and fuel depletion; however, power maneuvers, start-up and shutdown procedures, and all other operational measures that occur at off-rated power add extra complexity into the trending of critical k-eigenvalue that is ignored by the design k-eigenvalue. Figure 1-13 illustrates the actual critical k-eigenvalue, the associated design k-eigenvalue that was meant to mirror the true reactor conditions, and reactor power fluctuations during the failed Plant C reactor cycle. As illustrated in Figure 1-13, the design k-eigenvalue follows the general linear piecewise trend of the critical k-eigenvalue, but diverges most during any departure from rated operating power and at the end of cycle. The design k-eigenvalue is hoped to have an accuracy of 200 pcm for all off-rated power events, but can diverge much more because its trending is solely linear. Figure 1-14 illustrates the trending of the critical and design k-eigenvalue over the course of a specific off-rated power event. The design k-eigenvalue can be seen to accurately track the critical k-eigenvalue trending prior to the power event in Figure 1-14; however, following the event the critical and design k-eigenvalue lose agreement and diverge. This divergence during off-rated power conditions can propagate over the course of a given reactor cycle, consistently and considerably shifting the actual critical k-eigenvalue away

from the prediction, the design k-eigenvalue. Moreover, as previously stated, a poor prediction of critical k-eigenvalue can have significant impact on the flow rate map used for maintaining operational power and can result in reduced power production, as is clearly evident in Figure 1-13. Any reduction in power production for any sizeable amount of time represents a primary failure in the one of the most important objectives of an operating nuclear power plant and can result in a sizeable loss of profit in addition to the obvious reduced contribution to the electrical grid.

Creating an accurate prediction of the critical k-eigenvalue has therefore become more essential from a profitability and electrical production standpoint. This analysis aims to create such a correlation that predicts changes to the critical k-eigenvalue by using statistical regression techniques with the previously described major reactivity factors as trending information. Electrical production utilities requested more accurate critical k-eigenvalue prediction from the GE company following the reduction in operating margin and events like the 2004 power cycle shown in Figure 1-13. GE engineers established an initial, but unfinished and untested, methodology for predicting the critical k-eigenvalue. The GE methodology represented the first attempt to solve the problem of critical k-eigenvalue prediction and this analysis built on that methodology as a starting point. The initial GE methodology will be known as the patent methodology for the purposes of this analysis and to avoid confusion (Mertyurek, 2008). Prior to the commencement of this analysis, the patent methodology was not considered rigorous enough as well as incorporating too much variability. Over the course of this analysis, the patent methodology was examined for continued applicability, after being abandoned in 2008, with the aim of building on the initial prediction methodology by utilizing more demanding statistical methods and resolving unanswered questions. Specifically, investigation was performed to

determine whether a universal correlation for critical k-eigenvalue could be developed versus the correlations for poorly defined families of power plants as was developed in the initial methodology. The merits of correlations developed specifically for each power plant was also investigated and several thousand data points from eight operating nuclear power plants were utilized throughout all aspects of this examination.

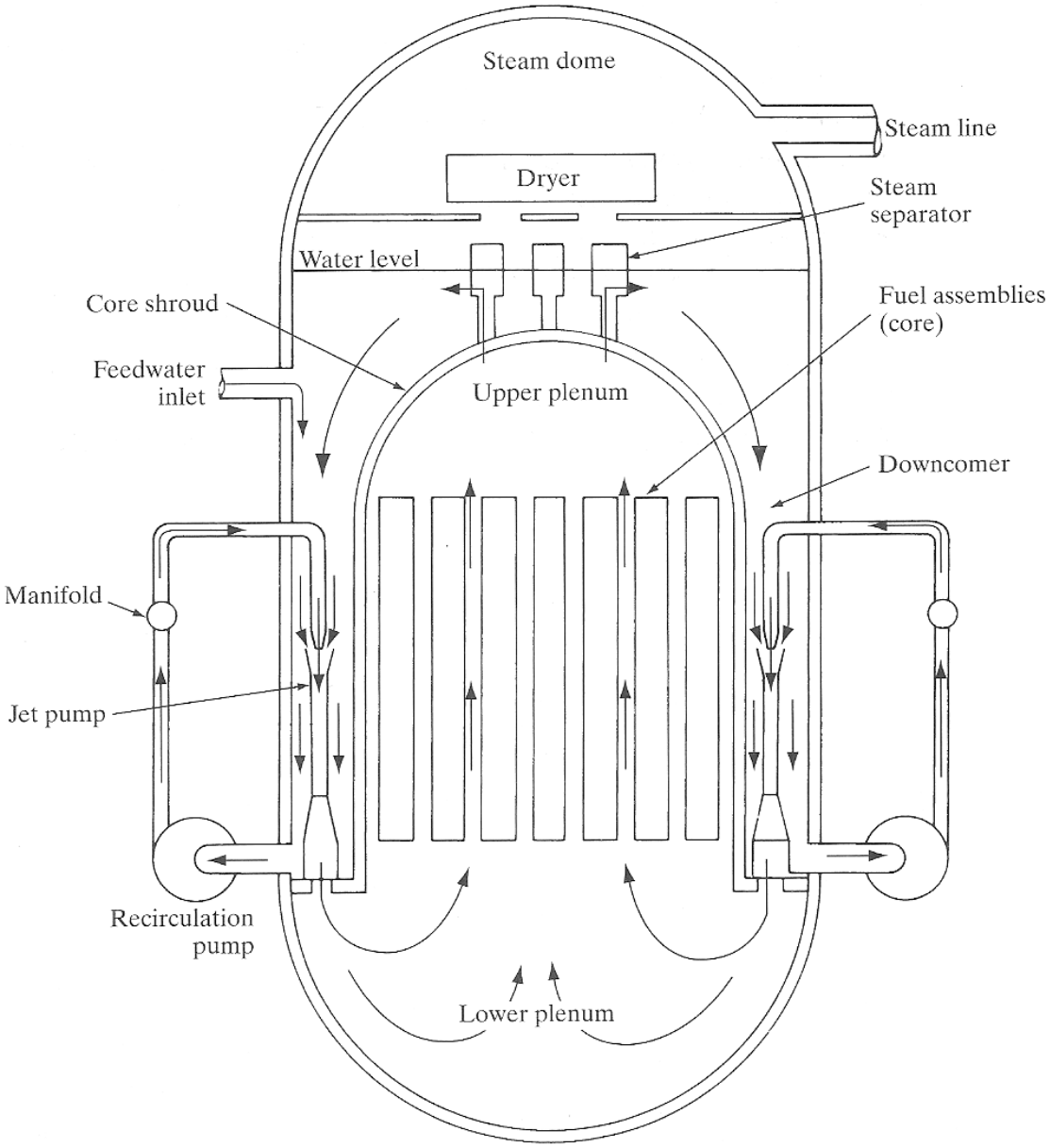

Figure 1-1. Flow schematic of a BWR reactor vessel (Lamarsh, 2001).

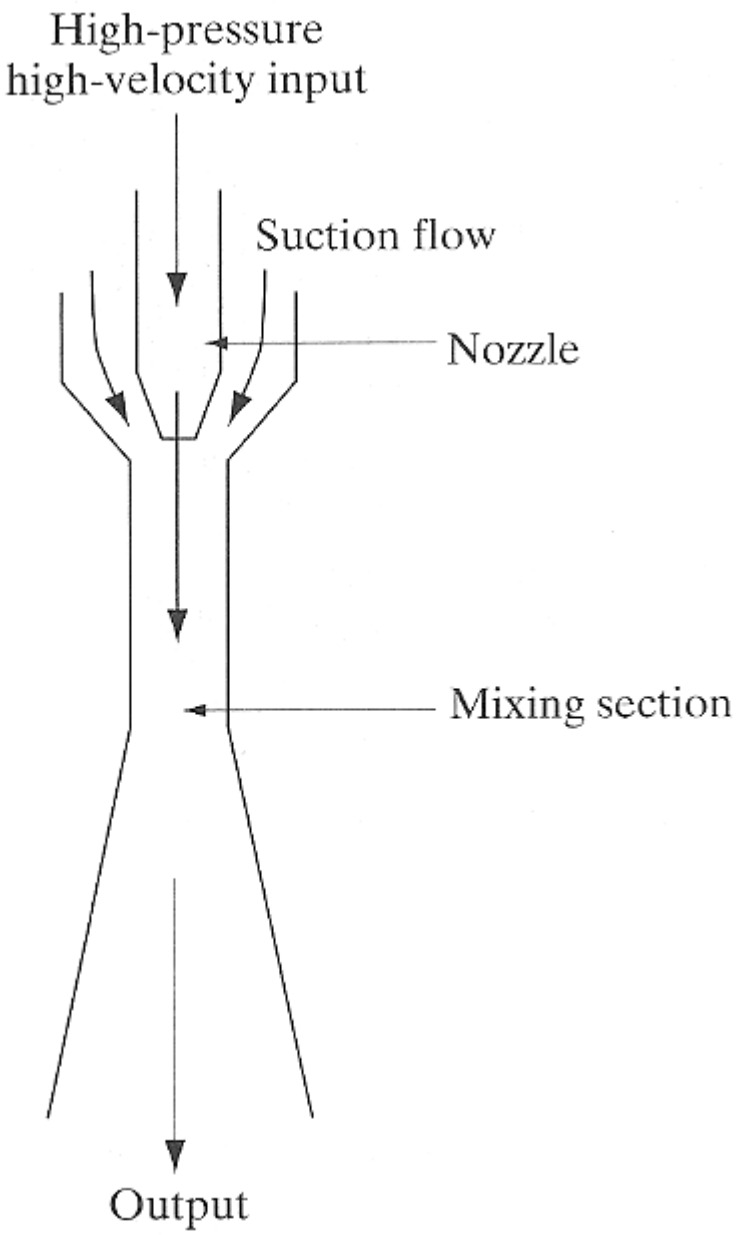

Figure 1-2. Schematic diagram of a jet pump, not shown to scale (Lamarsh, 2001).

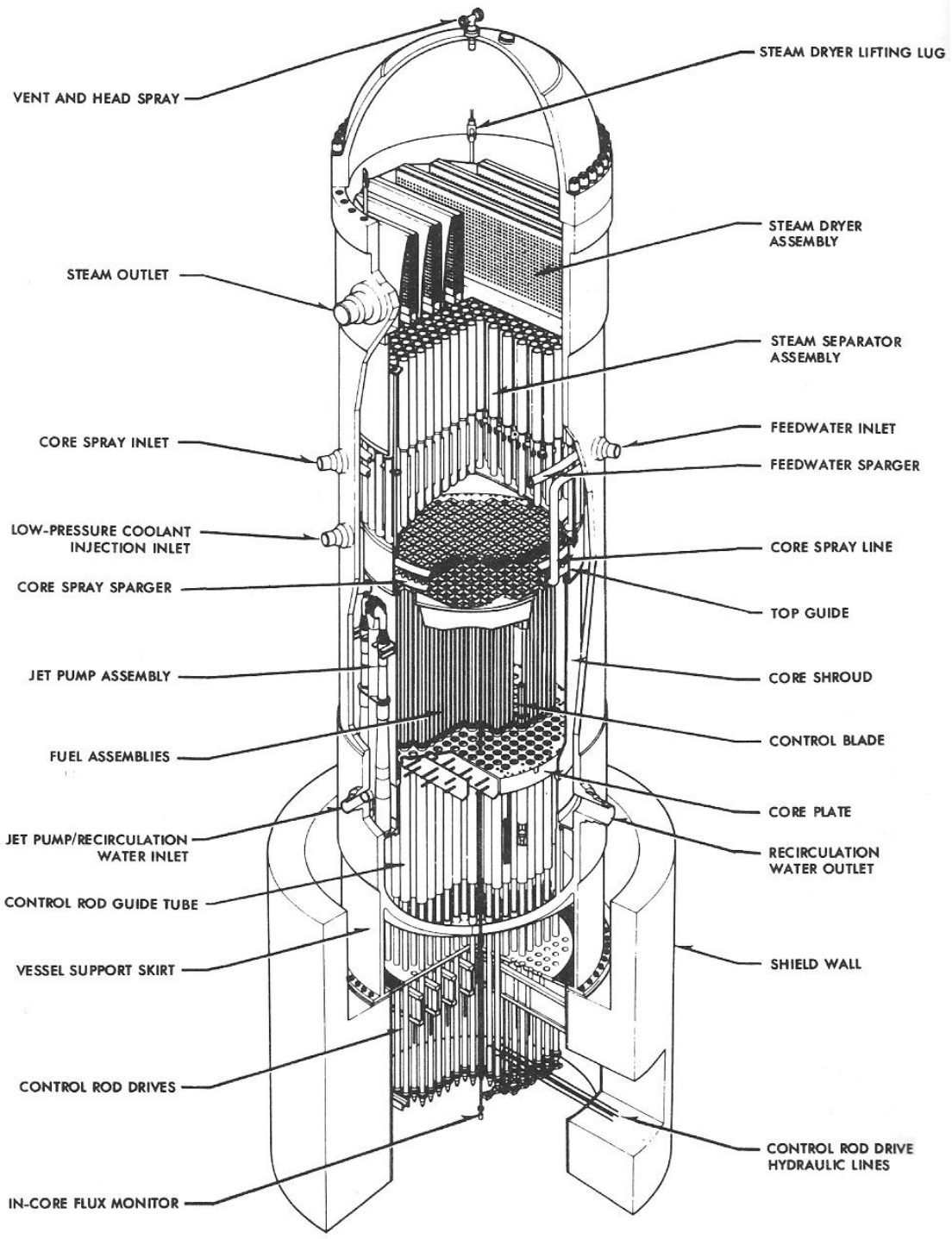

Figure 1-3. BWR/6 reactor pressure vessel (Lahey, 1977).

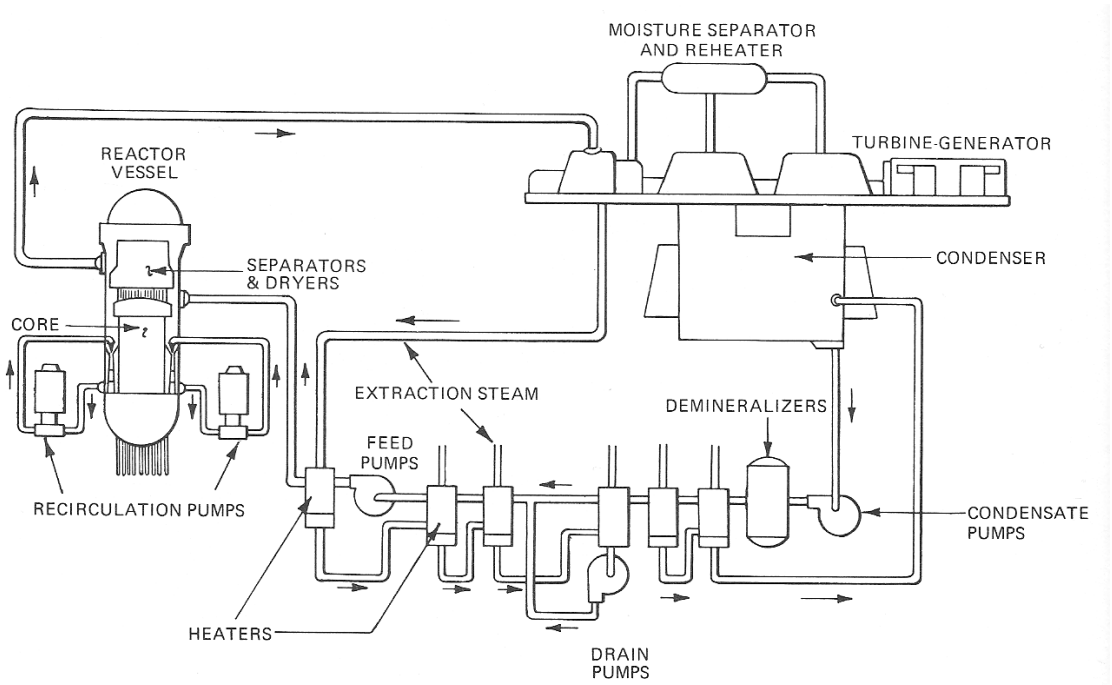

Figure 1-4. Direct cycle reactor system (Lish, 1972).

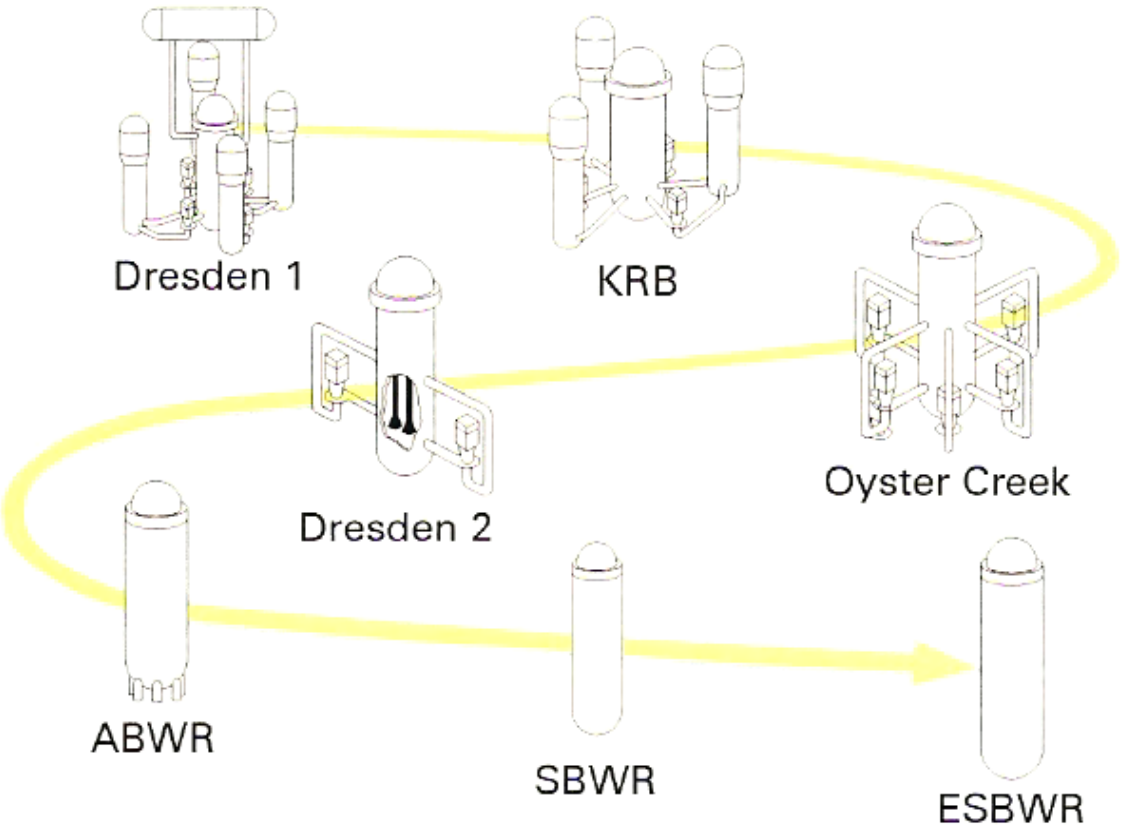

Figure 1-5. BWR reactor pressure vessel evolution (ESBWR, 2006).

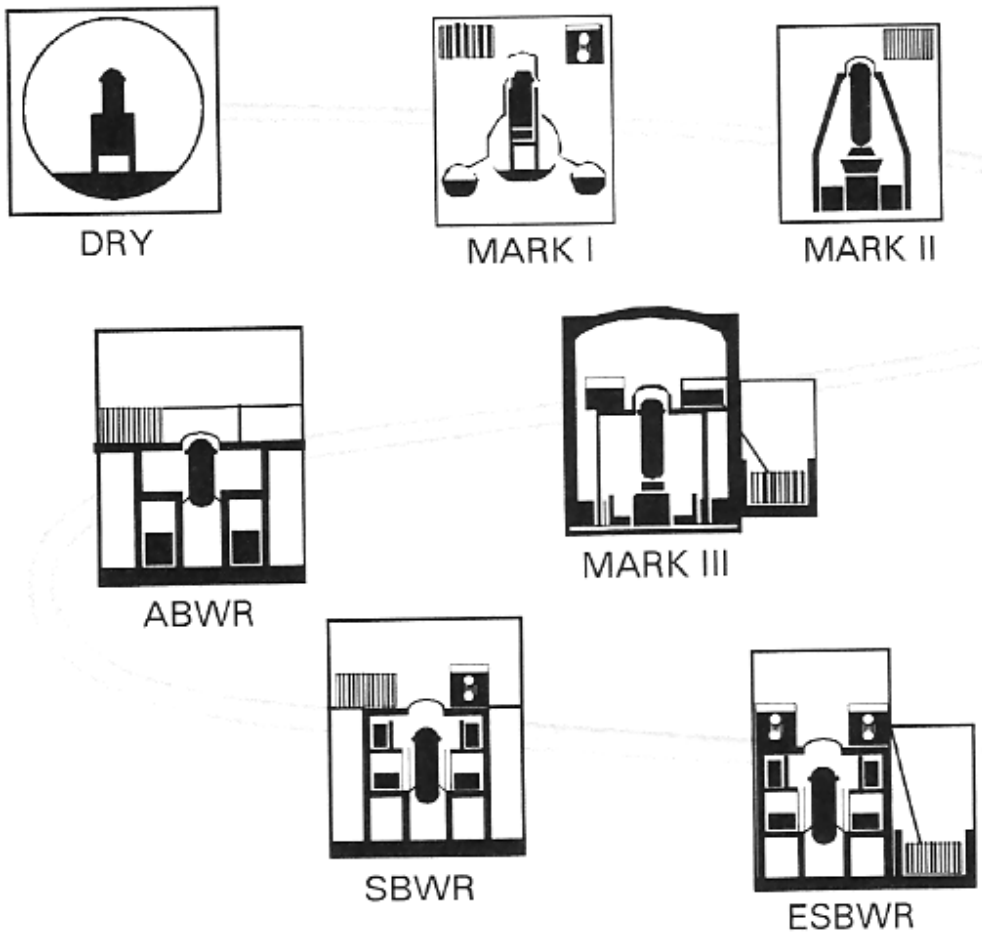

Figure 1-6. BWR containments and their evolution (ESBWR, 2006).

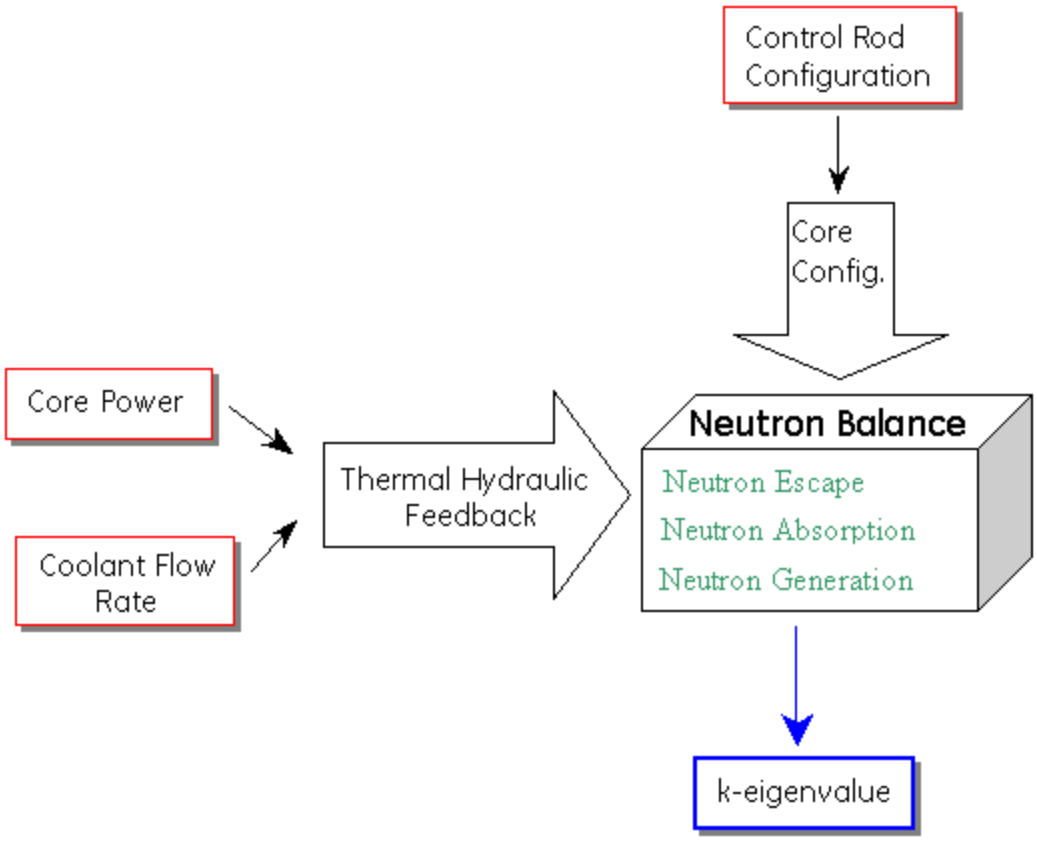

Figure 1-7. Operational neutron balance and k-eigenvalue calculation.

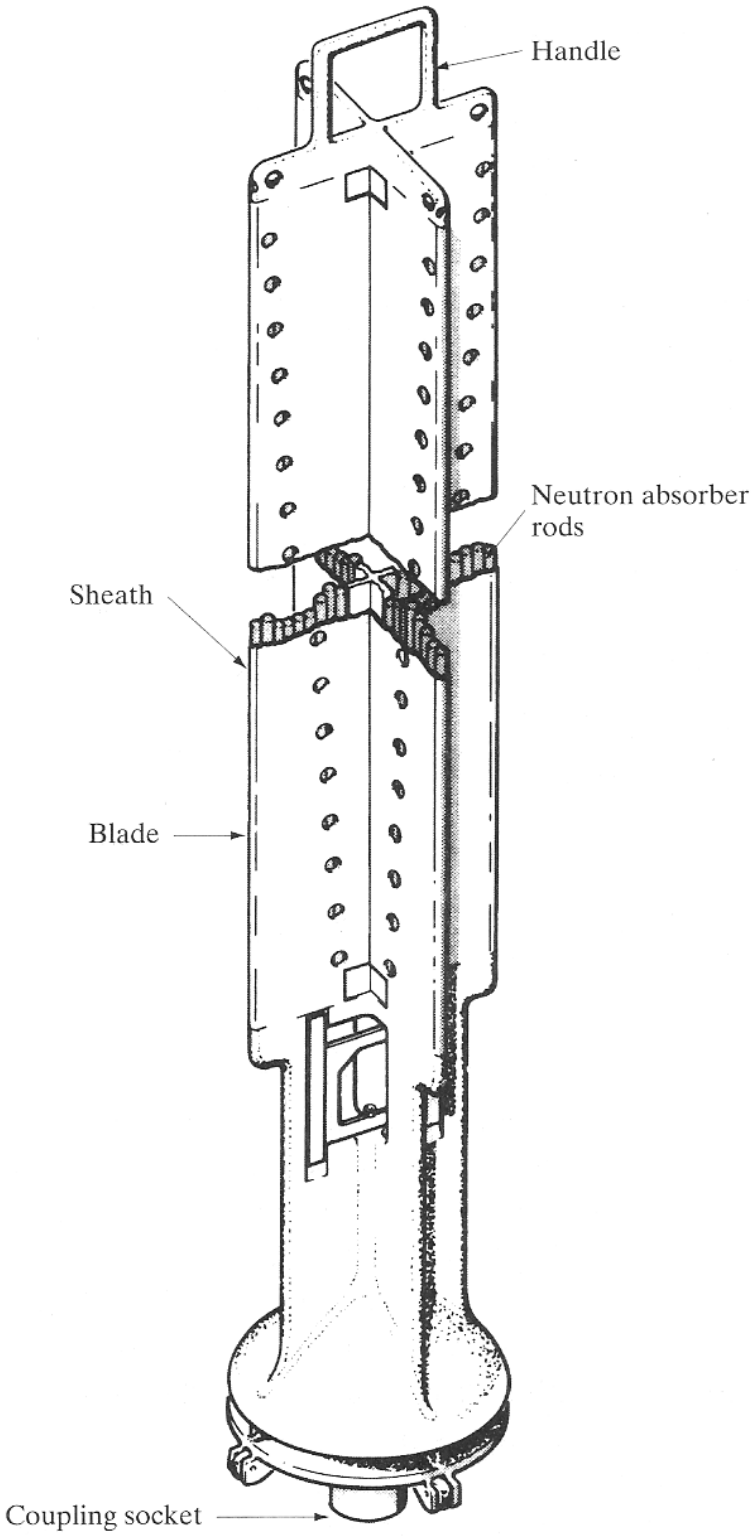

Figure 1-8. BWR cruciform control rod (Lamarsh, 2001).

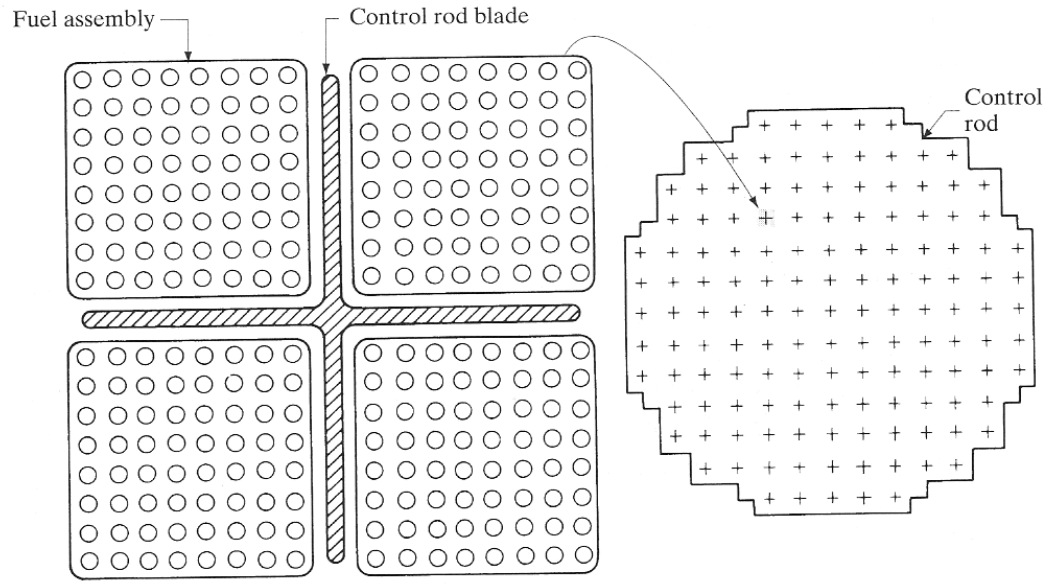

Figure 1-9. A BWR cruciform control rod between fuel assemblies and its location in the core (Lamarsh, 2001).

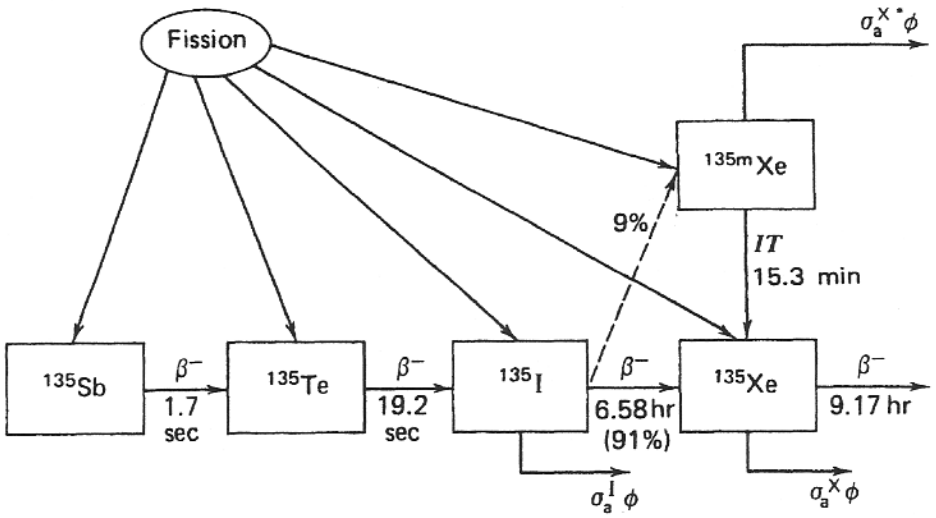

Figure 1-10. The xenon-135 fission decay scheme (Duderstadt, 1976).

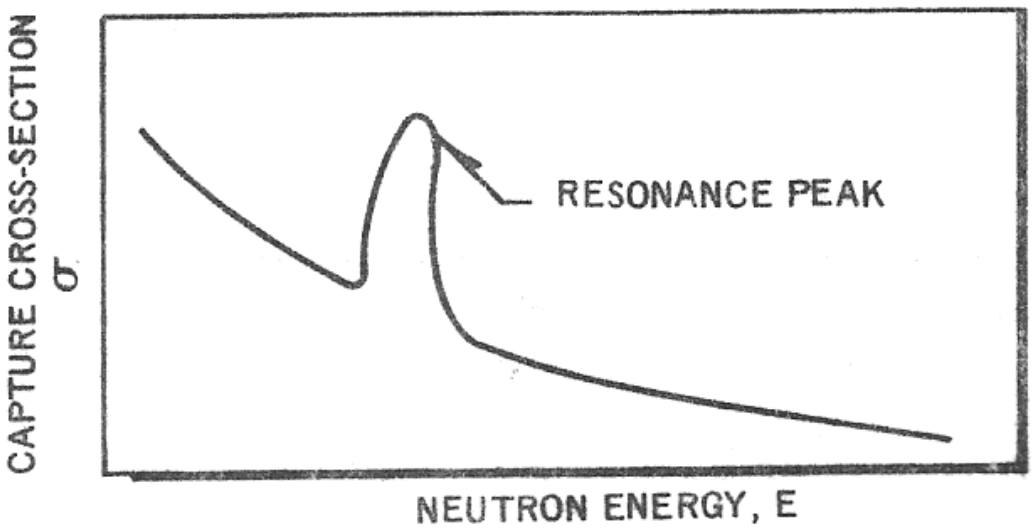

Figure 1-11. Typical resonance curve (BWR, 1971).

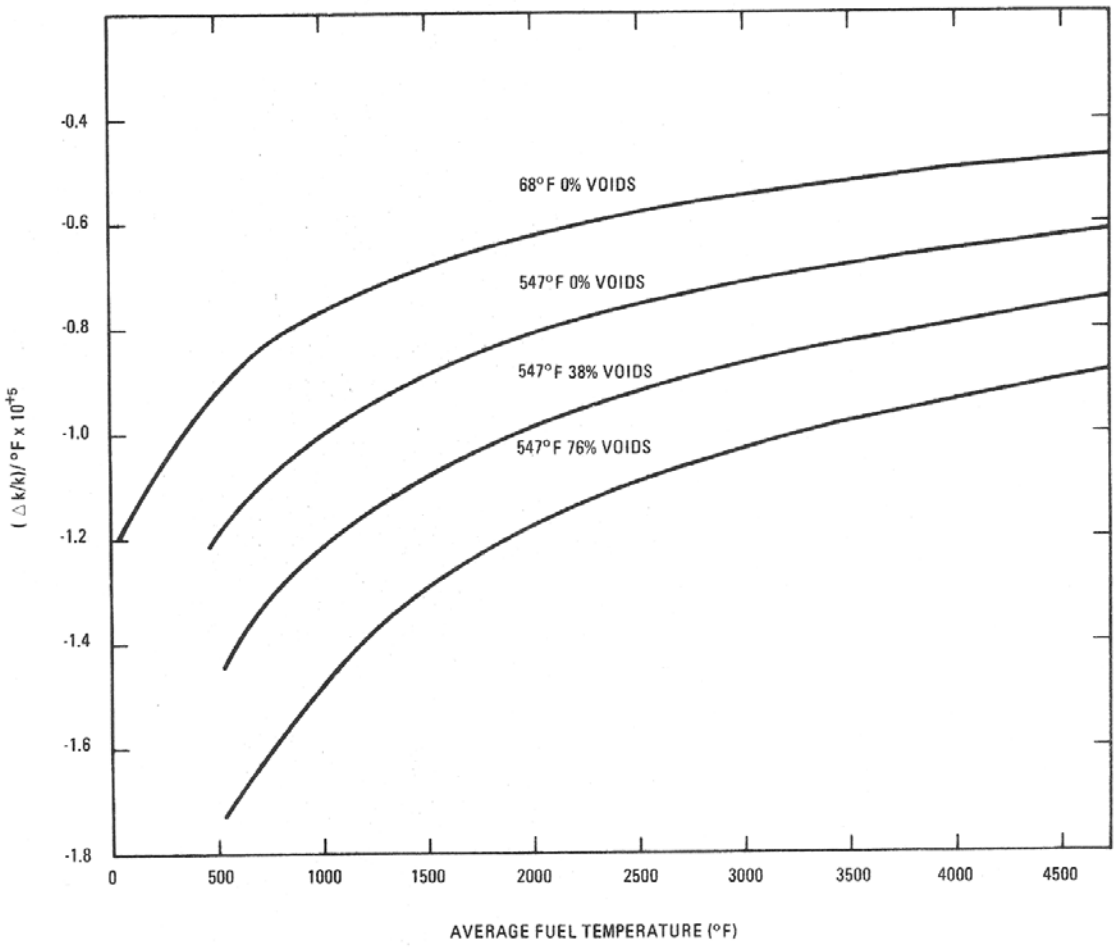

Figure 1-12. Doppler coefficient of reactivity temperature response (BWR, 1971).

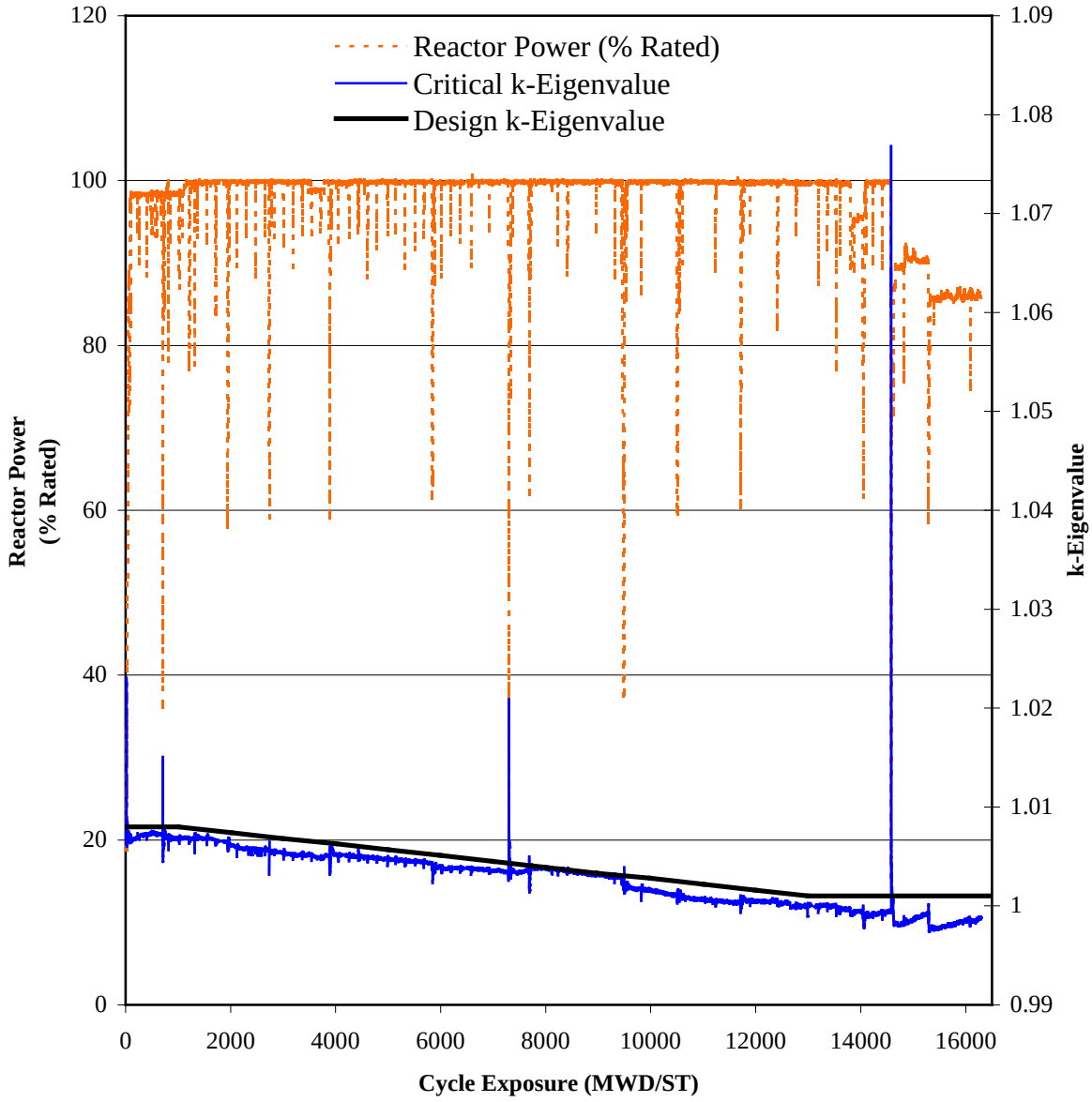

Figure 1-13. Plant C fuel cycle.

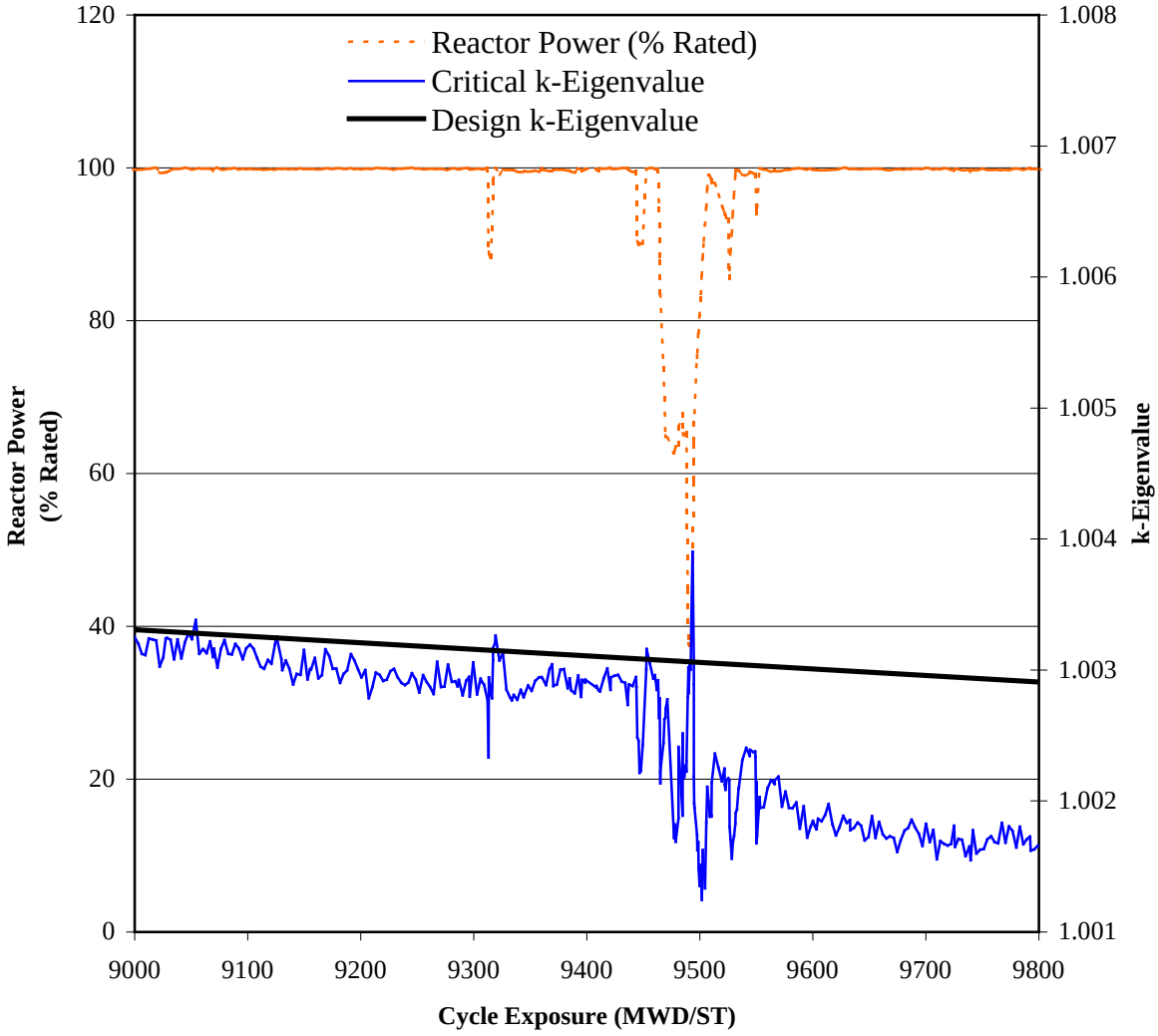

Figure 1-14. Plant C power maneuver.

Table 1-1. Boiling water reactor advancement and evolution.

BWR Product Line	Year of Introduction (Year of first Operation)	Characteristic Plant	Major Improvements
BWR/1	1955 (1960)	Dresden 1	First commercial BWR
BWR/2	1963 (1969)	Oyster Creek	First large direct cycle BWRs
BWR/3	1965 (1971)	Dresden 2	First usage of jet pumps and improved ECCS
BWR/4	1966 (1973)	Browns Ferry	Increased power density by 20%
BWR/5	1969 (1977)	Zimmer	Variable valve flow control and improved ECCS
BWR/6	1972 (1978)	Cofrentes	Increased power output and reduced fuel duty through new fuel arrangement and improvements to static systems such as steam separators and jet pumps

CHAPTER 2
DATA AND METHODOLOGIES

Sources of Data

In order to accomplish the aims of this analysis, data from eight different nuclear power plants was utilized. In order to abide by the privacy and proprietary information concerns of individual utilities, the eight plants used in this analysis will be know by a letter designator, A through H, and Table 2-1 lists some pertinent information about each plant. Plants A through H represent typical examples of the BWR fleet still in operation in the US and overseas, and plants were selected for inclusion in this study based on a preponderance of data and the generation of the reactor. Overall, data available from BWRs of the later generation was predominantly utilized as the most advanced generations are considered to be most representative of the fleet as a whole.

The data drawn from the eight power plants consisted of snapshots, or instantaneous accounts, of all the relevant plant parameters. Computationally, the reactor snapshots were drawn from two sources, PANAC11A (PANACEA), a BWR computer simulation program, and 3D MONICORE, a BWR monitoring and control program. In many ways, PANACEA and 3D MONICORE operate as a coupled computing system and were utilized independently as well as in conjunction for this examination. 3D MONICORE operates as a shell of programs built around and interfacing with PANACEA in order to give reactor operators trending information and help predict future operations. Figure 2-1 illustrates many of the different functions and interfaces of 3D MONICORE and its overlap with PANACEA. Figure 2-1 depicts that much of the main responsibility and function of 3D MONICORE deals with monitoring and predicting core operations and much of that responsibility is shared between the reactor operator and the engineer.

PANACEA

PANAC11A, also known as the BWR core simulator, is a static, three-dimensional, coupled neutronics and thermal hydraulics reactor core simulation. Primarily, PANACEA uses nuclear diffusion theory to model the neutron flux, balance, and reactor power, with a secondary coupled thermal-hydraulics package for completeness. Typically, PANACEA is used for operational calculation of important BWR parameters, such as power distributions, thermal limitations and performance, and neutron flux as well as three-dimensional reactor design and planning (Chopelas, 2007).

The neutronics package for PANACEA utilizes 1-1/2 group (quasi-two group), coarse mesh nodal, static diffusion theory in order to simulate reactor data and parameters. The highest energy group, or the fast group, is where solutions for the diffusion equation are obtained. The fast flux in the highest energy group is related to the resonance flux to account for resonance energy neutronic effects. The flux in the energy region below the fast, or the thermal group, is represented through an asymptotic slowing down approximation from the epithermal region, the region between thermal and fast. Of particular interest to this analysis, reactivity records are obtained for certain reactor parameters and tracked using spectral reactivity history and control rod reactivity history models. Additionally, PANACEA uses its coupled neutronics and thermal-hydraulics package to calculate the effect and reactivity worth of Doppler broadening, xenon production, gadolinium depletion, and void concentration (Chopelas, 2007). In conjunction with 3D MONICORE, PANACEA serves to record and monitor live record data and save them in a format that allows for reactor simulation outside of the 3D MONICORE and other reactor control systems. For this examination, individual PANACEA outputs represented live data state-points for a BWR and over ten thousand PANACEA outputs were employed to create histories for important reactor information over the course of a cycle. PANACEA live reactor data is

pulled from the 3D MONICORE system on the average of about every one to two hours and then saved for later use in long term monitoring and prediction.

3D MONICORE

The majority of the currently operating BWRs throughout the world utilize the 3D MONICORE system to provide information to evaluate future, current, and past fuel performance as well as monitor overall fuel and plant performance. The 3D MONICORE package consists of a group of program and algorithms working together to allow for observation and forecasting of future events, PANACEA being the most important component. The interface between PANACEA and 3D MONICORE allows for increased applicability and usability to operators in that the accuracy of the model used to simulate plant conditions in PANACEA is enhanced using adaptive algorithms coincident with actual plant data and calculated results. Additionally, the performance and function of local power range monitors and traversing in-core probes can be monitored and potentially corrected utilizing simulation and prediction data.

3D MONICORE is utilized during planning of a reactor cycle in order to create a flow map as well as design procedures for startup and shutdown or any power maneuvers. Incorporation of a more effective means of predicting the changes in the critical k-eigenvalue during these off-rated power conditions would improve reactor operations and would be an eventual final commercial application of this analysis. When necessary in this analysis, actual magnetic data storage tapes taken from nuclear power plant 3D MONICORE systems were replayed on a local 3D MONICORE system in order to obtain missing or extra live reactor data in the form of PANACEA outputs.

Statistics

As previously stated, the reactivity effects of control rods, xenon, gadolinium, and Doppler broadening can significantly alter and affect the critical k-eigenvalue during normal and off-rated

power conditions. As these four sources of reactivity play the biggest role in influencing the changes to the critical k-eigenvalue during off-rated conditions, the trending of and interactions between the four reactivity factors can be utilized to predict said changes.

Multiple Polynomial Regression

In statistics, two sources of data with a unit of association, or an element connecting two variables, can be linked and correlated to one another using a regression analysis. In the simplest form of regression analysis, one variable, or data source, serves as the independent or forecasting data for the other variable, the dependent or predicted data. However, a set of multiple independent variables can all affect the changes to a single dependent variable, dictating improved forecasting by utilizing the entire set of independent variables versus just one. Equation 2-1 illustrates a generic multiple polynomial regression model relating a dependent variable, y, to a set of independent variables.

$$y = \beta_0 + \beta_1 x_1 + \beta_2 x_2 + \beta_3 x_3 + \ldots + \beta_n x_n \quad (2\text{-}1)$$

In Equation 2-1, independent variables as well as the cross-products, equal to the value of two or more independent variables multiplied together, could be represented by one of the variables, x_j. The simplest multiple polynomial regression model would be first-order and omit any cross-products, while higher order, quadratic, cubic, or quartic models include them. A first-order model assumes the effects of the independent variables are additive in that the expected change in a dependent variable for a unit change in any independent variable depends solely on that independent variable and none other. On the other hand, the more advanced models seek to characterize the interaction between independent variables in the form of cross-products and can also include the independent variables raised to higher powers, in the with the goal of characterizing the higher order effects of such independent variables (Longnecker, 2004).

The other parameters in the Equation 2-1, β_j ($j \neq 0$), are known as the partial slopes or regression coefficients and relate the expected change in the dependent variable, y, to a unit change in any predictor parameter, x_j, while all the remaining prediction parameters are held constant. The regression coefficients represent trending for each of the independent variables or cross-products and each coefficient contributes to the overall fit of the final correlation. The overall fit of the regression model is tracked and interpreted using the coefficient of determination, R^2, whose calculation is shown in Equation 2-2.

$$R^2 = 1 - \frac{\sum_{i=1}^{n} (y_i - \dot{y}_i)^2}{\sum_{i=1}^{n} (y_i - \bar{y})^2} \qquad (2\text{-}2)$$

The coefficient of determination accounts for the fraction of the total variance in the dependent variable that is described by the regression model. In Equation 2-2, $\bar{y}$ represents the mean of the dependent variable, while $\dot{y}_i$ represents all the predicted values of the dependent variable using the regression model. As evidenced by Equation 2-2, the value of the coefficient of determination fluctuates from a maximum value of one to the minimum value of zero, where a higher value for R^2 indicates good prediction and a strong regression model (Longnecker, 2004).

Backwards Regression

When generating a higher order regression model, coefficients to explain the contributions of all cross-product terms and independent variable terms raised to powers must be first generated and many could be considered insignificant. An insignificant regression coefficient could be replaced with zero as the coefficient and still not extensively affect the ability of a regression model to achieve an accurate prediction. By utilizing a statistical hypothesis test to determine whether each regression coefficient's mean value is different from zero, the

significance of a regression coefficient can be quantified as a probability value between one and zero. Obtaining a high probability value for a regression coefficient would lead to accepting the hypothesis of the test, that the regression coefficient is not significantly different from zero. Probability values for a given statistical hypothesis test are obtained by first calculating the value of the test-statistic and then referring to the corresponding probability distribution. In the case of this analysis, the t-test was utilized, requiring calculation of the t-statistic and reference to the t-distribution for determining the significance of a regression coefficient. The t-statistic for determining the significance of a regression coefficient is calculated by dividing that regression coefficient by the coefficient's standard deviation. By finding the location of the calculated t-statistic within the t-distribution, the probability value associated with the determined test-statistic can be calculated as two times the area under the curve for values of the test statistic greater than what was calculated. For the purposes of this analysis, Microsoft Excel was utilized to calculate all statistical parameters as well as generate each and every regression model.

In a backwards regression analysis, a statistical hypothesis test is applied to each of the determined regression coefficients in a given regression model and the coefficients are then ranked according to their associated probability value. The regression coefficient with the highest associated probability value, higher than some threshold significance level, will be rejected as insignificant and removed from the regression model. In order to be assured that all regression coefficients have a 95% chance of playing a significant role, in affecting the value of the final prediction, a threshold significance level of 0.05 would be utilized. After removing the most insignificant of the regression coefficients in a given model, the regression coefficients would be recalculated with the contributions for the insignificant term omitted. Probability values from a statistical hypothesis test would then be calculated again for each of the new

regression coefficients, and the process would be repeated until all probability values are under the threshold significance level. The only time an insignificant regression coefficient might be retained and not omitted during a backward regression analysis is if its removal would reduce the value of the associated coefficient of determination for the model or disrupt the hierarchy of terms. In order for the hierarchy of terms to be maintained a regression model containing a cross-product term or an independent variable term raised to a higher power must also contain the constituent parts of each term raised to the first order.

Patent Methodology

The first attempt at critical k-eigenvalue prediction by the GE company introduced some of the important aspects and principles of this analysis. The initial k-eigenvalue prediction utilized several quadratic multiple regression models to predict changes to the critical k-eigenvalue over the course of a reactor event. Because many BWRs operate at different critical conditions, stemming from different fuel loadings and control rod arrays, prediction of the actual critical k-eigenvalue was thought to introduce too much complexity as similar reactivity conditions could dictate two different eigenvalues in two different reactors. To combat the disparity between different BWRs, the patent methodology sought to only predict instantaneous changes based on the immediate change to each of the reactivity parameters used as forecasting data. Because incremental changes in reactivity should initiate similar changes to the overall critical k-eigenvalue, regardless of critical arrangement, predicting and utilizing the change in a value, or its delta, improved the applicability of the prediction methodology. The final forecasting data used in the patent methodology consisted of the reactor power and the instantaneous change in the reactivity worth of the control rods, Doppler broadening effect, gadolinium, and xenon.

While the patent methodology represented a good step in the right direction for predicting the critical k-eigenvalue, much of it was done in a haphazard manner with a disregard for

statistical significance. Specifically, the patent methodology ended up creating an ill-defined family of five equations that were designed to describe all off-rated power conditions. Table 2-2 lists and numbers each of the five equations created by the patent methodology and are used later in this analysis for comparison purposes. The five equations also define several different off-rated power events for examination, down-power maneuvers, up-power maneuvers, and startup or shutdown situations. The main fault of the five equations stems from utilizing backward regression techniques to eliminate certain regression coefficients entirely from the model without considering the physical situations and arrangement of a given plant. Figure 2-2 depicts a flow chart describing the patent methodology with many OR gates represented at different steps of the methodology. The OR gates describe points during the patent methodology where plant parameters and physical arrangements should be utilized to determine which of the equations from the statistical analysis is most applicable. In the patent methodology, specific equations consider the reactivity effects of one of the reactor poisons, xenon or gadolinium, to be the overall driving force due to the statistical results. In the xenon-driven equation from the patent methodology, the reactivity effects of gadolinium are omitted as is similarly done for the xenon effects in the gadolinium-driven equation. The principle of the xenon or gadolinium reactivity effects overriding and negating the impact of other poison stems only from statistics and has no basis in the physical plant. Because a physical explanation does not exist in order to categorize plants that conform to the statistical parameters, eventual application of the patent methodology has been and will continue to be fraught with error and undue complexity. Moreover, one of the primary aims of the patent methodology was to generate the most simplistic regression models possible, those that contained a minimum number of regression coefficients. The objective of generating simple models lead, in some cases, to reduction in the overall quality of fit of the

model, in favor of ease of implementation and understanding. This analysis examined which of the five equations created in the patent methodology would operate during which regime and whether the determined plant conditions could lead one to utilize the correct prediction equation.

Advanced Methodologies

Building on the patent methodology, this analysis sought to develop more advanced methodologies and techniques for predicting changes to the critical k-eigenvalue. Compared to the patent methodology, the advanced methodologies incorporated more rigor and aimed to generate the best possible fit equations, without consideration for the simplicity or complexity of a regression model. All the advanced methodologies employ a cubic regression model, one order higher than the quadratic models used in the patent methodology. A cubic regression model includes more cross-product and interaction terms that a quadratic, and in the case of critical k-eigenvalue prediction, it is thought that the third-order interactions of forecasting data can play a role in the final prediction. In each of the advanced methodologies, backwards regression techniques were utilized to maximize the fit of the model and significance of each regression coefficient. Similar to the patent methodology, each of the advanced methodologies looked at the delta of, or change in each of the sources of prediction data and the dependent result in order to ensure applicability and improved prediction as was previously discussed. Like the patent methodology, the final forecasting data used in the advanced methodologies consisted of the reactor power and the instantaneous change in the reactivity worth of the control rods, Doppler broadening effect, gadolinium, and xenon. In contrast to the patent methodology, the advanced methodologies also treated the ill-defined up-power and down-power events to be two halves of the same power oscillation. Furthermore, the advanced methodologies sought to maintain accuracy and precision of the final regression models by rejecting any prediction models that consistently made forecasting errors greater than 100 pcm from the actual value.

Plant-Specific Approach

The patent methodology sought to characterize the entire reactor fleet with a small family of prediction equations, without consideration for variability of operation or design between reactors. The fact that the patent methodology ended up generating families of equations, each specifically tailored to a specific reactor type or condition, dictates that inconsistencies between plants can play a major role in the final prediction result. In order to combat the discrepancies between the plants, it was hoped that an approach that looked at each plant individually would result in accurate and precise final prediction of the critical k-eigenvalue. Plants with the most complete records for multiple cycles were examined in the plant-specific approach as it was the aim of this more advanced methodology to use previous fuel cycles to predict changes in the subsequent ones. Moreover, the plant-specific approach aimed to investigate the merits of a single equation for each reactor to describe all off-rated power events, or if certain events required separate and different treatment. Specifically, investigations were conducted to determine if in-cycle power maneuvers could be described in the same way as in-cycle and BOC startup and shutdown events.

Universal Approach

The universal approach developed in this analysis aimed to take the best aspects of the patent methodology while using physical considerations and accuracy concerns as the main over-riding factor versus simplicity and ease of implementation. Reactor events, from all data sources, with similar shape and duration in power fluctuations were grouped together and regression models were developed for each different reactor event across the entire BWR fleet. Similar to the plant-specific approach, the universal approach also investigated whether structure, duration, and cycle burnup or exposure of the power event could affect the final structure of the model. The main original aim of the universal approach was to create one

extremely robust and detailed equation predicting the critical k-eigenvalue for all off-rated power conditions. Due to reductions in statistical accuracy by incorporating all reactor events, some of which may be vastly different, it became necessary to develop multiple regression models, each describing an individual reactor event. Minimization of the total number of universal models then became the primary concern while still attaining accurate prediction.

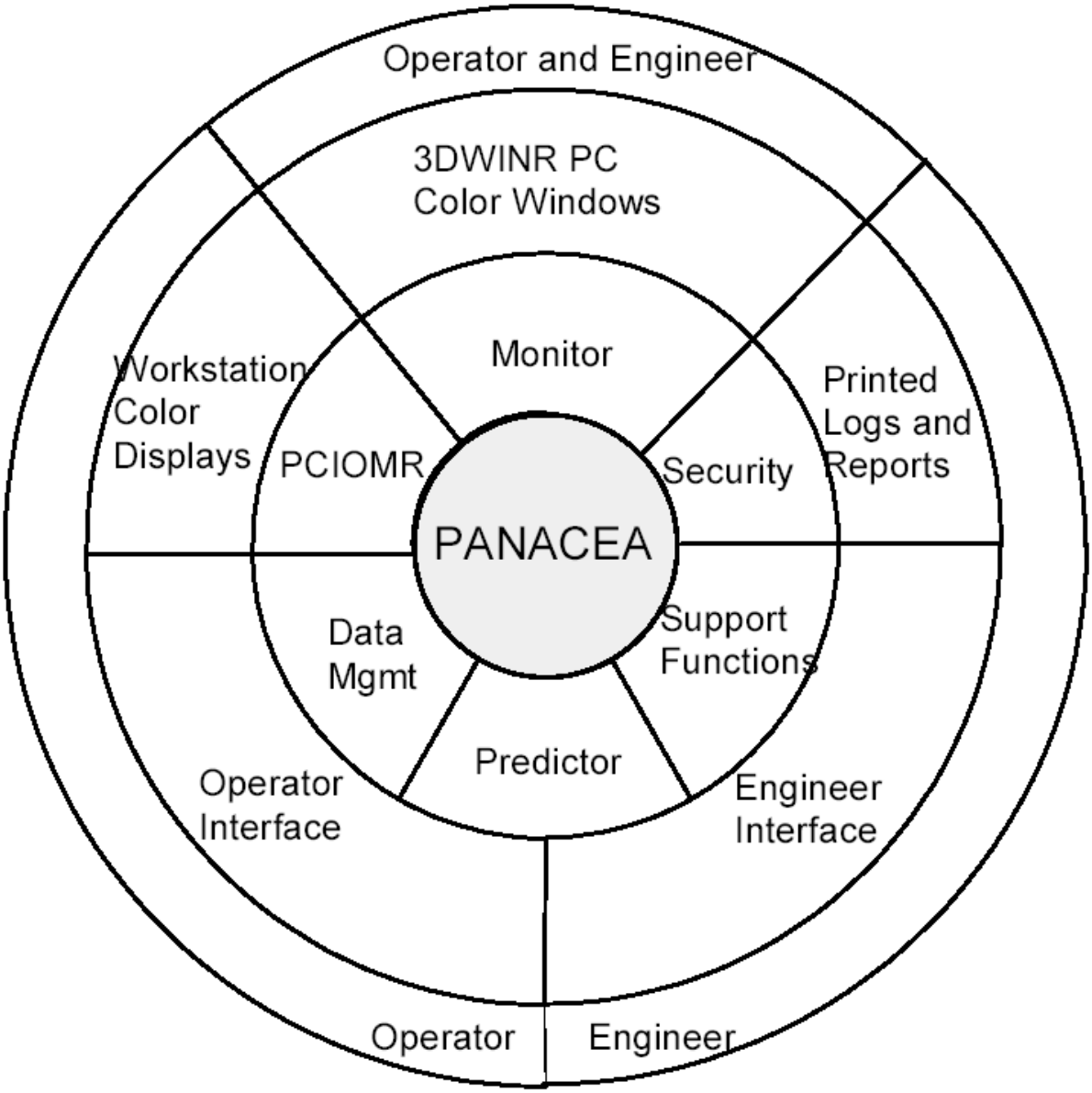

Figure 2-1. 3D MONICORE system features and overlap with PANACEA (3D MONICORE, 2004).

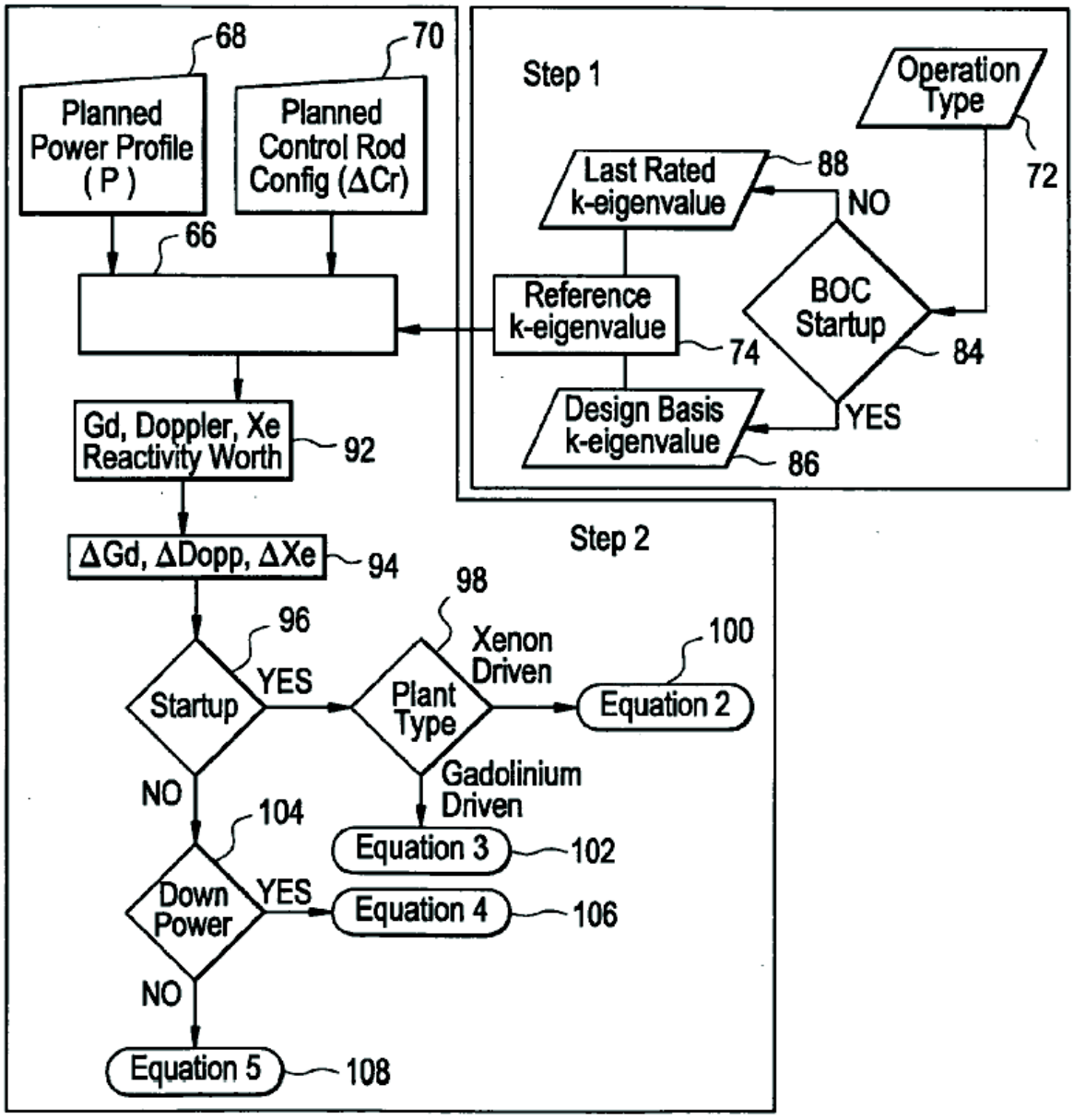

Figure 2-2. Patent methodology flow-chart (Mertyurek, 2008).

Table 2-1. Plant sources of data.

Plant	Plant Type	First Year of Commercial Operation	Thermal Reactor Power (MWth)	Dates of Acquisition of Live Reactor Data
A	BWR/4	1976	1593	April 2003
B	BWR/4	1988	3293	August 2004 – February 2005
C	BWR/4	1975	2436	March 2004 – February 2006
D	BWR/4	1979	2436	March 2004 – February 2007
E	BWR/4	1972	847	September 2007
F	BWR/4	1986	3293	September 2007
G	BWR/4	1974	3293	October 2004 and February 2005
H	BWR/6	1987	3579	September 2004 – January 2005, May 2005, and January 2006

Table 2-2. Patent methodology equation families.

Equation Number	Equation Name	Description of Applicability
1	BOC Startup	Useful only for the initial reactor startup
2	Xenon-Driven Startup	Useful for in-cycle and initial reactor startups where xenon reactivity effects are the overriding statistical concern
3	Gadolinium-Driven Startup	Useful for in-cycle and initial reactor startups where gadolinium reactivity effects are the overriding statistical concern
4	Power-Down	Useful for the initial decrease in reactor power during a power maneuver
5	Power-Up	Useful for the return to rated power following a power decrease during a power maneuver

CHAPTER 3
ANALYSIS, RESULTS, AND DISCUSSION

Applicability of the Patent Methodology

The first step in examining the patent methodology was an examination of the overall accuracy of the multiple regression models. As previously stated, the design k-eigenvalue is calculated with an estimated accuracy of 200 pcm over the course of all power maneuvers and oscillations; it is hoped that any critical k-eigenvalue prediction methodology should attain at least that level of accuracy. In order to reduce overall error propagation in flow rate calculation, it is thought that the 200 pcm level of accuracy for the design k-eigenvalue is not rigorous enough, hence the need to a more attain accurate prediction to within 100 pcm.

The patent methodology was applied to plant events and data that were not originally used to generate one of the five regression models. In order to accurately characterize the degree to which the patent methodology explained changes in the critical k-eigenvalue, plots, unless otherwise stated, are shown in terms of the difference between the predicted and actual value. Figure 3-1 illustrates a typical initial BOC startup and its associated power, specifically from Plant C. The equations developed in the patent methodology, described in Table 2-2, were all applied to the event depicted in Figure 3-1 and the resulting differences, actual minus predicted, are shown in Figure 3-2. Figure 3-3 shows a refinement of Figure 3-2, with the least accurate prediction equations removed for the sake of clarity. As evidenced by Figure 3-2 and 3-3, many of the equations from the patent methodology fail to explain the changes in critical k-eigenvalue to within the 200 pcm accuracy of the design k-eigenvalue, let alone the 100 pcm accuracy that was the aim of this analysis. Specifically, patent methodology equations 1, 2, and 3 should be the most applicable to the startup event shown in Figure 3-1; however, equations 1, 2, and 3 end up outside the 100 pcm accuracy region that was aimed for in this analysis. For the particular

event shown in Figure 3-1, it appears that Equation 1 generates the most accurate prediction and it is hoped that it would be the most applicable of all the patent methodology equations for BOC startups.

Having encountered difficulties in choosing and utilizing the correct prediction equation for reactor startup, another startup power event from Plant C was analyzed and the applicability of the patent methodology tested. Due to the fact that a BOC startup only occurs once per cycle, Figure 3-4 illustrates a Plant C startup from the cycle following the event in Figure 3-1. The Figure 3-4 startup event is from the same plant and it was hoped that the function of each of the patent methodology equation should be consistent from cycle to cycle. Figure 3-5 depicts the differences between the prediction and the actual changes in the critical k-eigenvalue for each of the five patent methodology equations. Equations 1, 2, and 3 should once again be the most applicable to the startup event, and Figure 3-6 depicts the differences, actual minus predicted, for the more accurate of the five equations, 1 and 2. As evidenced by Figure 3-5, Equation 3, which should have been applicable to the startup event, falls several thousand pcm away from the prediction and was excluded from Figure 3-6 for the sake of clarity. On the other hand, the most accurate of the two prediction equations, Equation 1 falls outside the 200 pcm accuracy regime sought by the design k-eigenvalue. The inability of the patent methodology equations to characterize changes in the critical k-eigenvalue as accurately as the piecewise linear trending of the design k-eigenvalue challenges the overall applicability of the patent methodology.

A BOC startup event, such as those characterized in Figures 3-1 and 3-4, represents an extremely short timeframe during the course of a reactor cycle as well as a small portion of the overall function of the patent methodology. While Equation 1 is solely described as a BOC startup equation, Equations 2 and 3 can be utilized to characterize in-cycle reactor restarts,

known as in-cycle startups in this analysis. In-cycle startups are similar to a BOC startup in that reactor power climbs from a low percentage of rated power in much the same way the power comes up from below 50 percent in an initial BOC startup. As opposed to a normal reactor power maneuver, where the lowest power achieved is between 50 and 60 percent, an in-cycle startup could reach a lower final power, as low as 20 percent rated. Figure 3-7 illustrates a typical in-cycle startup, from Plant C and for the same cycle as Figure 3-1. Figure 3-8 shows the application of the five patent methodology equations by once again showing the differences between the predicted change and actual change in the critical k-eigenvalue. Figure 3-9 represents a refinement of Figure 3-8, with the least accurate prediction equation, Equation 1, removed. The inability of equation 1 to characterize an in-cycle startup confirms that Equation 1 is most accurate at BOC, while the failure of Equations 2 and 3 to clearly follow critical k-eigenvalue trending raises questions about their function. However, with the predictions generated by Equations 2 and 3 removed from Figure 3-9, shown here as Figure 3-10, it can be seen that the final difference in the actual versus the predicted k-eigenvalue change for the remaining equations is quite small. While the final difference at the end of each event is of primary concern, the fluctuations that occur mid-event are detrimental to usage of the prediction in that a result drawn mid-event will most likely be far from actual due to fluctuations and oscillations. Figure 3-11 shows a zoomed in view of the end of the power event and the associated predictions from Equations 4 and 5, with the 100 pcm acceptance region labeled. While Equations 4 and 5 fluctuate greatly over the course of power event, the end result of Equation 4 remains within the acceptance region while the end result of Equation 5 remains just slightly outside the acceptance region. The large variations and fluctuations in the prediction equations, shown in Figures 3-8, 3-9, and 3-10, are troublesome from a standpoint of achieving

accurate prediction prior to the end of the power event. The equations all peak above the value of 1000 pcm and should the prediction be utilized prior to the end of the event, the resulting final eigenvalue could be up to five times further off from the design k-eigenvalue, let alone being up to 1000 pcm away from the actual value. However, because the patent methodology predicts the overall change, rather than the local change (the change from start to finish rather than between each data point during the event), the final results in Figure 3-11 will predict changes with more accuracy than the design k-eigenvalue. Unfortunately, Equations 4 and 5 are the power-down and power-up equations, respectively, dictating less applicability to the event in Figure 3-7 versus the startup Equations, 2 and 3. The analysis performed on the three power events, Figures 3-1, 3-4, and 3-7, indicates the inability to determine which equation should accurately predict a power event solely based on the predicted power shape and event type.

The final remaining area left to determine the applicability of the patent methodology was during a normal power maneuver, one where the power level drops to around 50 to 60 percent of rated power before rebounding back to the rated power level. Equations 4 and 5 should be the most applicable to normal power maneuvers and Figure 3-12 illustrates a typical power maneuver, again from Plant C. All five of the patent methodology equations were applied to the power event in Figure 3-12 and the resulting differences in the change in k-eigenvalue, actual minus predicted, is shown in Figure 3-13. Figure 3-14 depicts the resulting prediction using what was supposed to be the two most applicable prediction equations, Equations 4 and 5, according to the patent methodology. Figure 3-14 shows the 100 pcm accuracy region aimed for during this analysis and Equations 4 and 5 clearly fall well outside that accuracy region as well as outside the 200 pcm accuracy regime of the design k-eigenvalue. On the other hand, two equations, Equations 2 and 3, unexpectedly accurately predict the change in critical k-eigenvalue

within the sought after 100 pcm acceptance region as shown in Figure 3-15. While the use of patent methodology equations 2 and 3 would generate accurate and proper results for a normal power maneuver, in this situation, complications arise from the fact that the patent methodology would incorrectly choose less accurate predictions based solely on the categories the equations were divided into.

While most of the investigation into the applicability of the patent methodology utilized two Plant C cycles as the main and standardized sources of data to which the patent equations were applied, certain other plants were examined to ensure Plant C events were representative of the fleet as a whole. A normal power maneuver from Plant H is shown in Figure 3-16 with the associated k-eigenvalue differences, actual minus predicted change, are shown in Figure 3-17. Figure 3-18, represents a refinement of the plot in Figure 3-16, with the least accurate prediction equation, Equation 1, removed for the sake of clarity and understanding. Comparing the Plant C and Plant H power events, Figures 3-12 and 3-16, respectively, it is evident that the prediction equations result in similar results across plants. Figure 3-18 depicts the inability of the power-down and power-up equations, Equations 4 and 5, respectively, to accurate characterize a normal power maneuver, the main purpose of the two equations. Moreover, similar to Figures 3-14 and 3-15, Equations 2 and 3 represent the most accurate predictions in Figure 3-18, contrary to the categorical applicability that was originally determined for each equation. Equations 4 and 5 should be more accurate than Equations 2 and 3 for a normal power maneuver and fall well outside the 200 pcm accuracy regime of the design k-eigenvalue let alone the sought after 100 pcm accuracy.

In almost all the cases examined over the course of this analysis, the patent methodology failed to accurately predict the trending in the critical k-eigenvalue. Specifically, the equation

categories seem to have significant overlap between one another and the resulting inability to select the most accurate equation prior to application challenges the methodology's final usage. Additionally, it was extremely uncommon for any of the five equations to predict changes within the 200 pcm accuracy regime of the design k-eigenvalue, let alone the aimed for 100 pcm. Specifically, of all the patent methodology prediction equations, Equations 2, 3, and 5 were the only models that achieved the sought after 100 pcm accuracy; however, their usage, function, and title all seem to be in conflict. In terms of final implementation and usage of the patent methodology, the analysis performed herein illustrates that the most accurate prediction equation will not always be selected by the steps used in Figure 2-2. On the other hand, the impact of disparities between reactors was found to be negligible across the Plants utilized in this analysis as evidenced by Figures 3-14, 3-15, and 3-18. The cross-plant applicability of the patent methodology adds to the value of its overall usage; however, the inability to select the proper equation remains the biggest and most overriding concern.

Plant-Specific Methodology

The plant-specific methodology stipulates that future behavior can be predicted by past behavior for a single reactor and for similar events. In order to determine the merits of such an approach, the first step required obtaining as much uninterrupted data from a single plant as possible. In the case of this analysis, Plant C represented the most complete source of data with information available from nearly two entire complete cycles, or over the course of three full years. The earlier of the two cycles from Plant C, cycle C-1, occurred between March 2004 and January 2006 and represented the data pool from which all of the plant-specific prediction equations were created. The created plant-specific equations were then applied to the later cycle from Plant C, cycle C-2, occurring between March 2006 and January 2008, in order to judge the versatility and effectiveness of the plant-specific approach. Based on difficulties encountered in

the patent methodology and obstacles initially encountered in the plant-specific approach, a separate BOC startup equation was created in addition to the plant-specific equation describing power maneuvers. The power maneuver equation from the plant-specific data was created in such a way as to also model an in-cycle startup event and it was hoped that such an equation would function better for a specific event than the associated patent methodology equation. Accuracy on the order of 100 pcm was sought after and equations from the patent methodology corresponding to the proper event were also applied with the plant-specific equations in order to determine which is more accurate and effective.

Figure 3-19 shows the cycle C-2 BOC startup power shape with the differences, actual minus predicted change in eigenvalue, obtained from plant-specific BOC startup equation and patent methodology Equation 1 shown on top of the power shape. The 100 pcm acceptance region is shown in Figure 3-19 and all of the final values from the applied prediction equations fall outside of the 100 pcm threshold and the 200 pcm accuracy of the design k-eigenvalue. Moreover, the final value of the patent methodology BOC startup equation, Equation 1, falls consistently outside the 100 pcm acceptance region, but maintains a more uniform trending and change versus the plant-specific BOC startup equation. The inaccuracy of the plant specific BOC equation stems mostly from a lack of plant-specific BOC startup events resulting in a poor data pool for generating prediction equations. On the other hand, even though the patent methodology equation takes into account many other BOC startup events, outside of Plant C, the accuracy remains outside what is desired for both predictions, from the plant-specific approach and patent methodology.

The plant-specific approach next investigated the ability to describe changes in the critical k-eigenvalue during power maneuvers and events other than BOC startups. Figure 3-20

depicts a cycle C-2 in-cycle startup and the associated power shape. The application of the in-cycle startup equations from the patent methodology, Equations 2 and 3, and the plant-specific power maneuver equation is shown in Figure 3-21. Once again, Figure 3-21 shows the differences in the actual versus predicted changes in the eigenvalue in order to clearly gauge the accuracy of each prediction technique. Observing the trends in Figure 3-21, it is clearly evident that the three prediction equations characterize the eigenvalue changes well at the end of the power event and tend to oscillate quite a bit towards the middle and beginning of the event. While the oscillations are troublesome in that a prediction that is utilized prior to the end of a power event will achieve a very inaccurate critical k-eigenvalue prediction, whereas the final result of all three equations would be virtually exact. Figure 3-22 illustrates an enhanced view of Figure 3-21, with the scale adjusted to only show the 100 pcm acceptance region. Figure 3-22 illustrates how all three prediction equations fall well within the 100 pcm acceptance region following some oscillations and fluctuations. The plant-specific prediction equation differences fall closer to a value of zero, about 35 pcm off, than the patent methodology equations, indicating a better final critical k-eigenvalue from the plant-specific approach. While all three prediction equations generate accurate final results, the best results come from the plant-specific approach even with larger variations mid-event versus the patent methodology.

Another in-cycle startup from cycle C-2 was examined in order to see if the plant-specific methodology maintained its accuracy for events occurring later in the cycle, and Figure 3-23 shows the power shape for this event. Specifically, Figure 3-23 represents a blending of a normal power maneuver and an in-cycle startup and therefore, four of the five patent methodology equations, excluding the BOC startup equation, were applied to the power event along with the plant-specific power maneuver equation. The resulting differences obtained

between the actual and predicted k-eigenvalue changes for the Figure 3-23 power event are shown in Figure 3-24. Figure 3-24 clearly illustrates that all of the prediction equations experience large fluctuations from the actual value during the course of the power event even though the final values of the differences fall close to zero, as shown by the zoomed in view of Figure 3-24, Figure 3-25. Figure 3-25 shows only the tail-end of the power event, scaled to the 200 pcm accuracy sought by the design k-eigenvalue and the 100 pcm acceptance region labeled on the plot. Examining Figure 3-25, it is clearly evident that all five equations fall within the 200 pcm accuracy of the design k-eigenvalue, while only two equations fall within the 100 pcm acceptance region, the plant-specific equation and patent methodology Equation 4, the power-down equation. As far as the patent methodology is concerned, confusion would arise in an attempt to characterize this event in that it would be difficult to determine which of the four applicable prediction equations would work best prior to conclusion of the power event. Moreover, Figure 3-26 shows how the most accurate patent methodology prediction equation, Equation 4, remains more consistently outside the 200 pcm design k-eigenvalue accuracy region than the plant-specific equation even though the final result is closer to the actual change. This variations over the course of the event would make drawing eigenvalue changes mid-event extremely difficult and inaccurate, and the plant-specific approach seems to have more merit for such a situation than the patent methodology.

Finally, the plant-specific approach investigation examined a normal power maneuver from cycle C-2, the power shape of which is shown here as Figure 3-27. Figure 3-28 shows the resulting k-eigenvalue differences obtained, actual minus predicted changes, for application of the plant-specific power maneuver and the two applicable patent equations, Equations 4 and 5. The 100 pcm acceptance region is shown in Figure 3-28 and it is clearly evident that only the

plant-specific prediction equation obtains the desired accuracy in the final prediction value. Additionally, even though the plant-specific approach varies and fluctuates to values outside of the accuracy desired by the design k-eigenvalue, the patent methodology equations are once again more consistently outside of the sought after accuracy region. The inability to consistently predict the change throughout the entire course of the event introduces unneeded complications into the prediction process and seems to devalue the approach of the patent methodology.

Throughout Plant C cycle C-2, the plant-specific approach, seemed to have more merit and improved accuracy versus the patent methodology. Specifically, the 100 pcm accuracy desired during this analysis was more consistently achieved by the plant-specific approach and many of the patent methodology results were even outside of the 200 pcm accuracy of the design k-eigenvalue. Moreover, in certain cases, such as the mixed power maneuver and in-cycle startup shown in Figure 3-23, the plant-specific approach introduces less opportunity for error by utilizing a single power maneuver equation versus the multiple equations and regimes employed by the patent methodology. On the other hand, the plant-specific BOC startup equation achieved less accuracy than the patent methodology for describing the cycle C-2 BOC startup, even though neither approach achieved the desired accuracy. The inability to characterize the cycle C-2 BOC startup by the plant-specific approach most likely stems from a lack of more BOC startup events from Plant C prior to cycle C-2 and should be improved with incorporation of such data. The failure of the plant-specific approach to characterize BOC startups is one of many reasons why the universal approach was investigated, as it was thought that between similar plants, BOC startups should have analogous trending and therefore be useful in predicting final changes.

Universal Approach

The universal approach sought to pool data from all plants collectively and apply the resulting prediction equation across the fleet in order to achieve accurate prediction. Similar power events from all the power plants were taken as a whole in order to generate universal prediction equations for all plants. In order to maintain statistical accuracy and ensure fit arises from trending across the reactors, the only events that were excluded from the pool of prediction data were those that were used for validation. As in the two previous methodologies, it was again thought the differences between BOC startups and normal power maneuvers would result in complications so a separate universal prediction equation was created for BOC startup as well as for all power maneuvers.

The first step in the universal approach was to investigate the ability to describe changes during a BOC startup event. The power event shown in Figure 3-19 was utilized and the universal methodology BOC startup equation was applied to the event, along with the patent and plant-specific methodologies BOC startup equations, and the resulting differences from the actual change in eigenvalue are shown in Figure 3-29. Examining Figure 3-29, it becomes apparent that even though the universal methodology fluctuates and varies less than the plant-specific approach, the patent methodology remains consistently closer over the course of most of the event. However, Figure 3-30 shows a zoomed in view of the end of the power event, with the 200 pcm design k-eigenvalue accuracy region labeled, and illustrates how both the patent methodology and universal approach achieve similar, if opposite, final values just outside the 200 pcm accuracy region. In fact, the universal methodology BOC startup equation achieves a prediction that is about 50 pcm closer to the actual change than the patent methodology. While none of the three equations achieve 200 pcm accuracy, let alone the 100 pcm accuracy desired, the universal approach would result in the best possible prediction out of the three methods.

Next the analysis on the universal approach turned to its applicability to an in-cycle startup event and the event whose power shape is shown in Figure 3-20 was first investigated. Figure 3-31 shows the application of the universal approach and plant-specific normal power maneuver equations along with the most accurate of the patent methodology equations, as determined by Figures 3-21 and 3-22. Figure 3-31 depicts increased accuracy of the universal approach in that the large fluctuations in the plant-specific approach and the smaller oscillations in the patent methodology have all been reduced. Figure 3-32 shows a refinement of Figure 3-31, scaled to only show the changes that occur with a 1000 pcm accuracy region and the large oscillations from the plant-specific approach removed for the sake of clarity. Figure 3-33 is scaled to show the 100 pcm accuracy region and it is evident that the universal approach is most consistently within its bounds. The lack of significant oscillations ensures that a prediction could be pulled at any point during the course of the event and still achieve accurate results. Figure 3-33 shows the tail-end of the power event with the final values obtained from the four prediction equations: universal, plant-specific, and the two from the patent methodology. Of paramount concern would be the fact that the universal approach achieves a more accurate final value than both the plant-specific and patent methodologies. In fact, the predicted changes from the universal approach achieve around 15 pcm accuracy relative to the actual value, a two fold improvement from the plant-specific approach and a three-fold improvement from the most accurate equation developed for the patent methodology.

The final area the universal approach examined was the ability to describe normal power maneuvers and the first event to be analyzed was the maneuver whose power shape is shown in Figure 3-27. Figure 3-34 shows the k-eigenvalue difference, actual minus predicted changes, obtained from both the plant-specific and universal approach as well as the two most applicable

equations from the patent methodology, Equations 4 and 5. The 100 pcm acceptance region is also shown in Figure 3-34 and the universal approach is most consistently within the desired accuracy as compared to the other two methodologies. Additionally, even when the universal methodology falls outside the desired accuracy, the peaks and troughs are much less severe and the universal approach is always within the 200 pcm accuracy of the design k-eigenvalue. On the other hand, the final value of the plant-specific approach achieves closer agreement with the actual eigenvalue than the universal methodology; however the final difference between the two methodologies is less than 30 pcm. Unfortunately, the plant-specific approach is more regularly outside of the desired 100 pcm accuracy region and sometimes falls outside the 200 pcm accuracy of the design k-eigenvalue, illustrating the reduced versatility of that approach versus the universal one.

Because the universal approach seeks to characterize all BWRs as a whole, the universal approach prediction equations were then applied to an event outside of Plant C. While the majority of the events that the universal approach was analyzed against came from Plant C in order to best compare against the plant-specific approach, a Plant H power event was also analyzed to ensure cross-plant applicability. The Plant H power event previously analyzed in the patent methodology investigation and whose power shape is shown in Figure 3-16 was selected for analysis with the universal approach in order to be able to compare its applicability to that of the patent methodology. Figure 3-35 shows the application of four of the patent methodology equations to the Figure 3-16 power event along with universal approach normal power maneuver prediction equation. As previously stated, patent methodology Equations 4 and 5 should be the most accurate of the patent methodology equations on the basis of the categories each equation is assigned to; however, Equations 2 and 3 achieve significantly more accurate results. Comparing

Equations 2 and 3 results to the universal approach, it is evident that all three achieve accuracy within 100 pcm, but the universal approach is more accurate by the order of 10 to 20 pcm. Figure 3-36 shows Figure 3-35 with Equations 4 and 5 omitted in order to better depict the fluctuations that occur between the best the patent methodology can offer and the universal approach. Unfortunately, Equation 2 from the patent methodology seems to be consistently closer to the actual change in eigenvalue over the entire course of the event when compared to the universal approach, whose biggest difference from actual peaks just around 400 pcm off. Nevertheless, the final prediction obtained by the universal approach is closer to actual and confirms the ability of the universal approach to use a single equation to describe similar events across different plants.

When comparing the results from the universal approach to both the patent methodology and plant-specific approach, the universal approach almost always achieves better results. Specifically, the use of the universal approach ensures that the opportunities for error presented by the patent methodology, in the form of being forced to select an applicable equation, no longer exists and accurate prediction can be achieved. BOC startups remain an issue for the universal approach as the methodology achieved the most inaccurate result for BOC startups when compared to the other events analyzed. Additionally, the number of events analyzed for the universal approach had to be limited, as each additional event analyzed needed to be removed from the data pool from which the predictions were created. It was thought that the removal of any event from the universal approach data pool would reduce overall accuracy of the final prediction equations and the limited number of events shown in this examination were analyzed because of it.

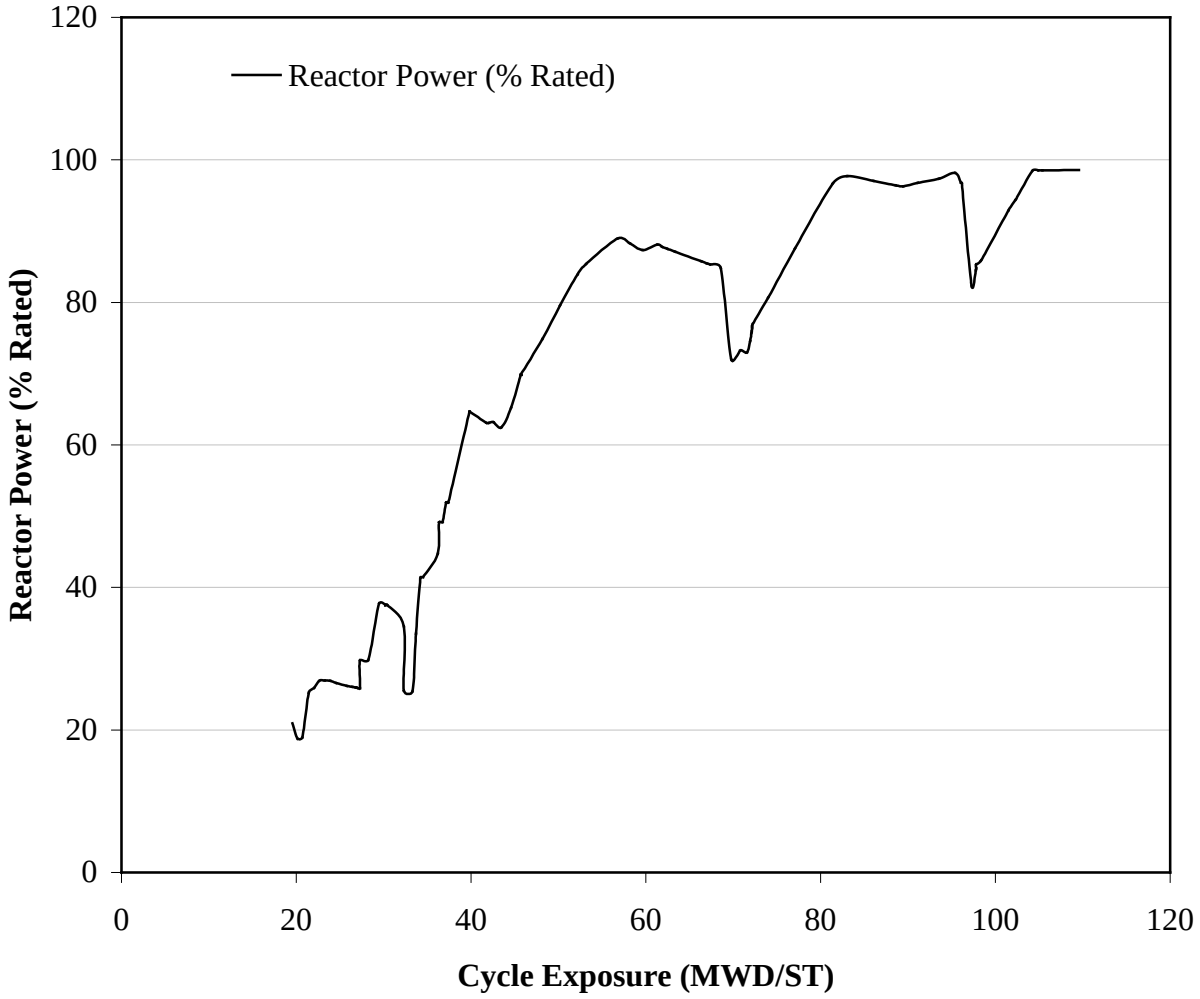

Figure 3-1. Power shape for Plant C startup event number 1

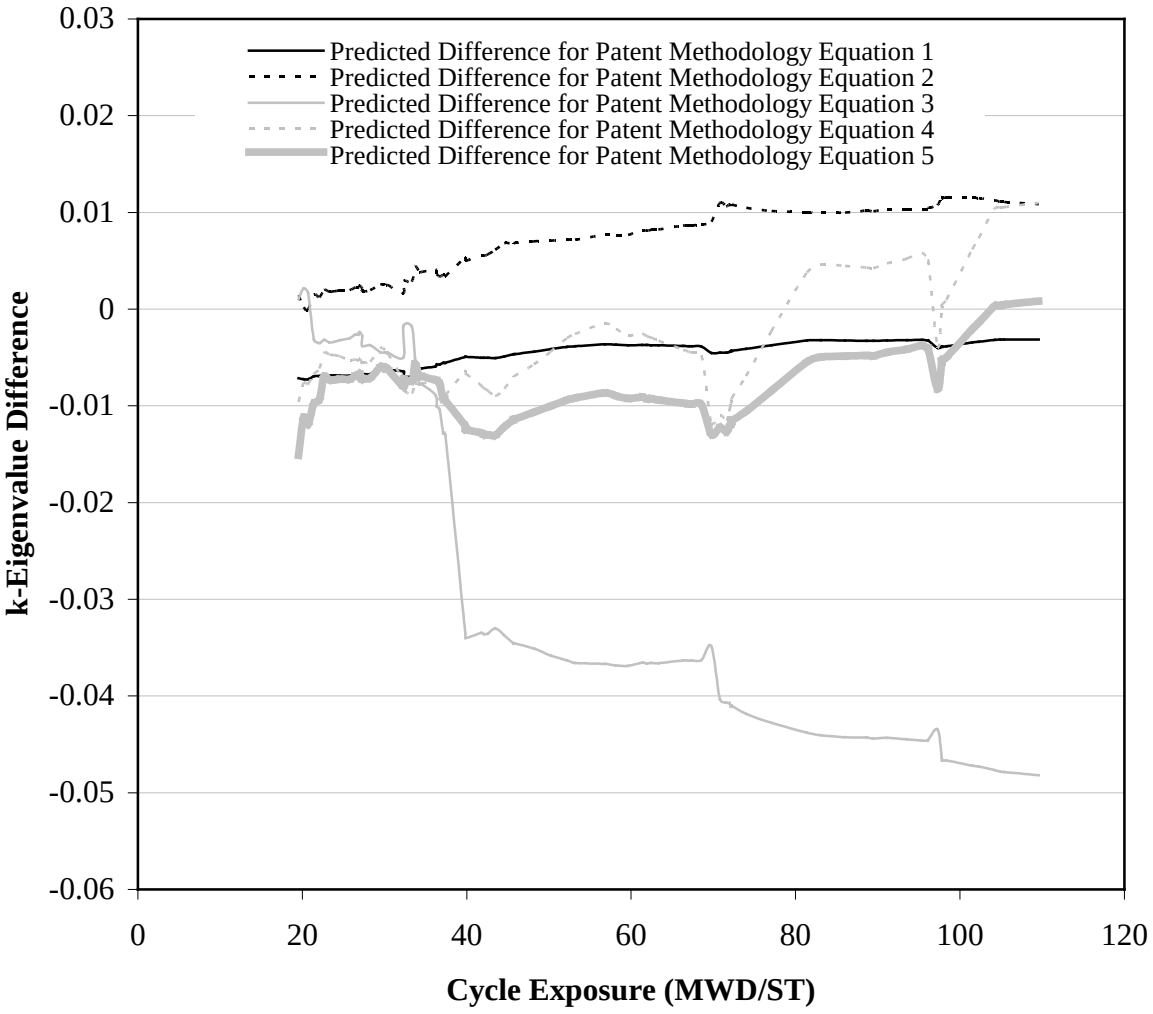

Figure 3-2. Patent methodology equations applied to Plant C startup event number 1

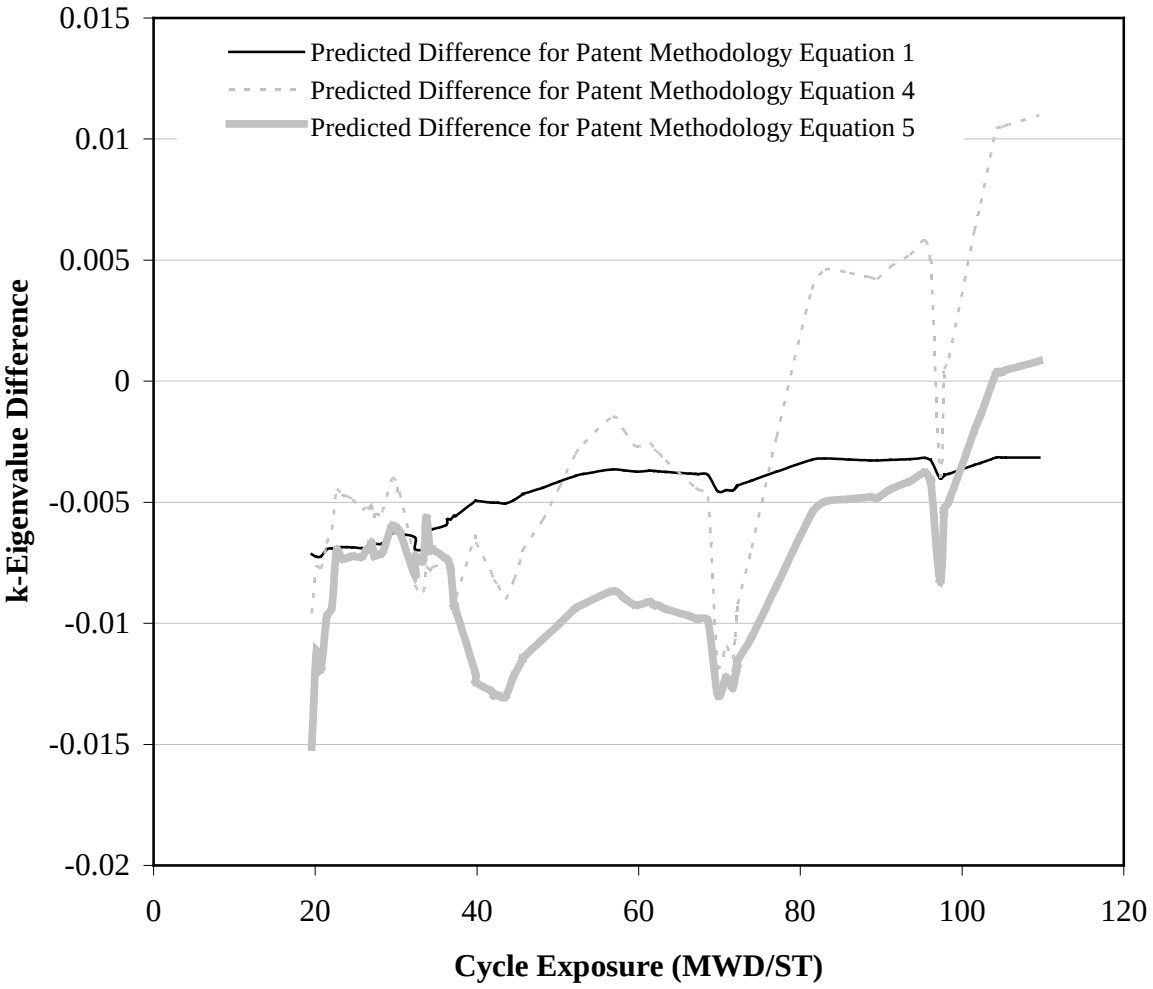

Figure 3-3. Patent methodology equations applied to Plant C startup event number 1, with the most inaccurate predictions omitted

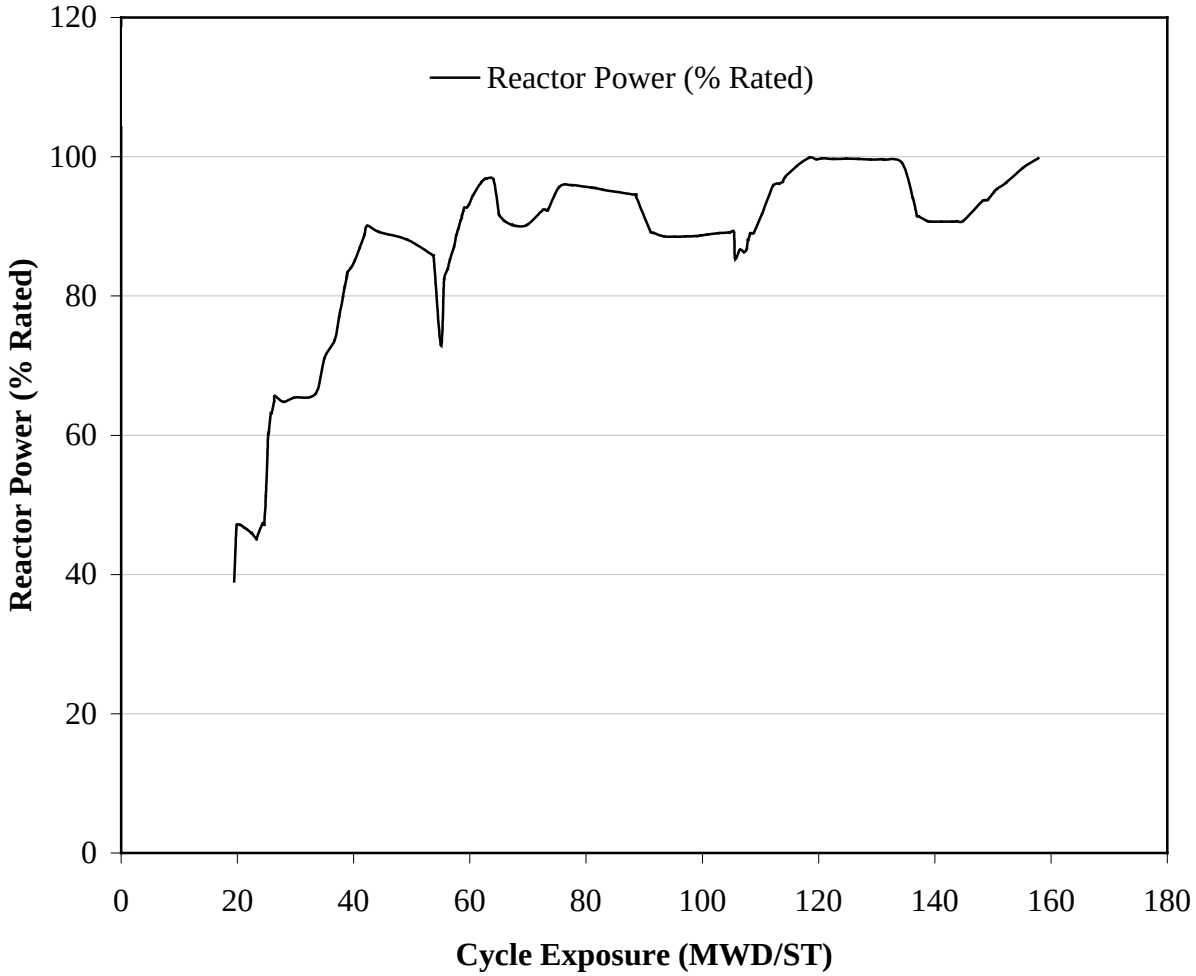

Figure 3-4. Power shape for Plant C startup event number 2

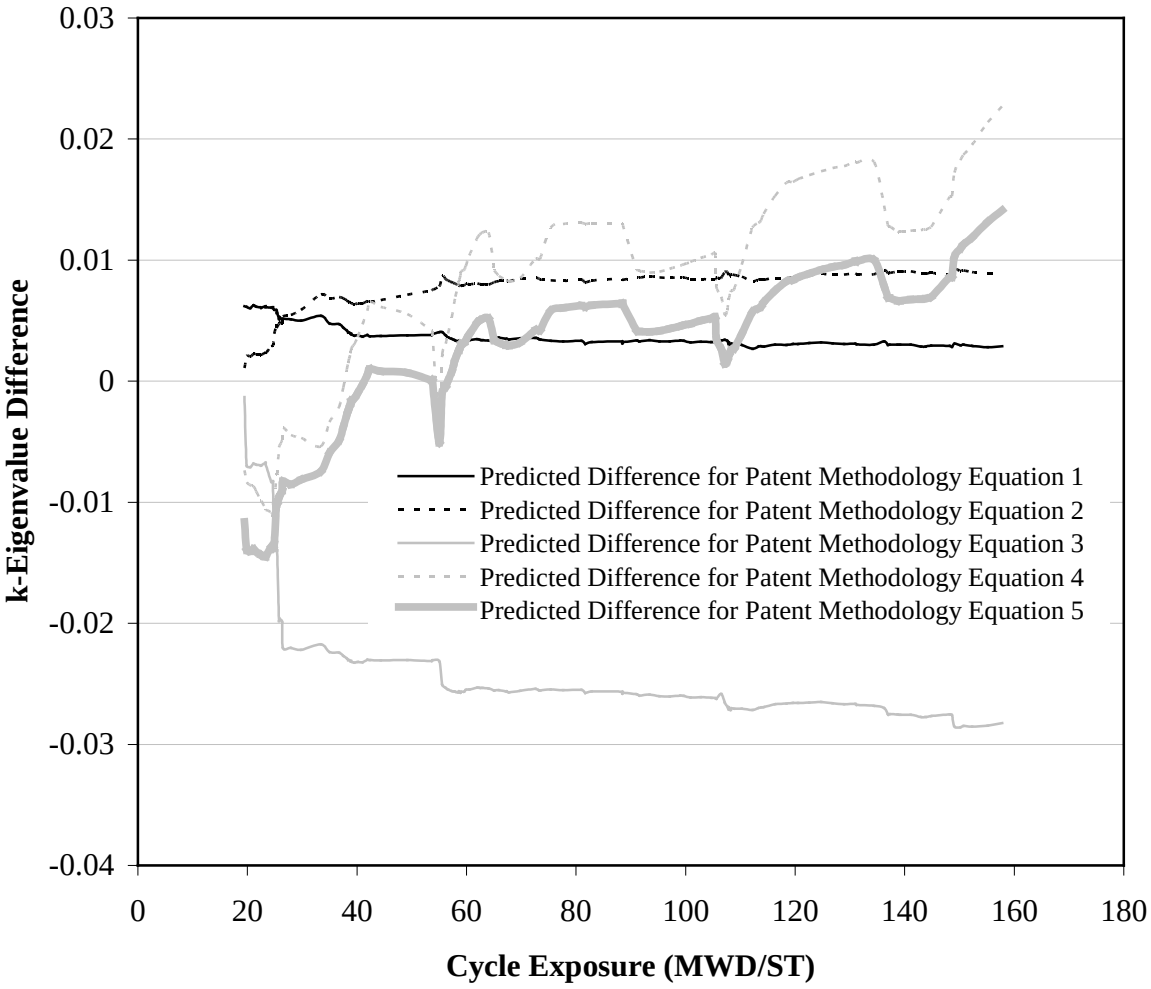

Figure 3-5. Patent methodology equations applied to Plant C startup event number 2

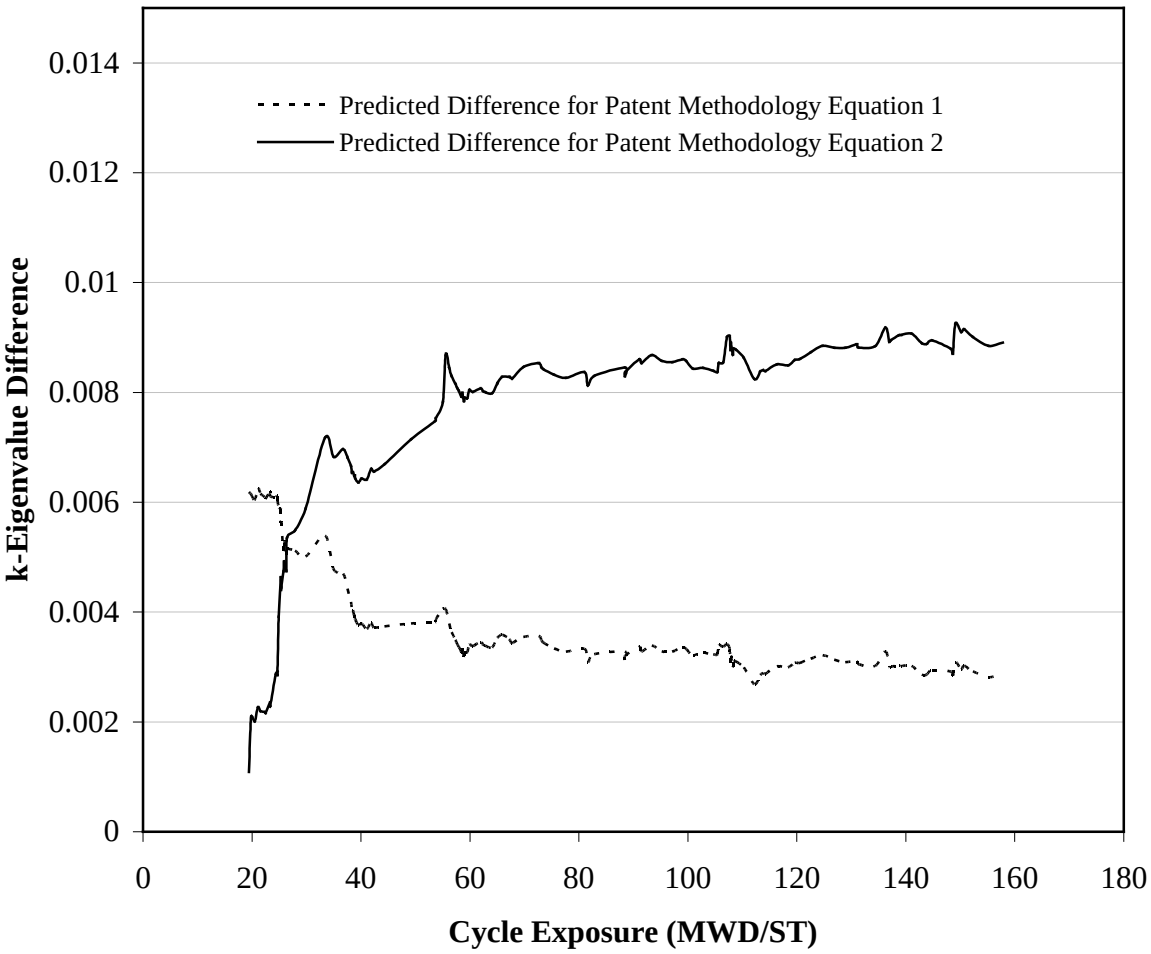

Figure 3-6. Patent methodology equations applied to Plant C startup event number 2, with the most inaccurate predictions omitted

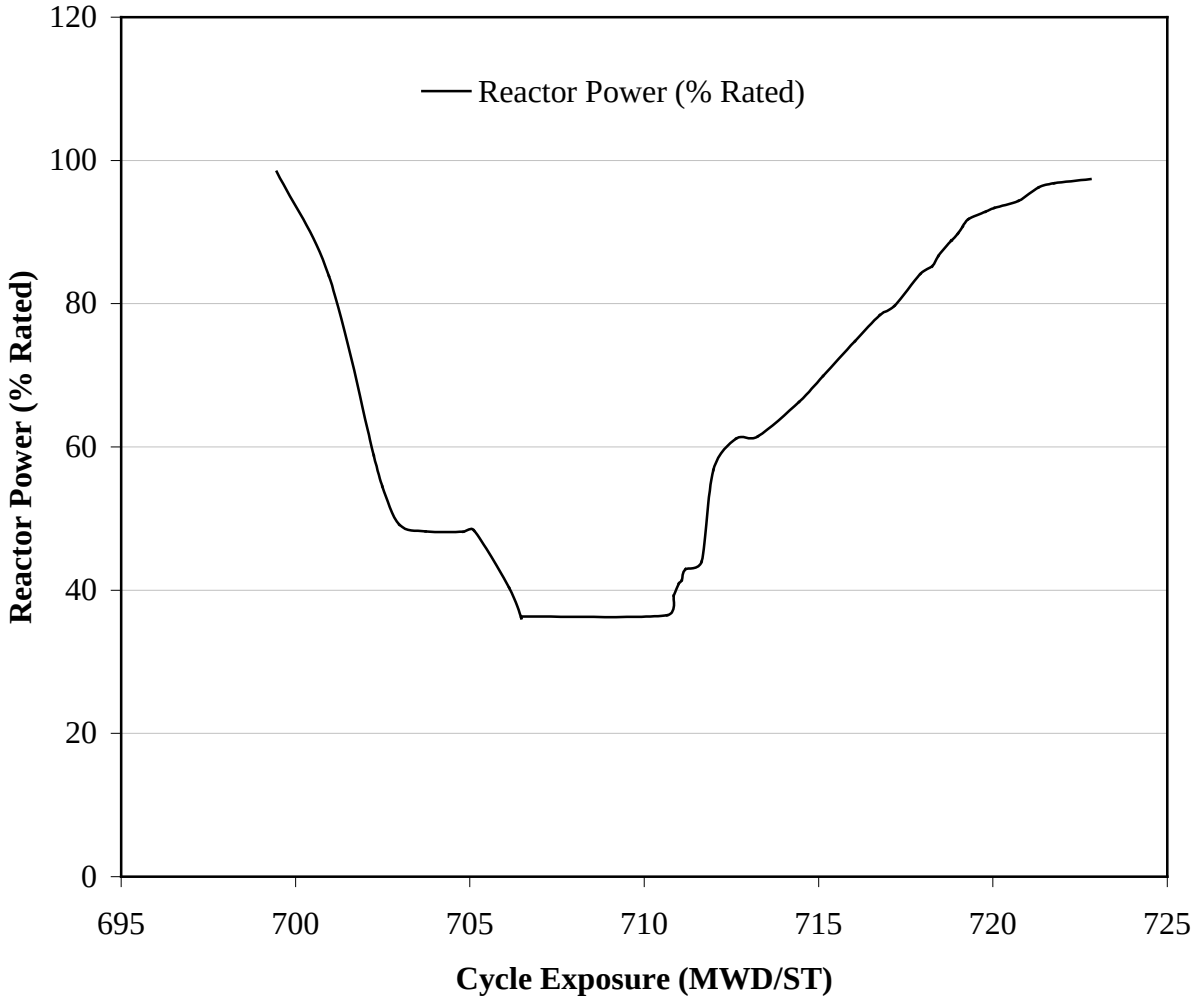

Figure 3-7. Power shape for Plant C in-cycle startup event number 1

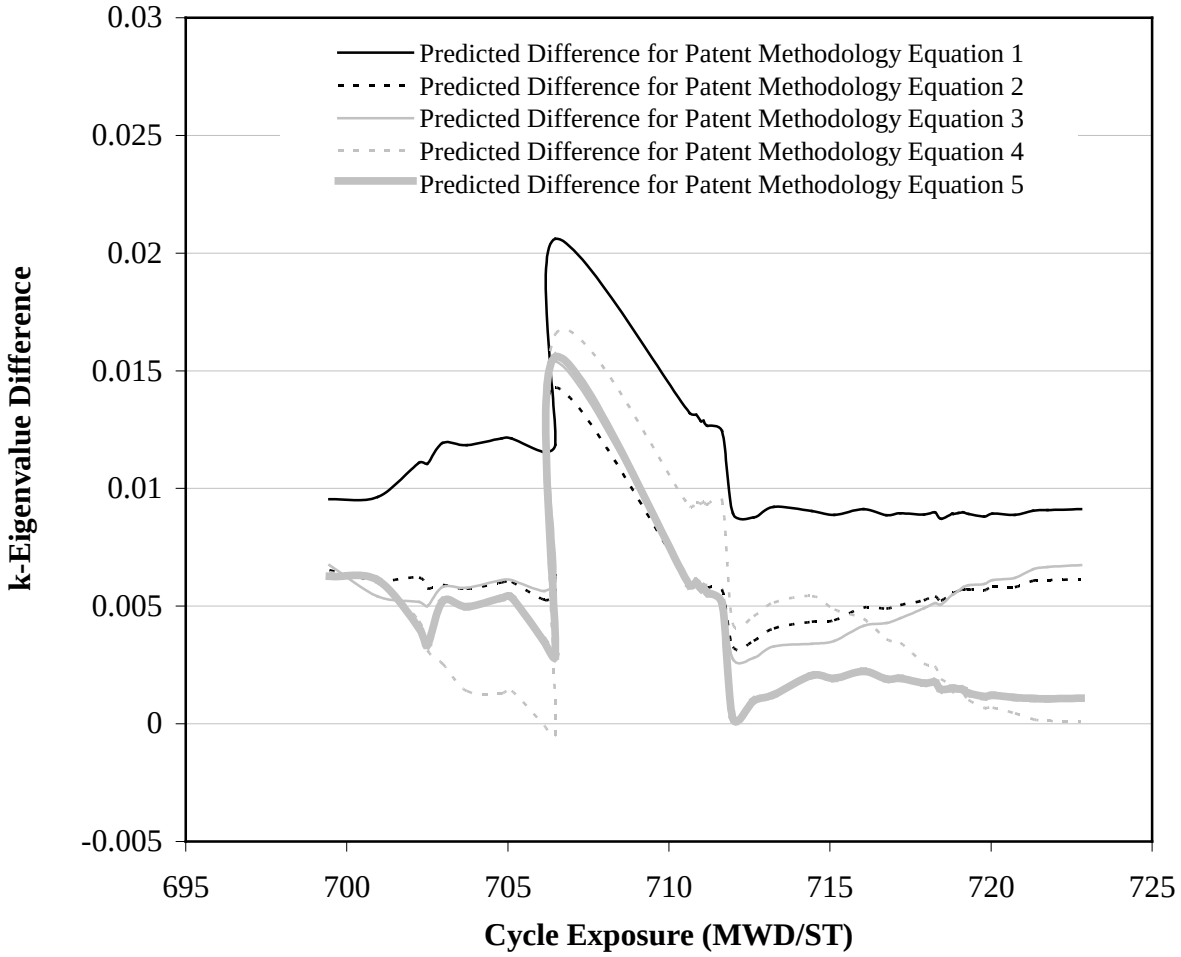

Figure 3-8. Patent methodology equations applied to Plant C in-cycle startup event number 1

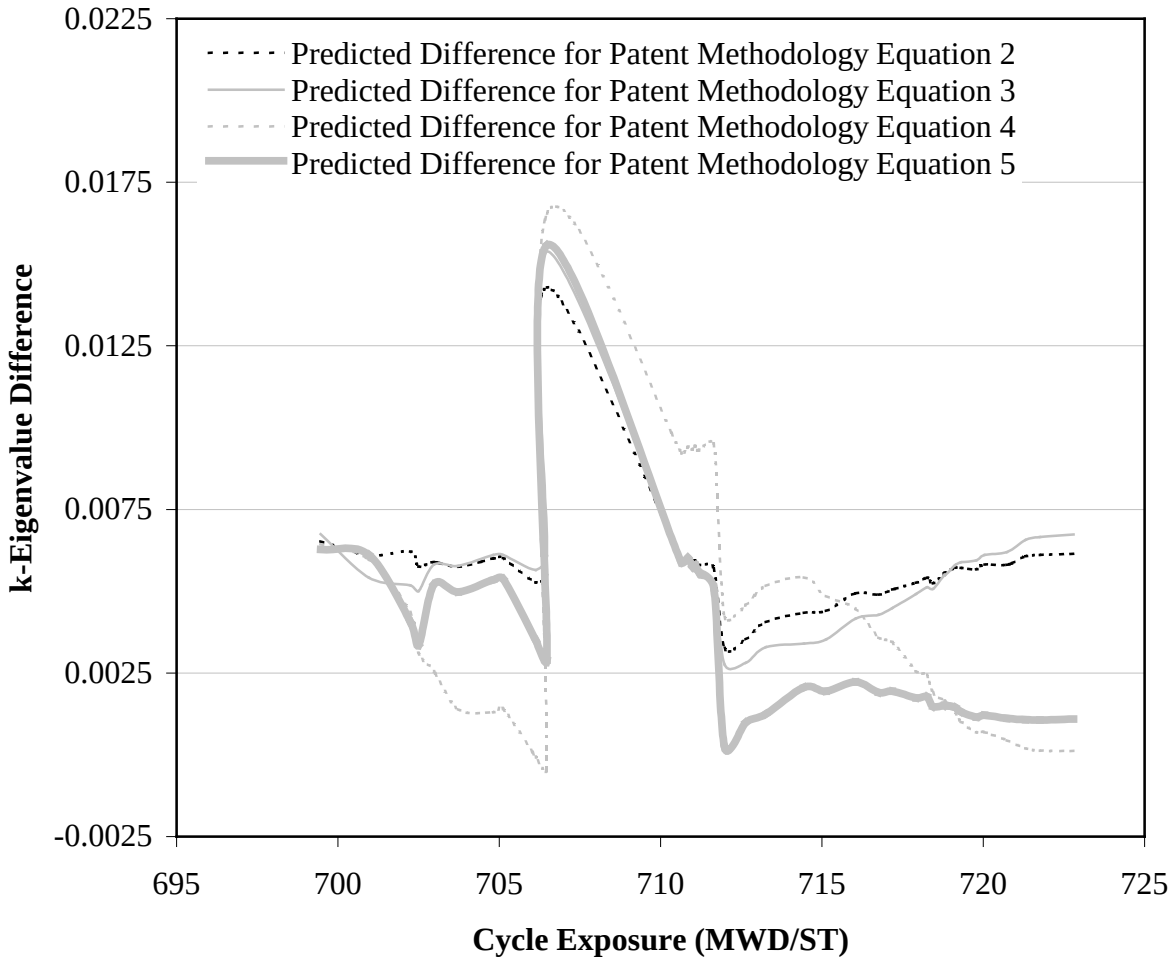

Figure 3-9. Patent methodology equations applied to Plant C in-cycle startup event number 1, with the least applicable prediction omitted

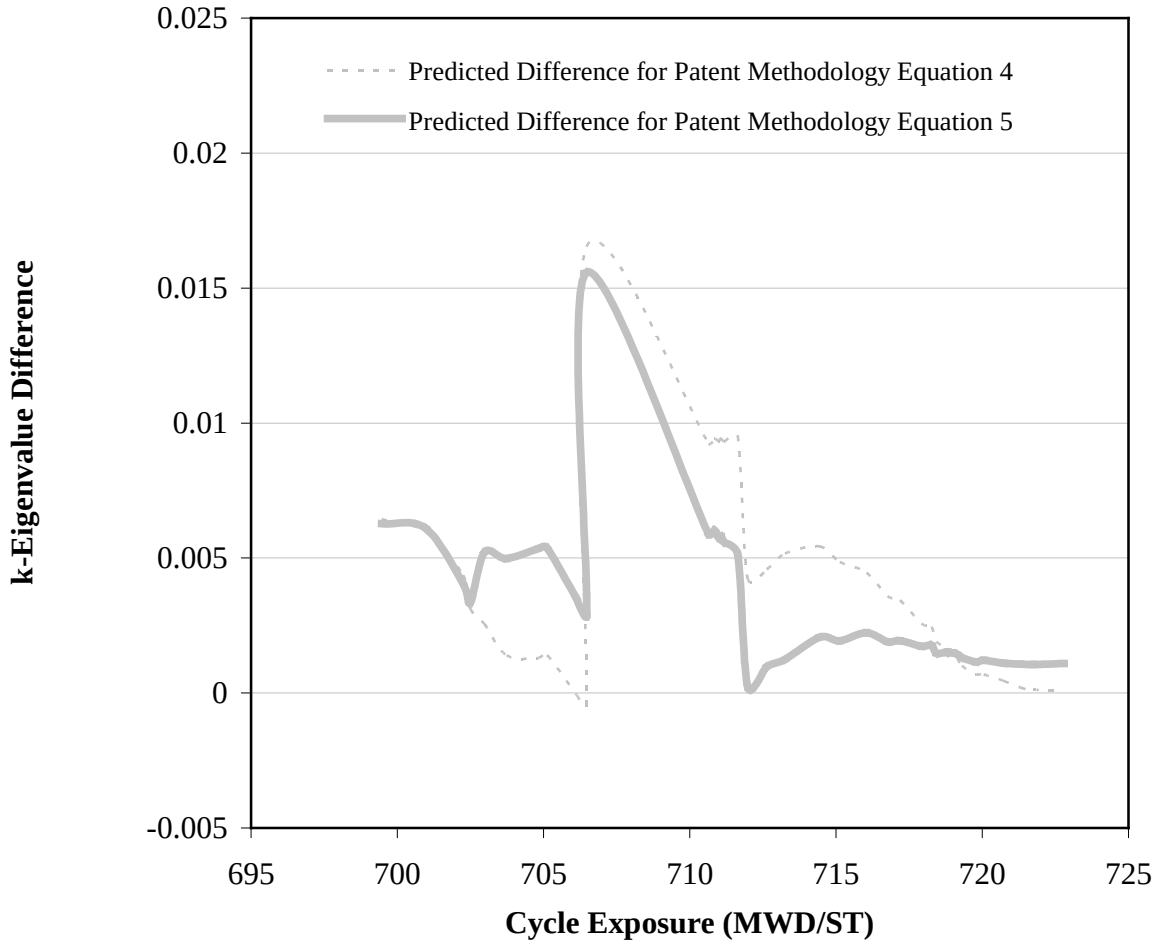

Figure 3-10. Patent methodology equations applied to Plant C in-cycle startup event number 1, with the least applicable prediction and the least accurate predictions omitted

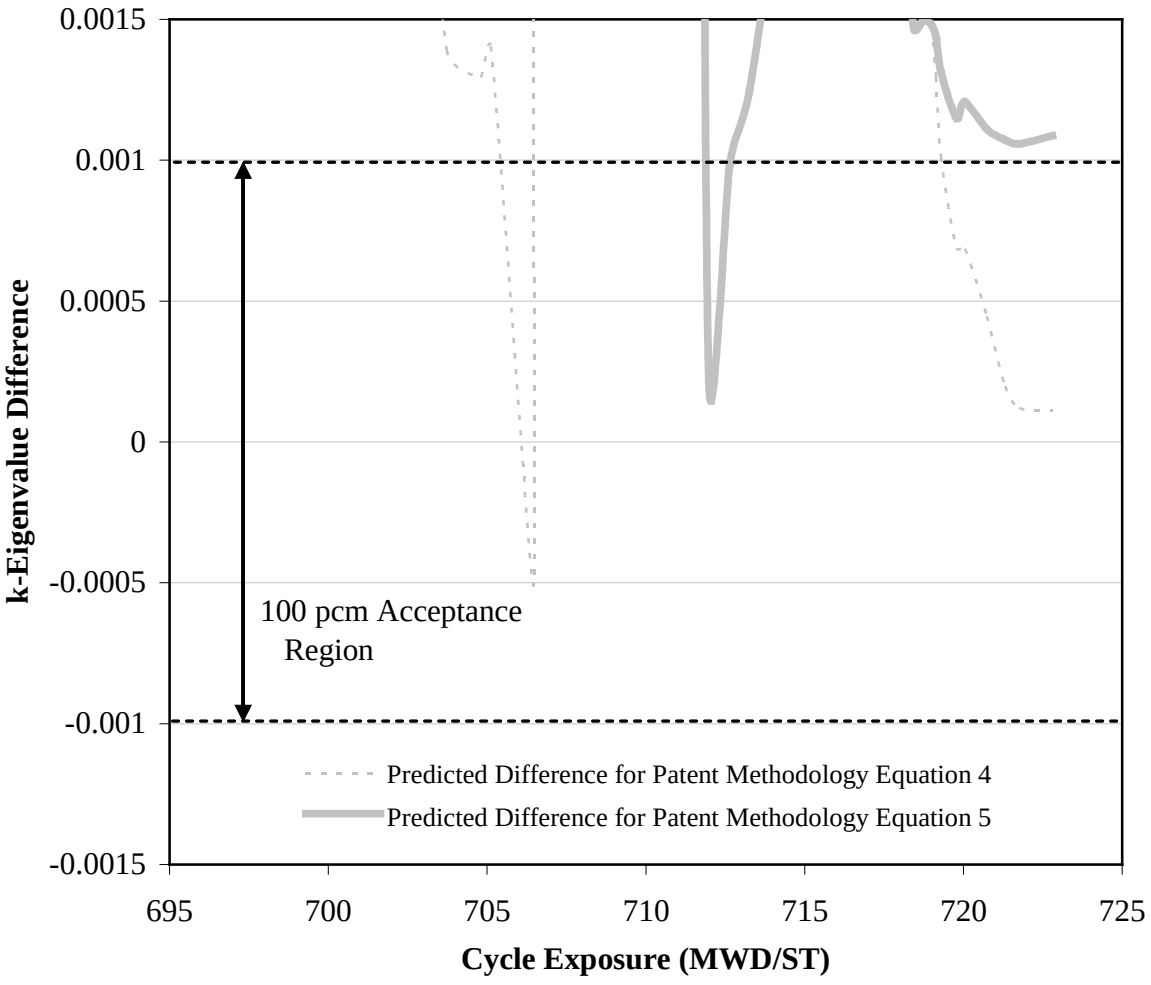

Figure 3-11. A zoomed-in view of the finale predictions obtained from the patent methodology equations applied to Plant C in-cycle startup event number 1, with the least applicable prediction omitted and the least accurate predictions omitted

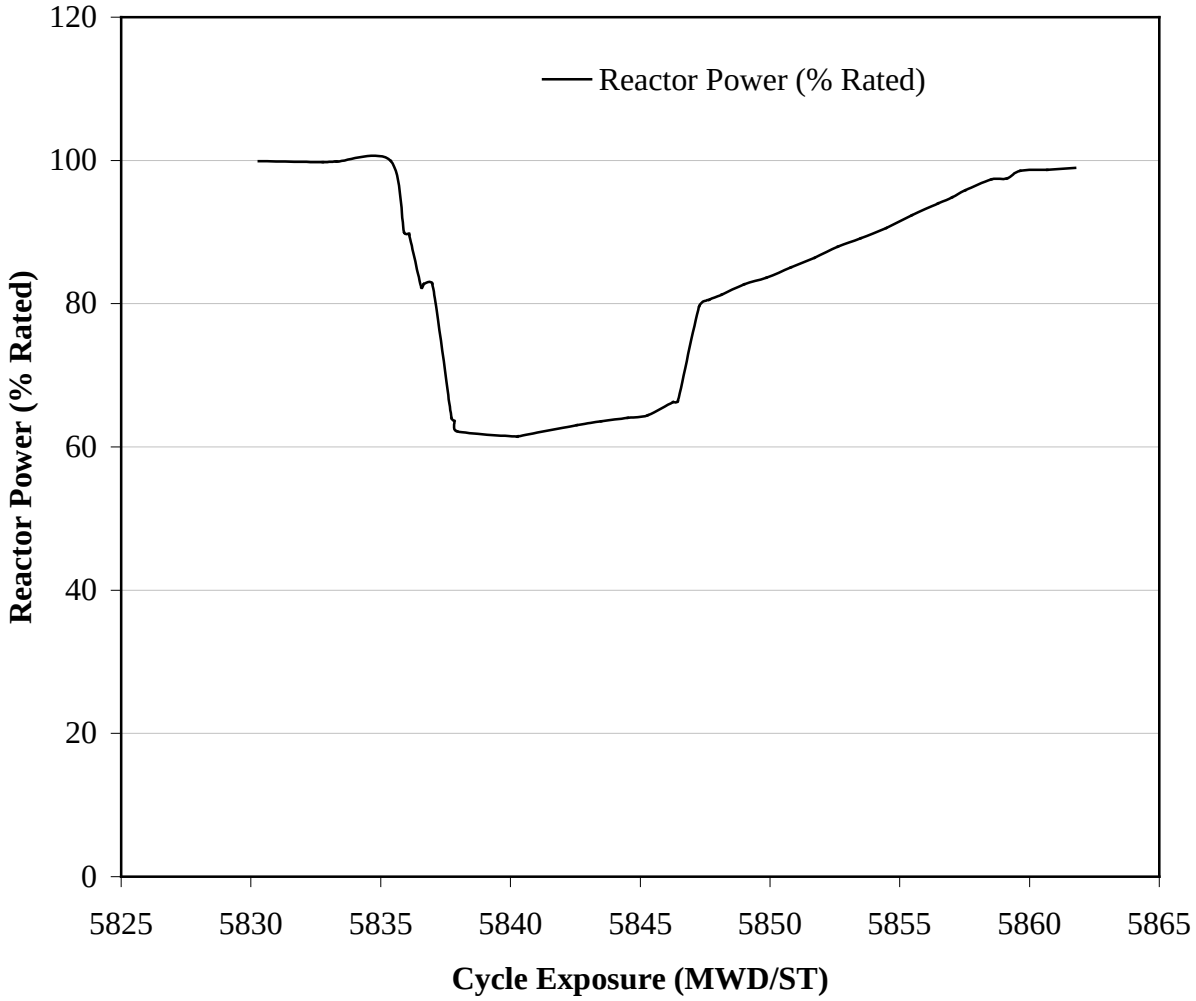

Figure 3-12. Power shape for Plant C power maneuver event number 1

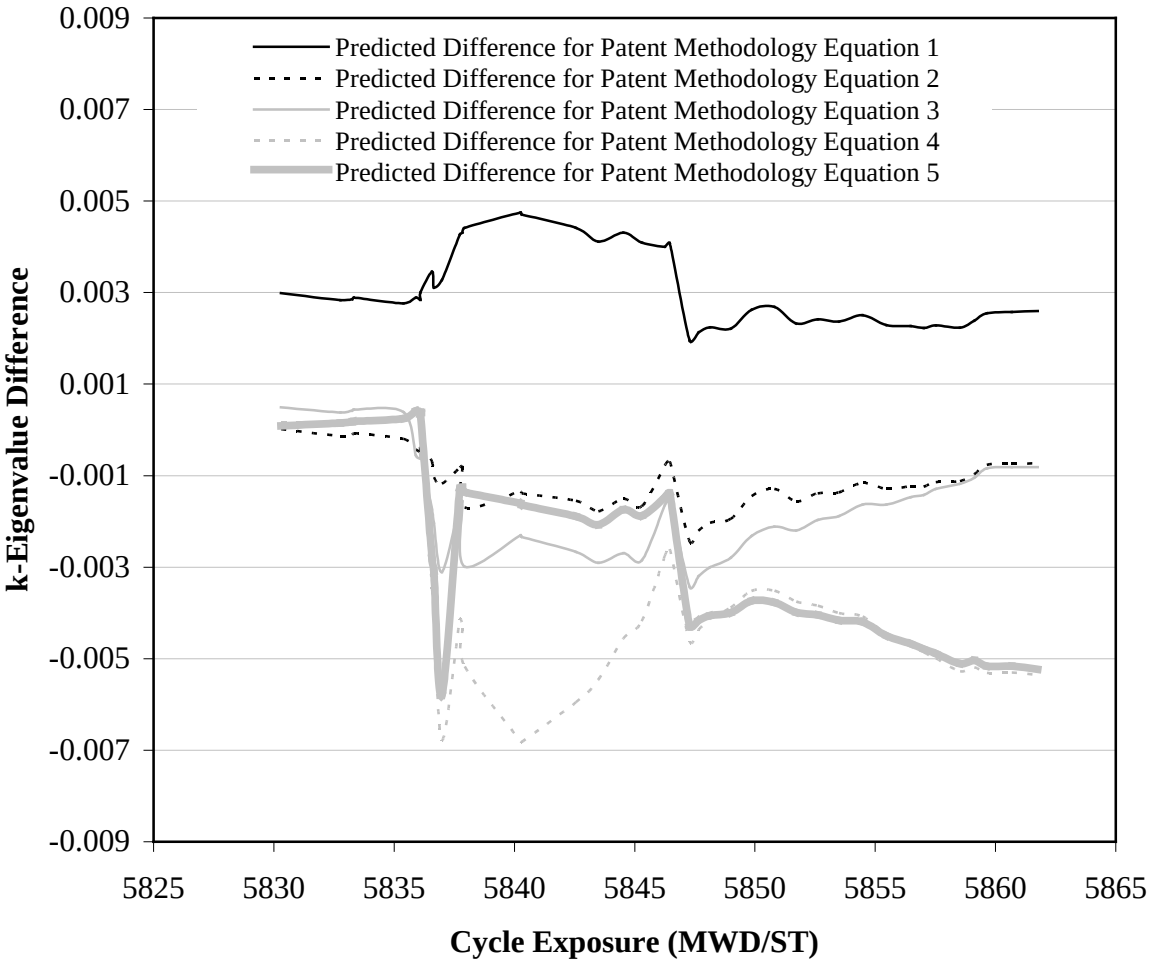

Figure 3-13. Patent methodology equations applied to Plant C power maneuver event number 1

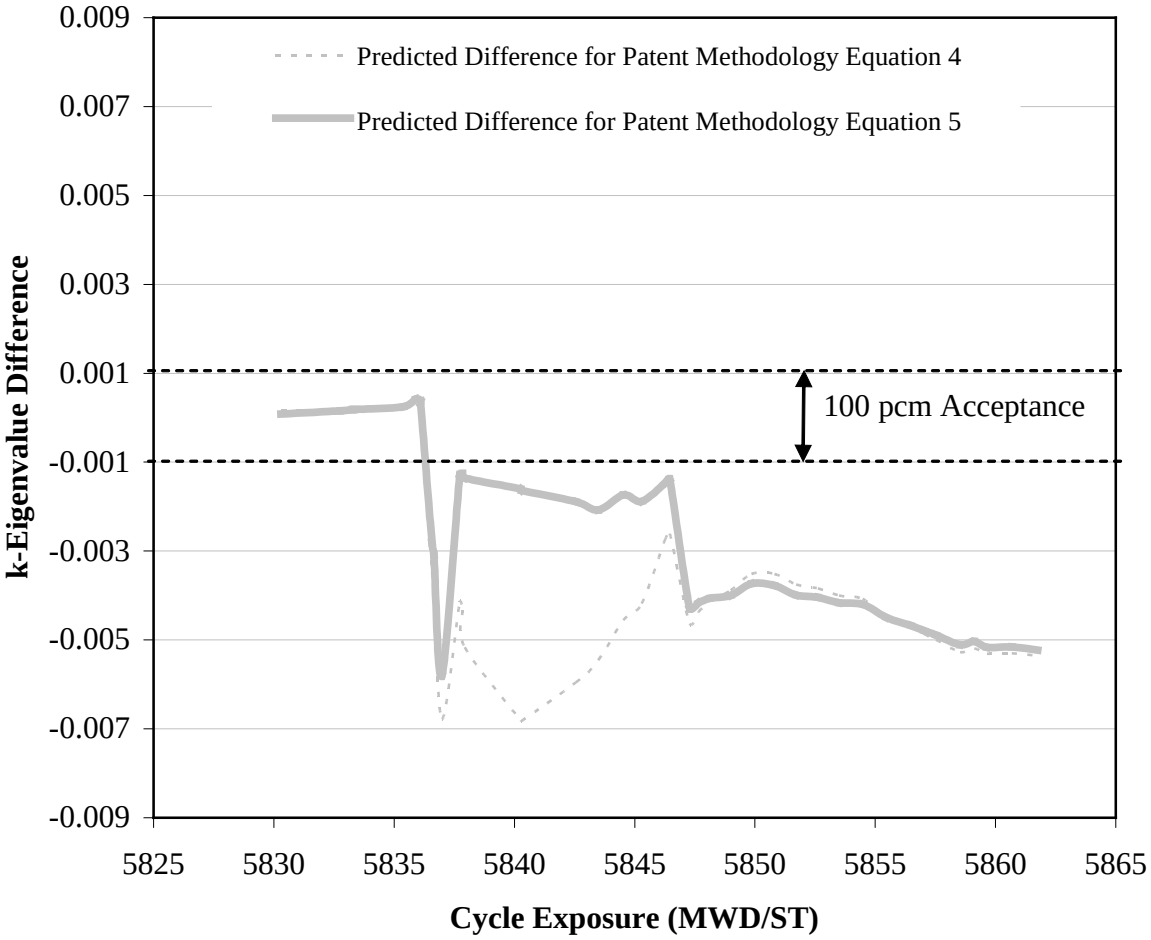

Figure 3-14. Patent methodology equations applied to Plant C power maneuver event number 1, with only the most applicable prediction equations shown

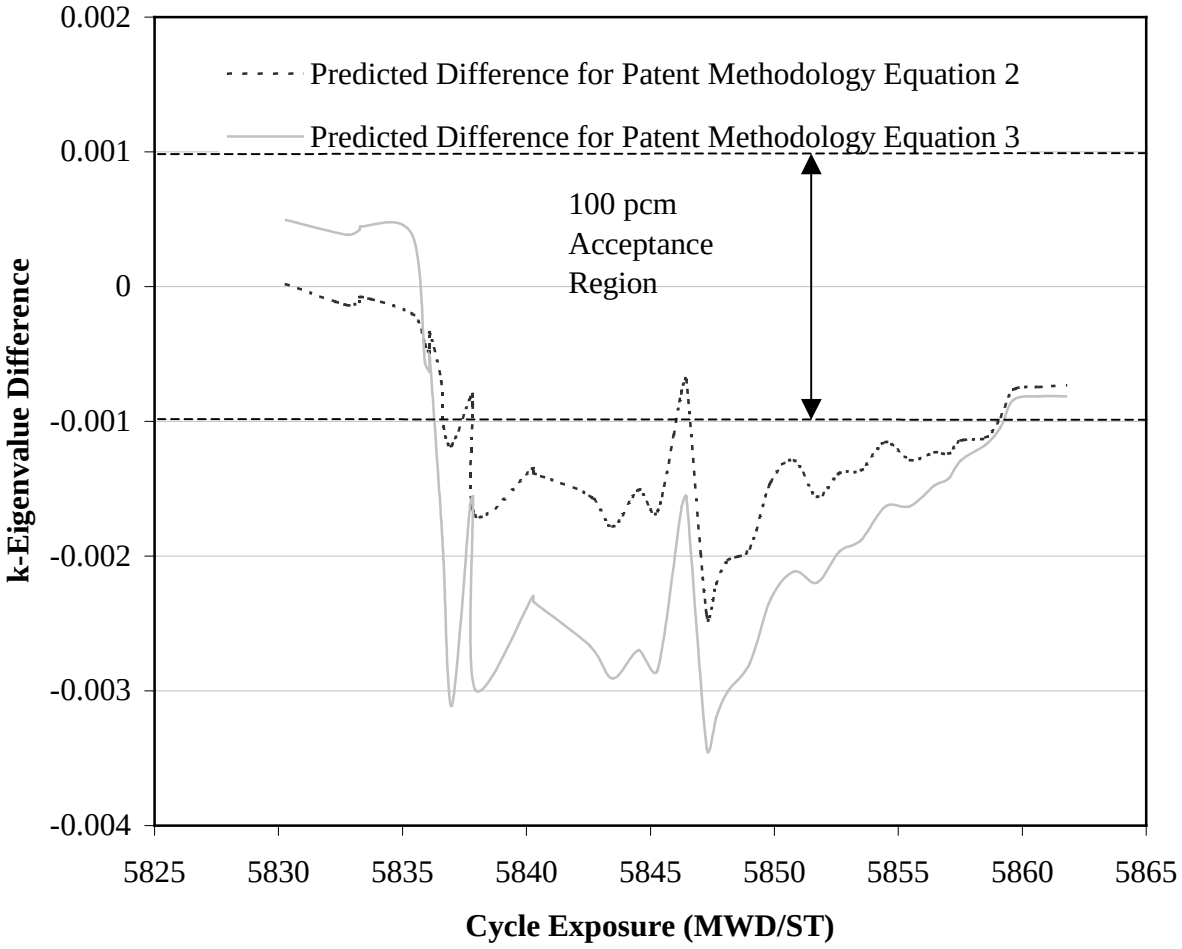

Figure 3-15. Patent methodology equations applied to Plant C power maneuver event number 1, with only the most accurate prediction equations shown

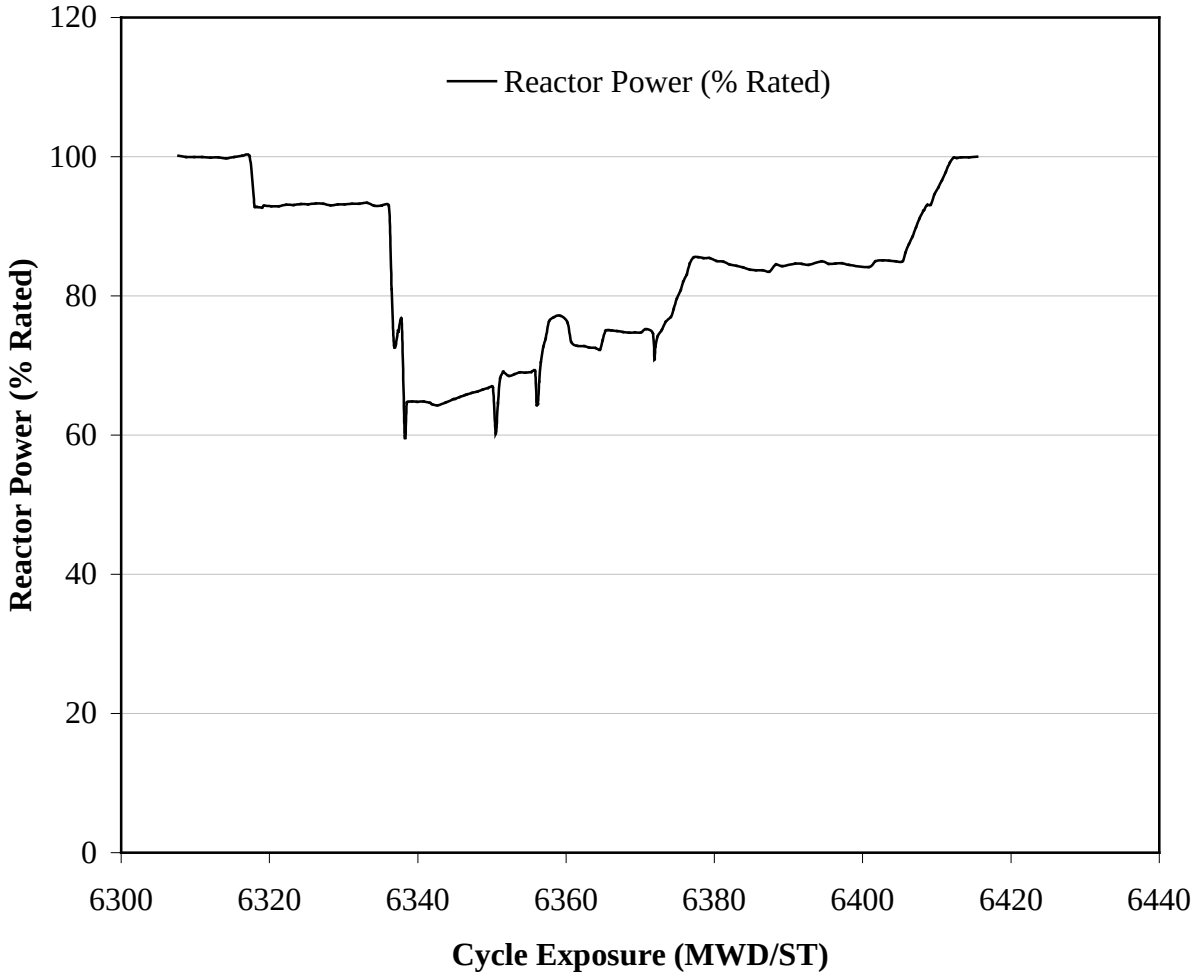

Figure 3-16. Power shape for Plant H power maneuver event number 1

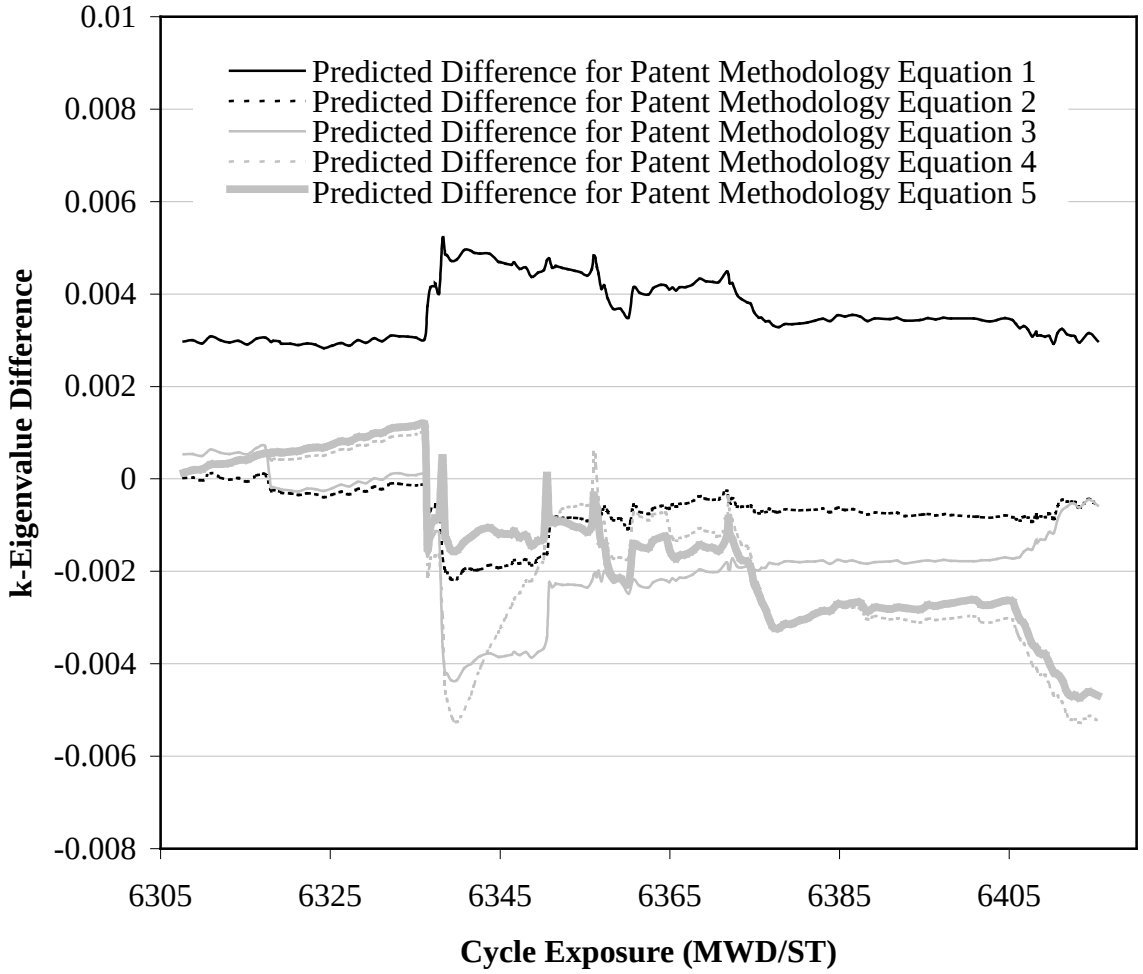

Figure 3-17. Patent methodology equations applied to Plant H power maneuver event number 1

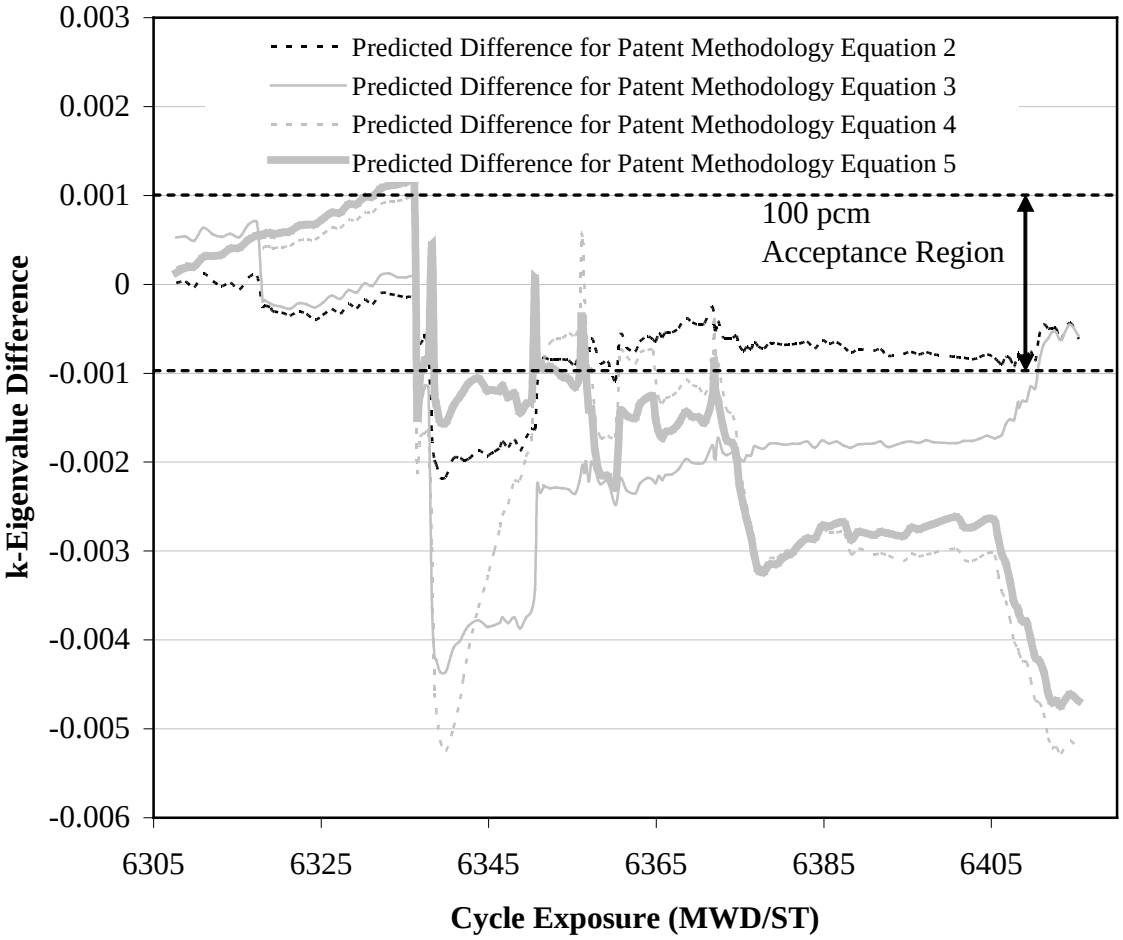

Figure 3-18. Patent methodology equations applied to Plant H power maneuver event number 1, with the least applicable prediction omitted

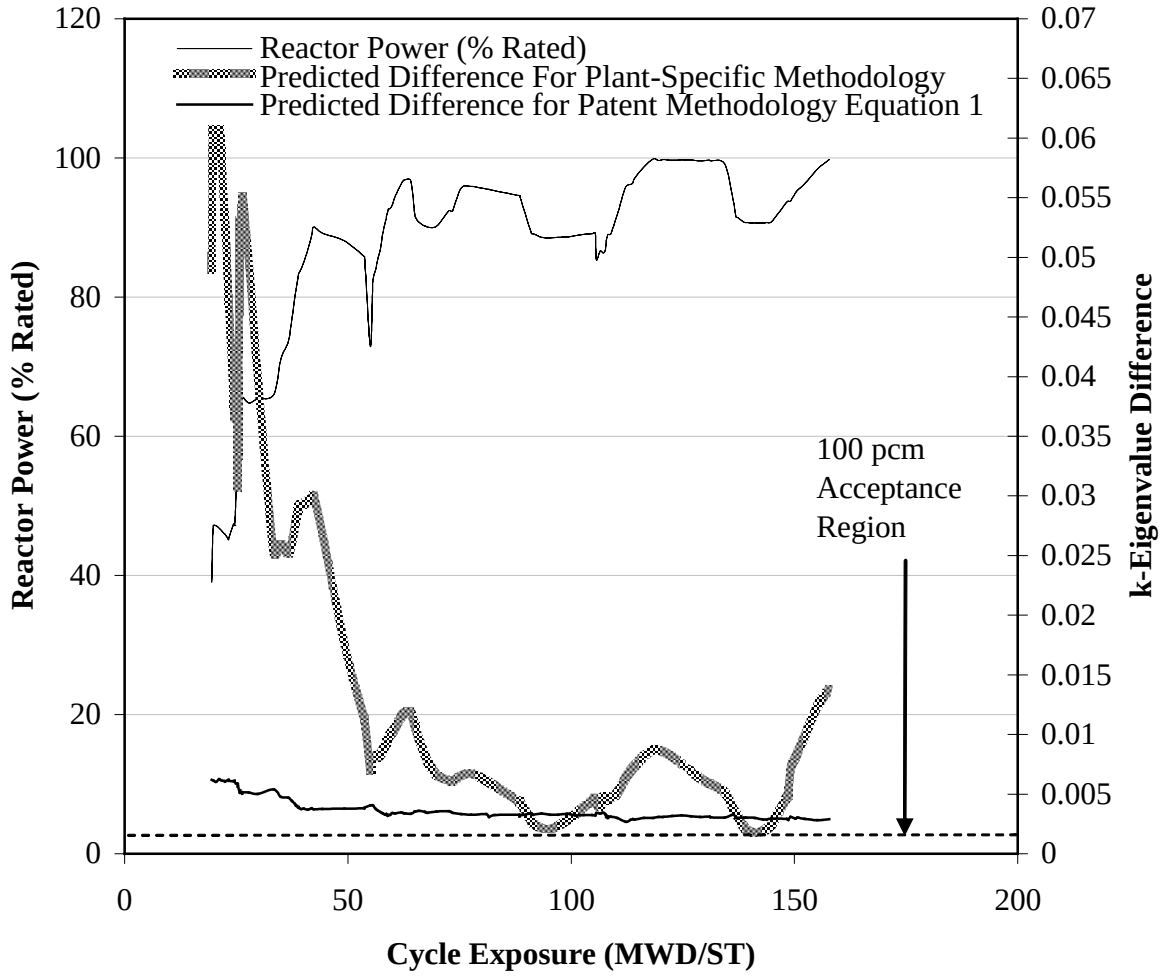

Figure 3-19. The plant-specific methodology startup equation and the most accurate and applicable patent methodology equation applied to Plant C startup event number 2, cycle C-2, and the associated power shape

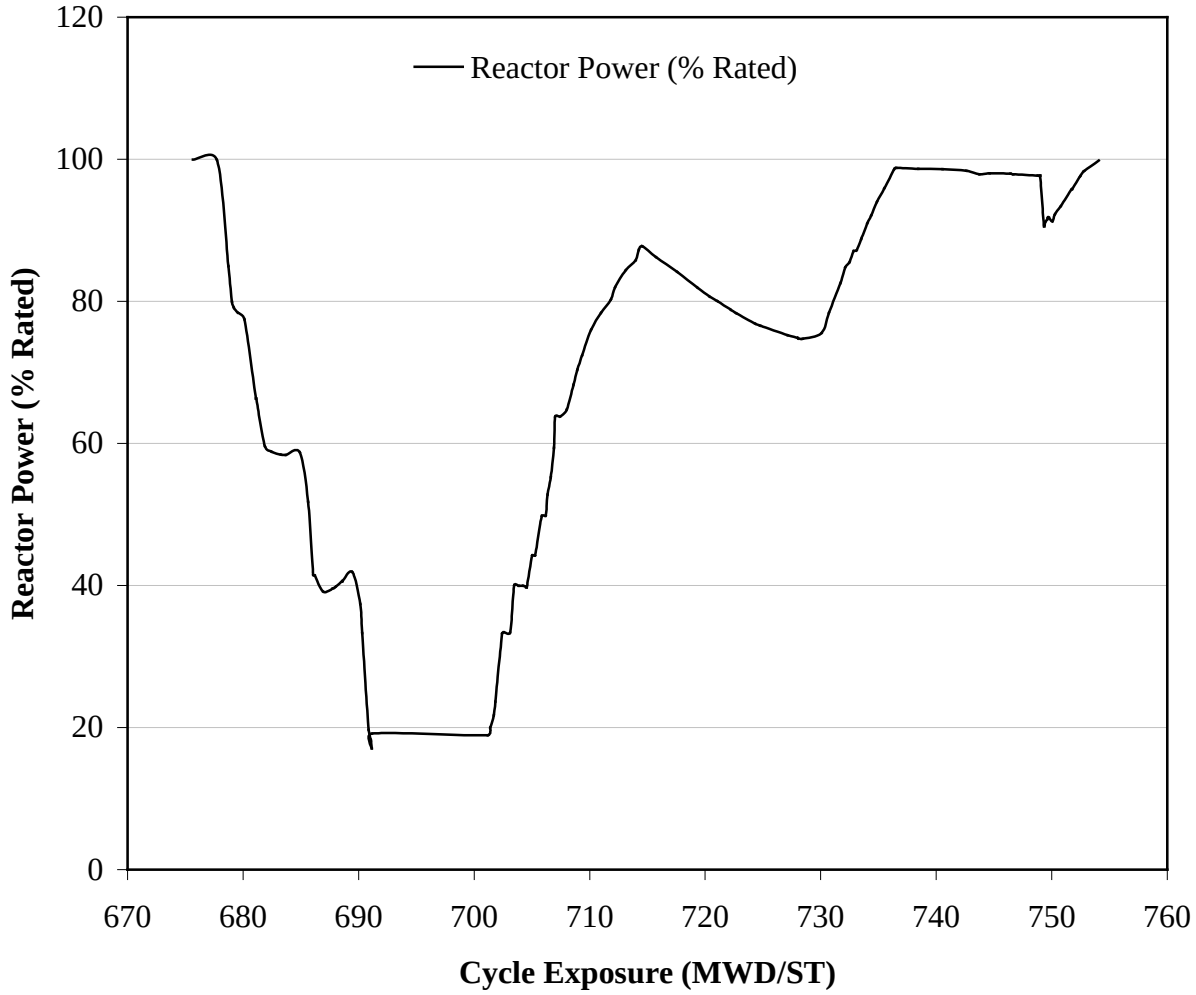

Figure 3-20. Power shape for Plant C in-cycle startup event number 2, cycle C-2

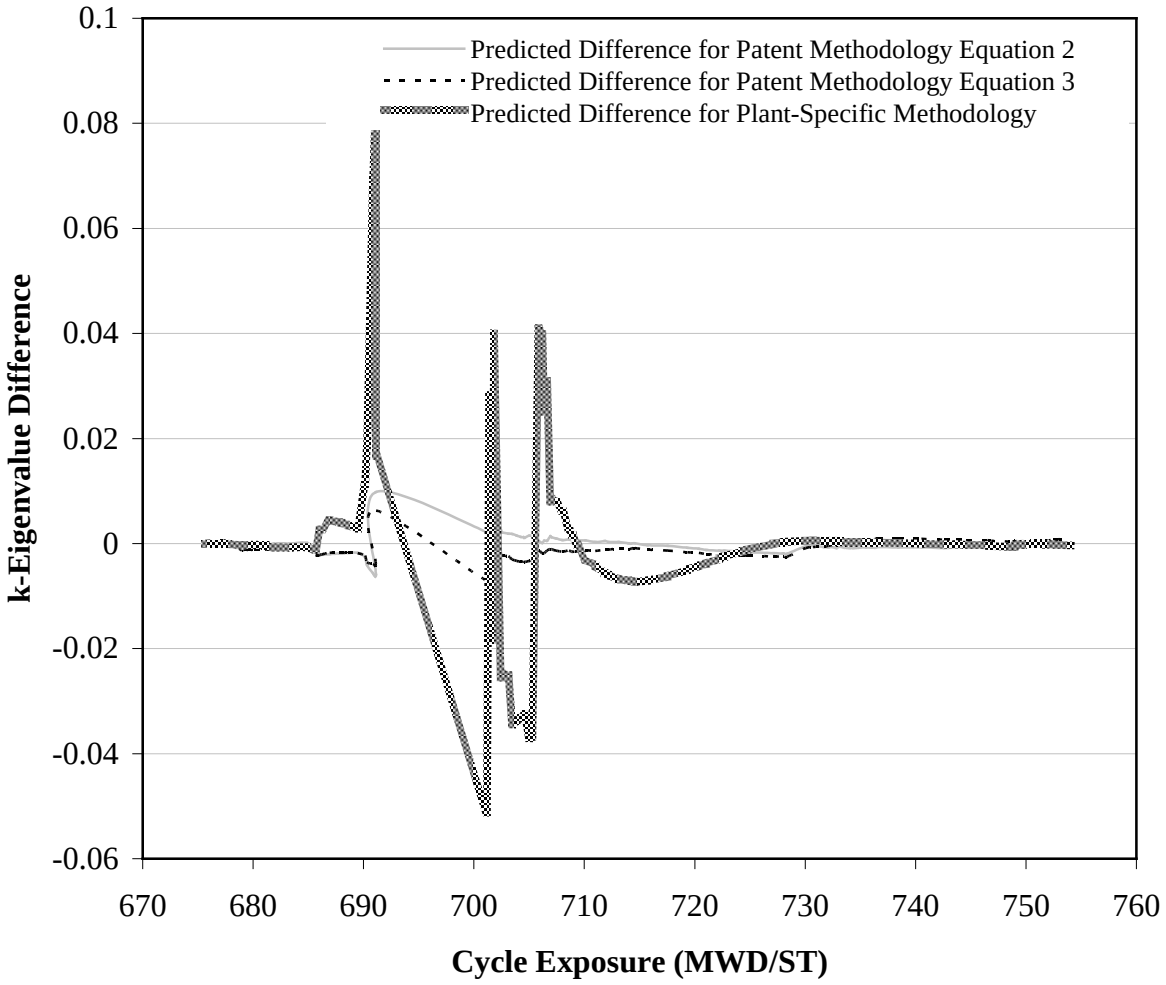

Figure 3-21. The plant-specific methodology normal power maneuver equation and the most applicable patent methodology equations applied to Plant C in-cycle startup event number 2

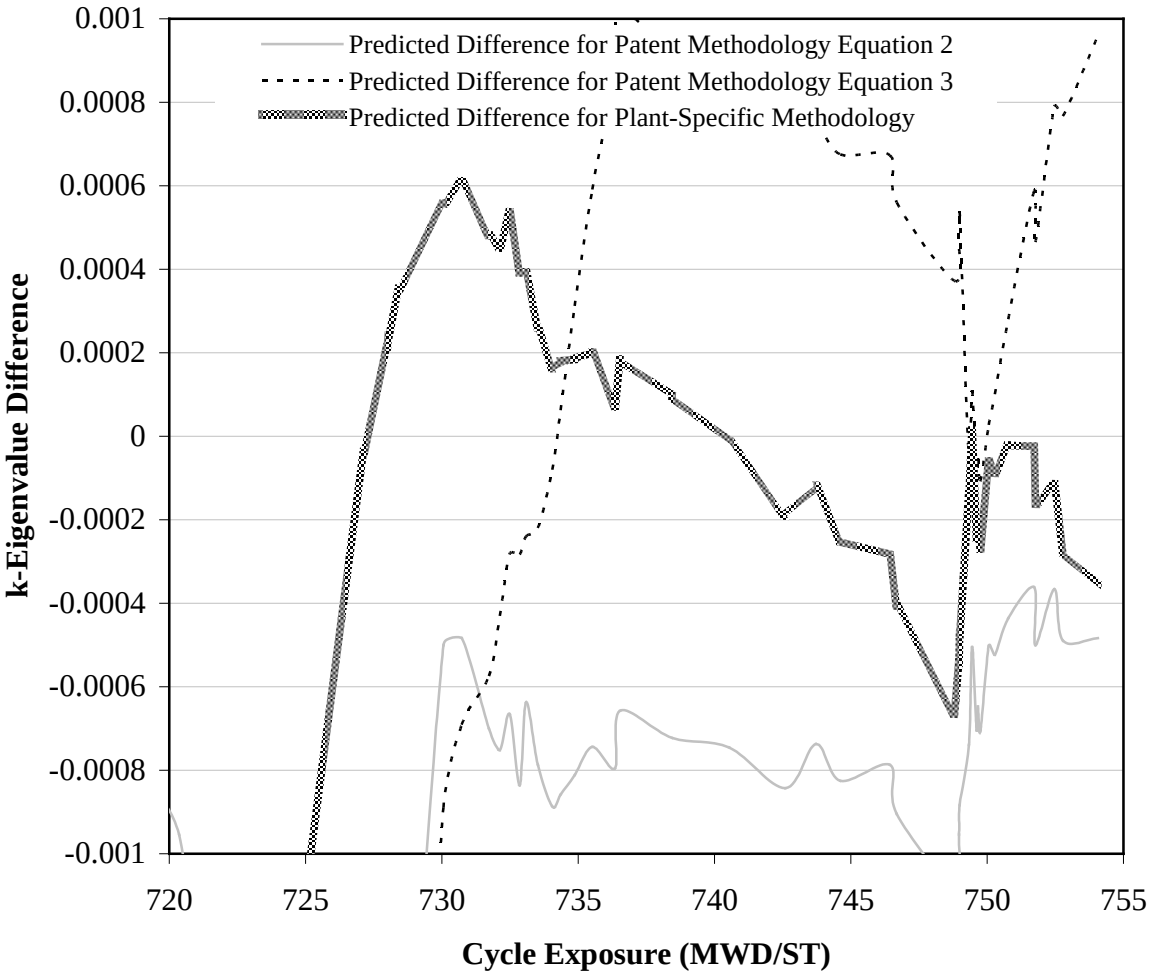

Figure 3-22. A zoomed-in view of the final predictions obtained from the plant-specific methodology normal power maneuver equation and the most applicable patent methodology equations applied to Plant C in-cycle startup event number 2

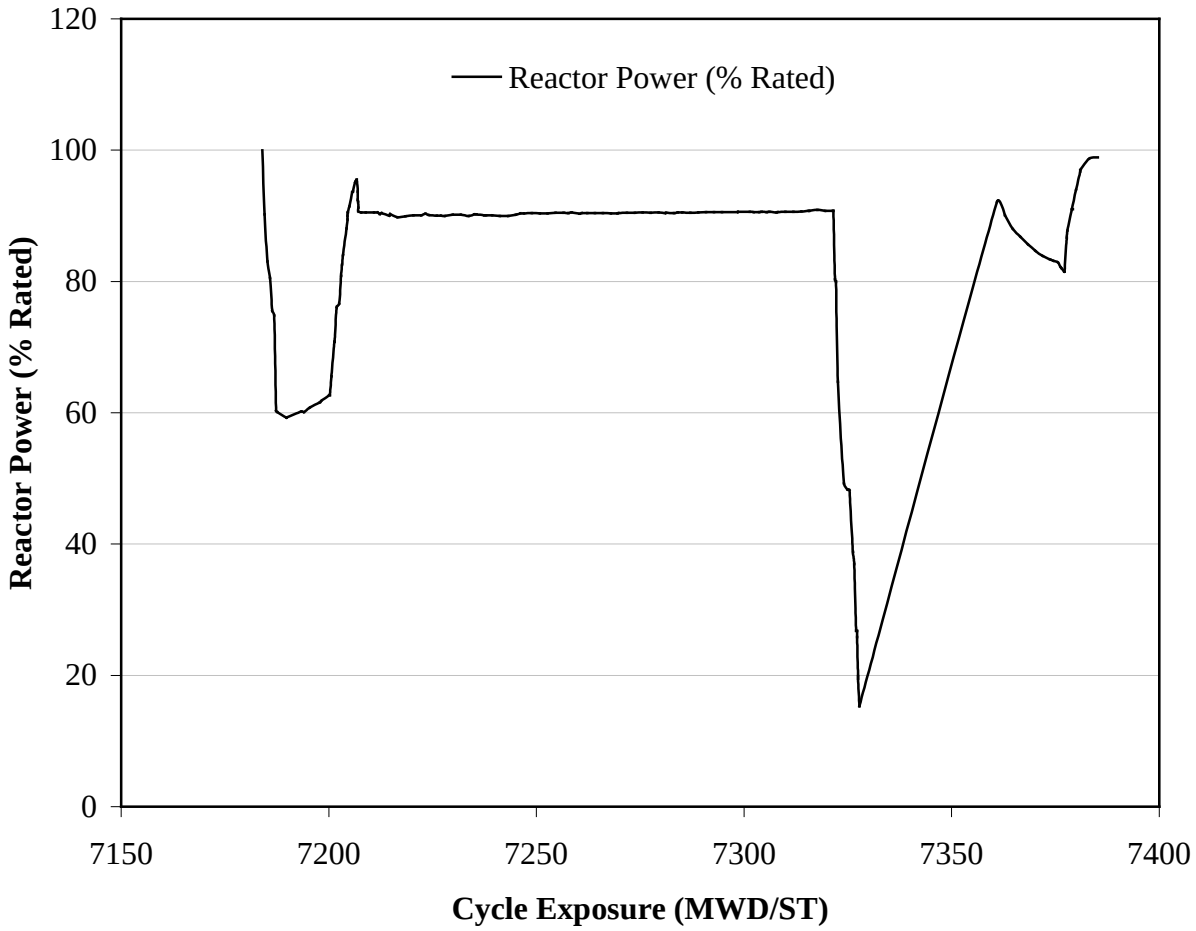

Figure 3-23. Power shape for Plant C in-cycle startup event number 3, cycle C-2

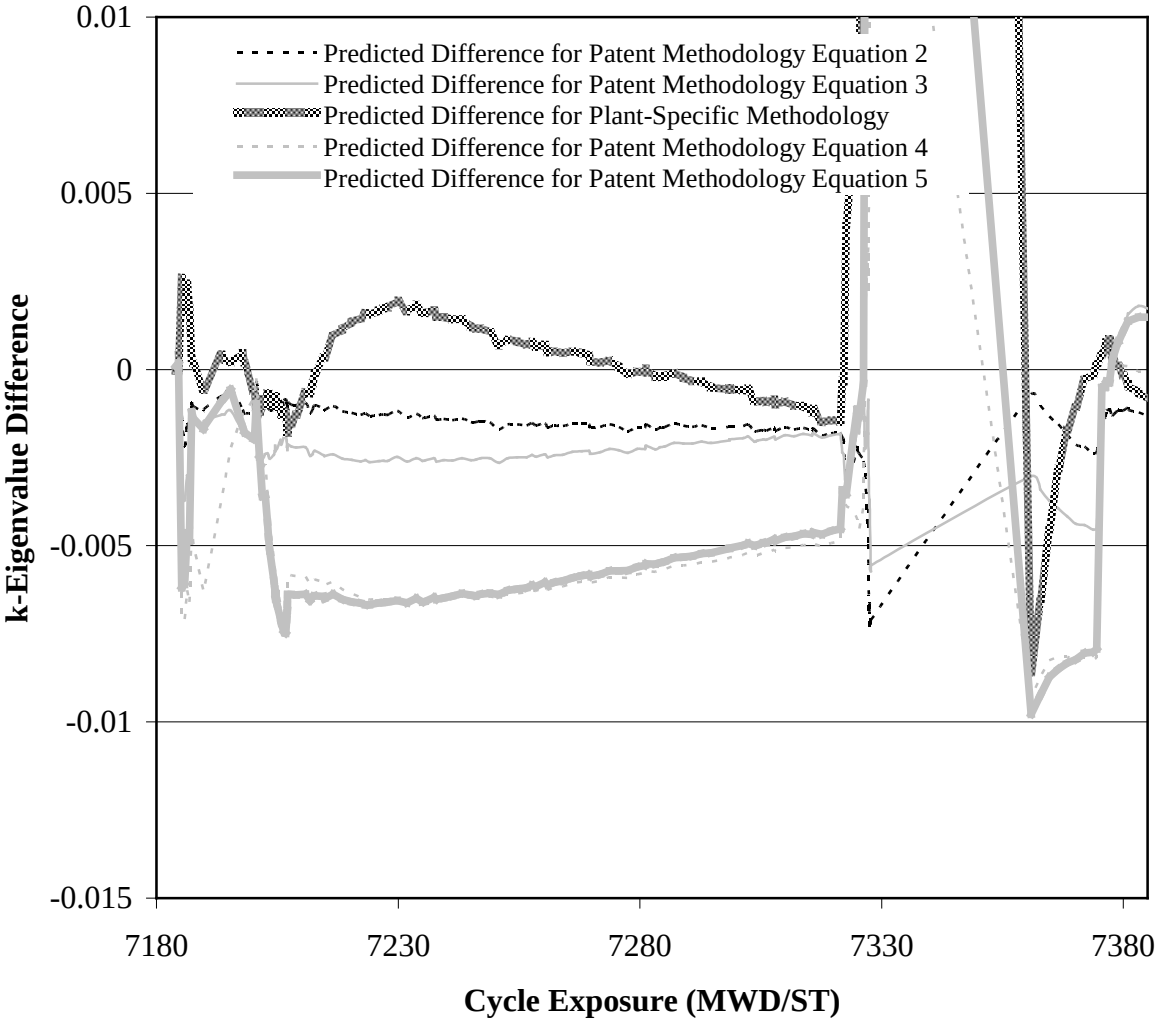

Figure 3-24. The plant-specific methodology normal power maneuver equation and the patent methodology equations applied to Plant C in-cycle startup event number 3, with the least applicable patent methodology equation omitted

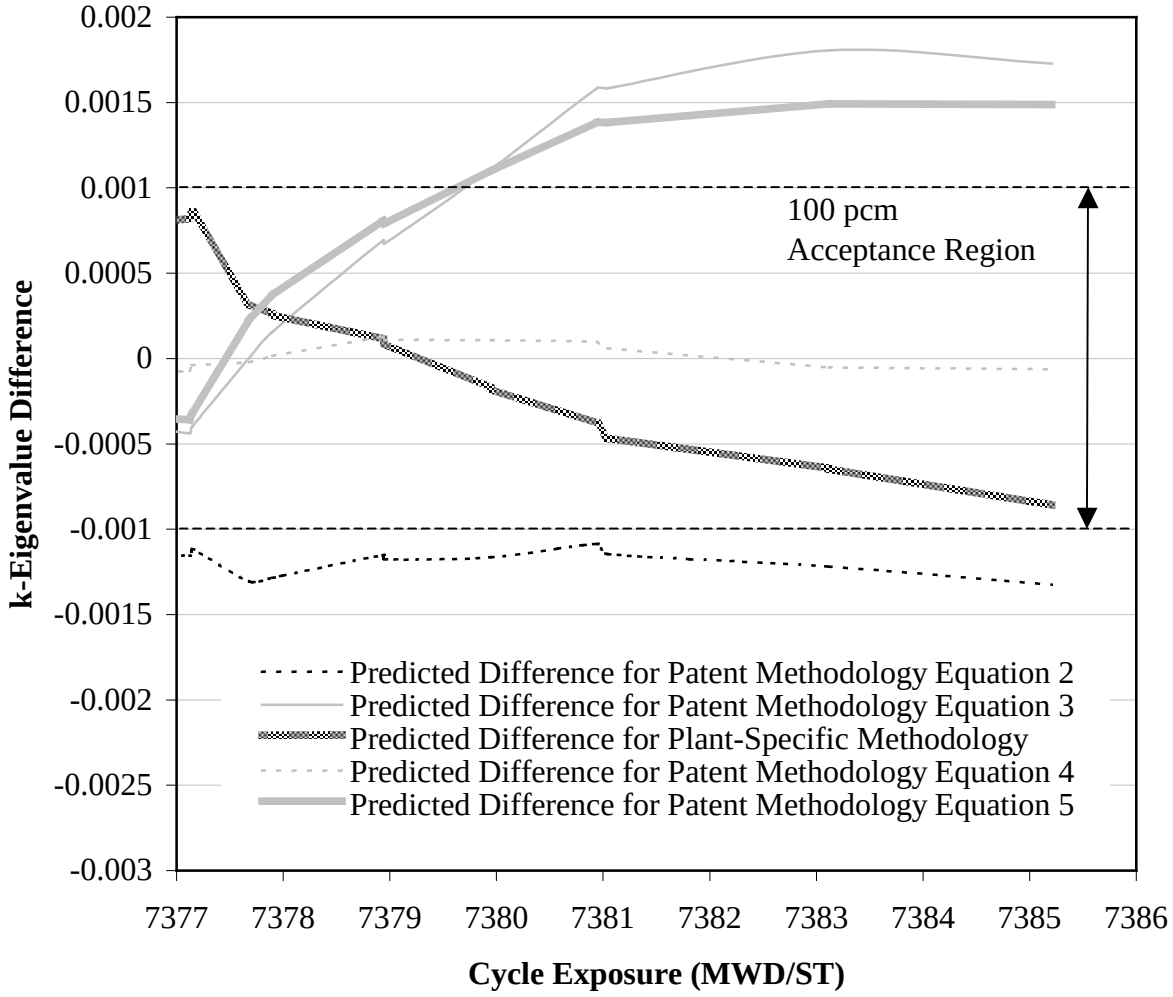

Figure 3-25. A zoomed-in view of the finale predictions obtained from the plant-specific methodology normal power maneuver equation and the patent methodology equations applied to Plant C in-cycle startup event number 3, with the least applicable patent methodology equation omitted

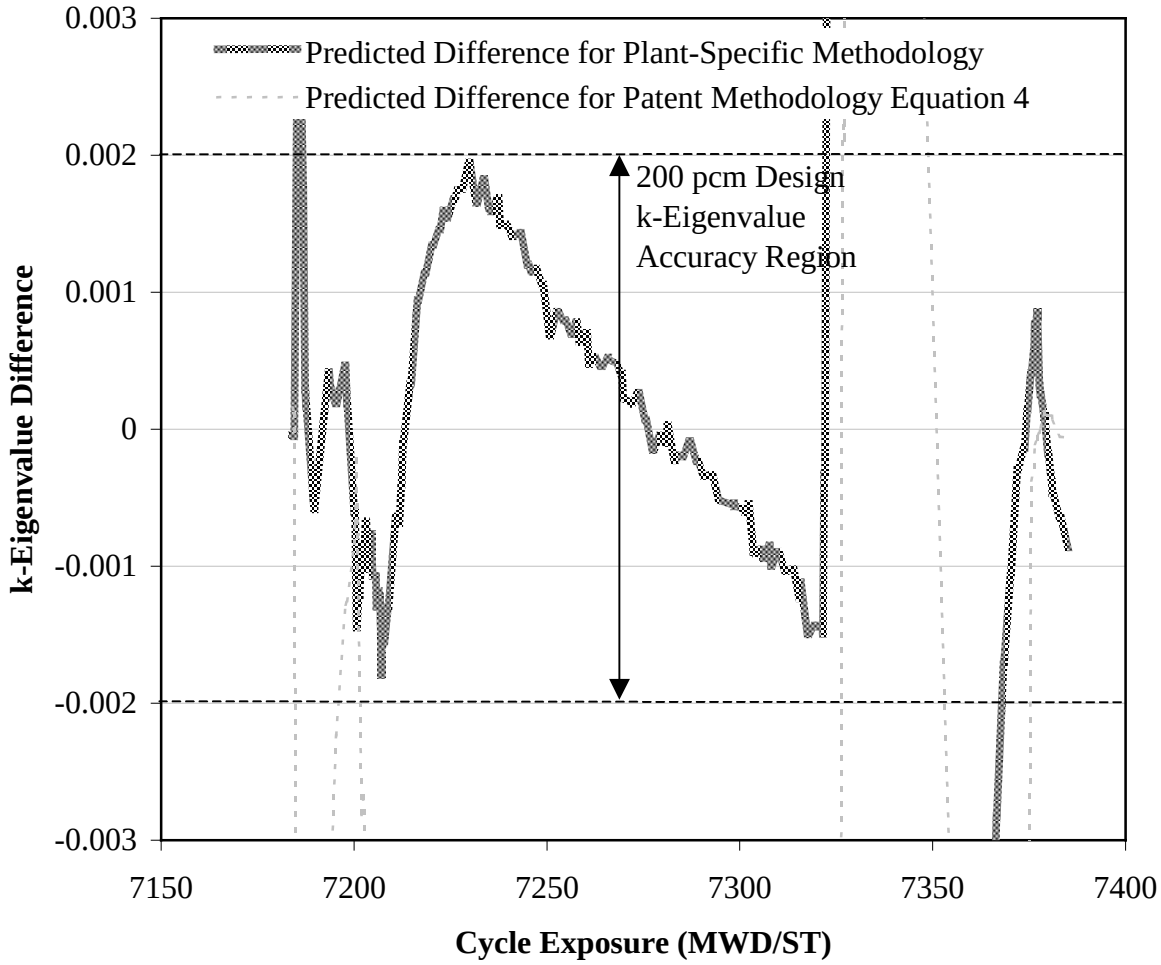

Figure 3-26. A comparison view of the fluctuations in predictions obtained from the plant-specific methodology normal power equation and the most accurate patent methodology equation applied to Plant C in-cycle startup event number 3

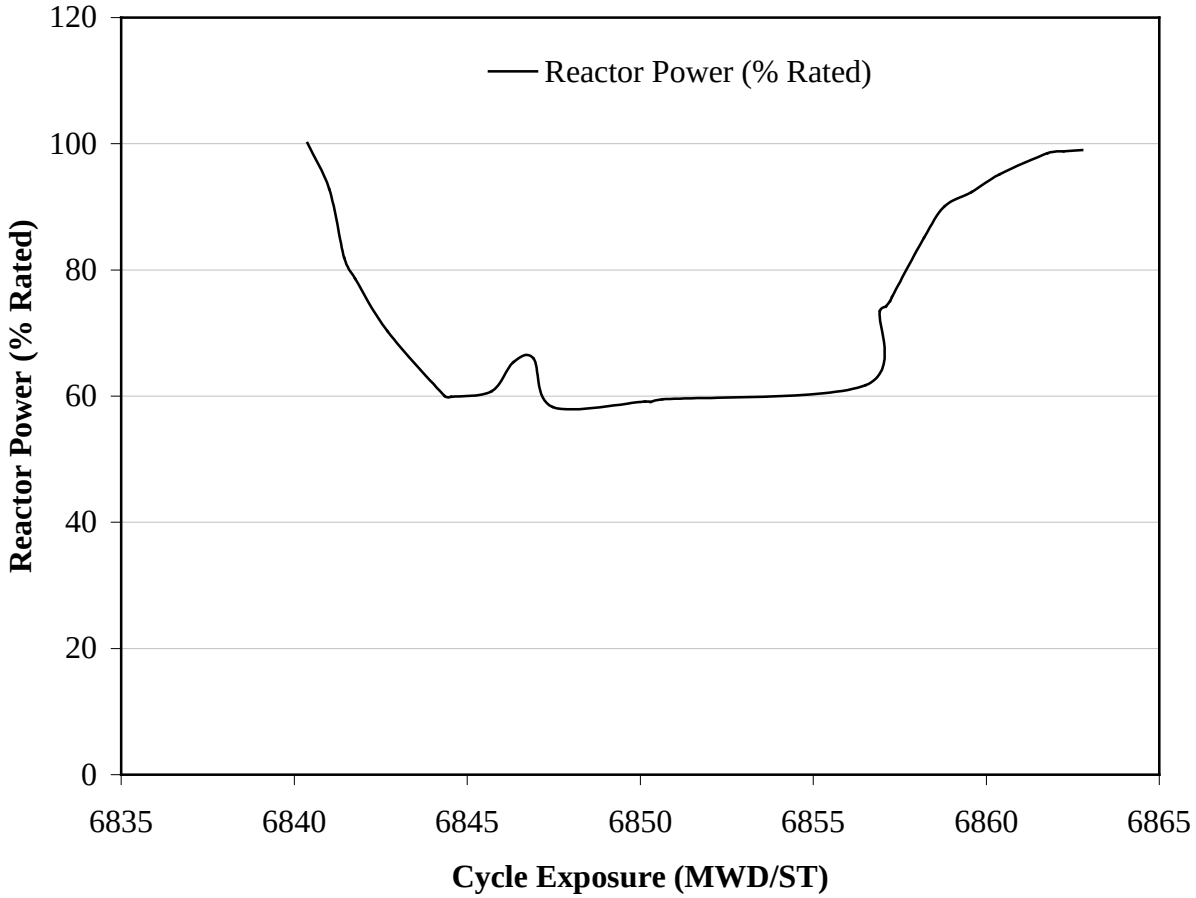

Figure 3-27. Power shape for Plant C power maneuver event number 2, cycle C-2

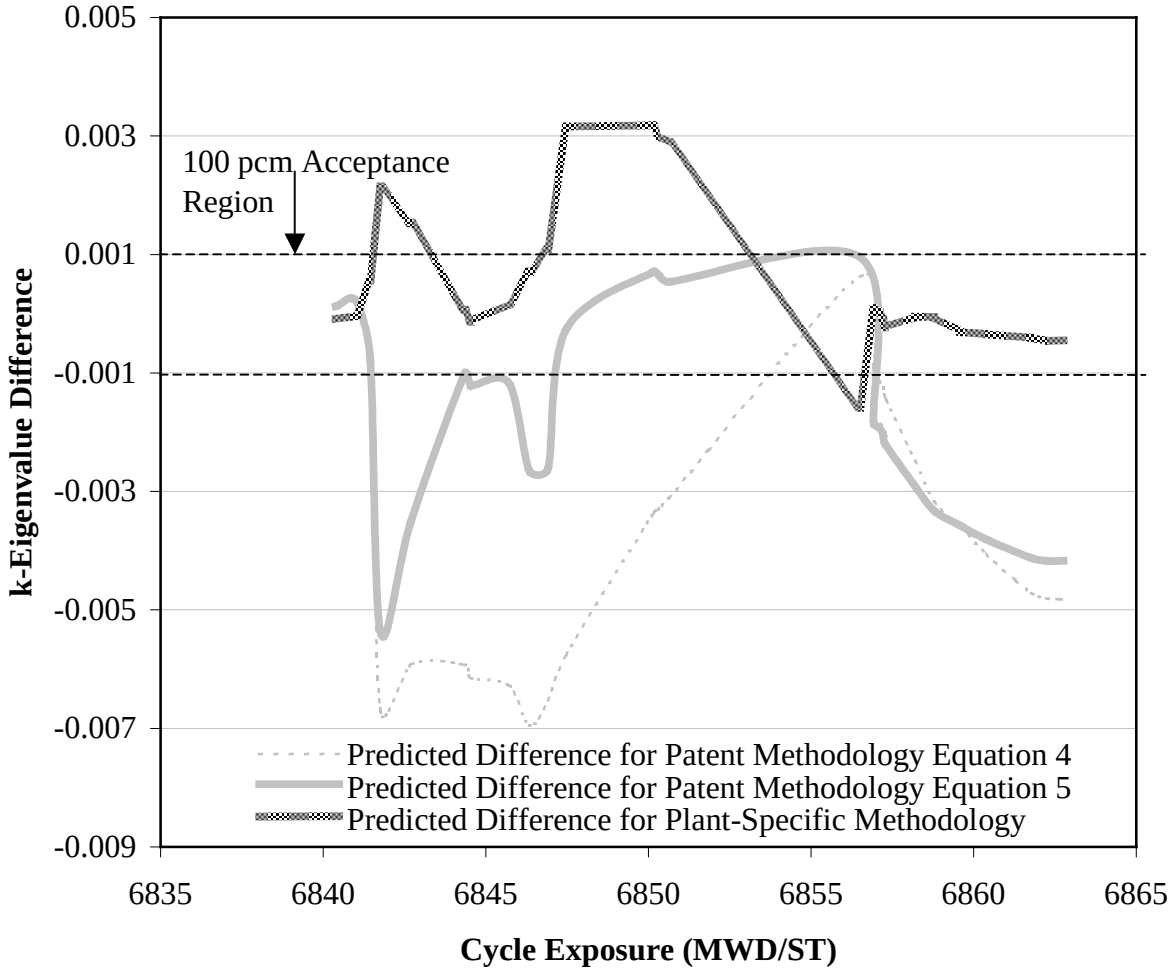

Figure 3-28. The plant-specific methodology normal power maneuver equation and the most applicable patent methodology equations applied to Plant C power maneuver event number 2

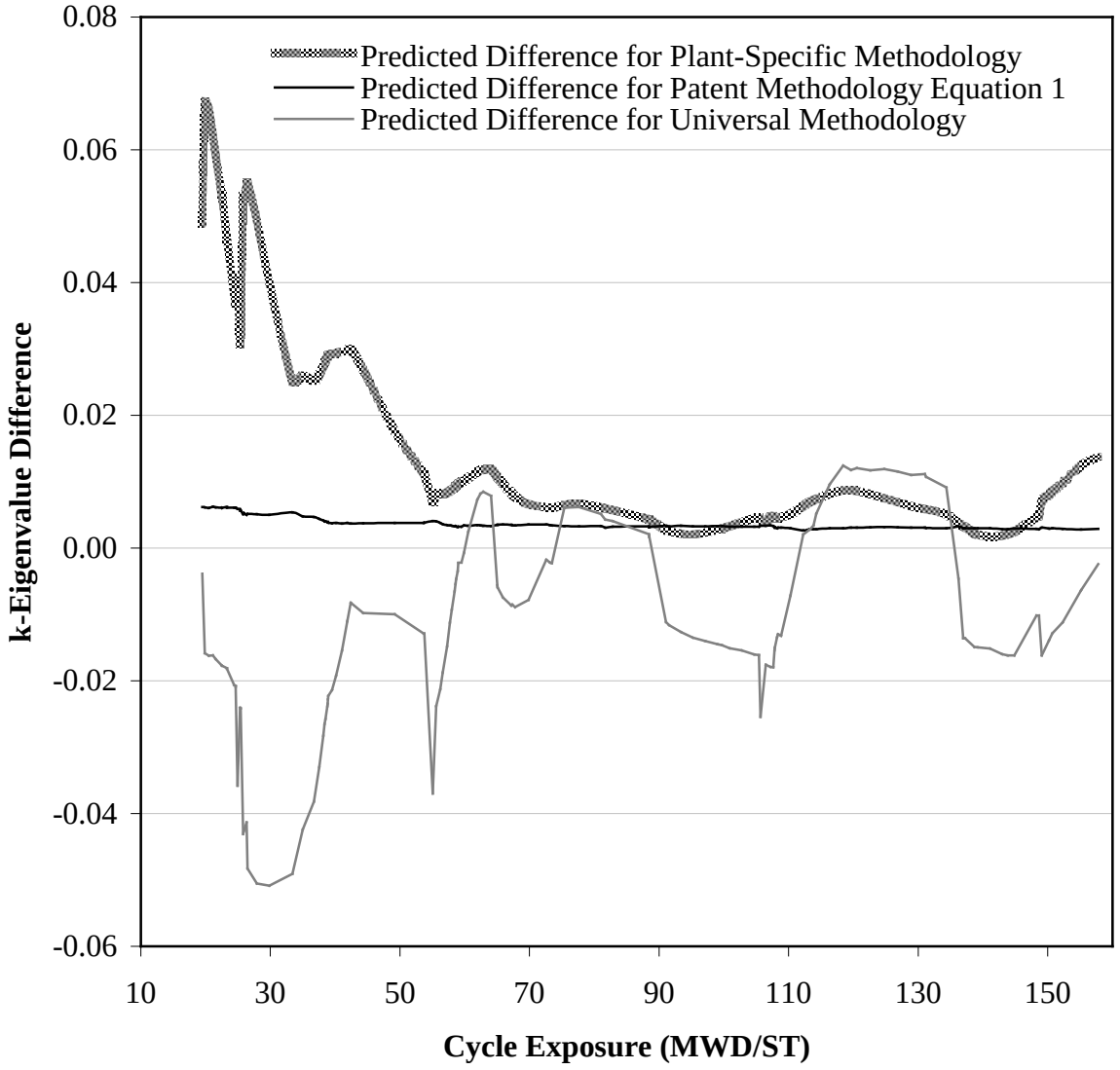

Figure 3-29. The universal methodology startup, the plant-specific methodology startup, and the most accurate and applicable patent methodology equations applied to Plant C startup event number 2

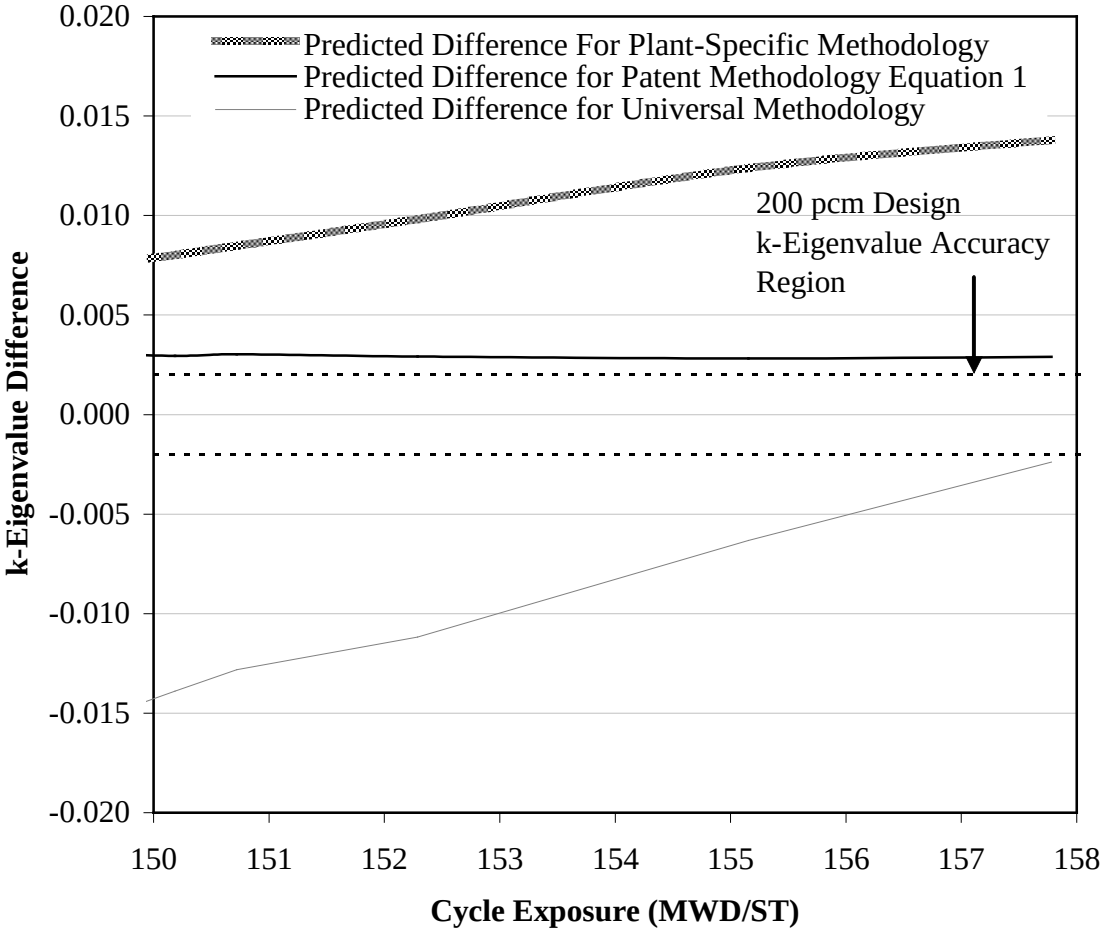

Figure 3-30. A zoomed-in view of the finale predictions obtained from the universal methodology startup, the plant-specific methodology startup, and the most accurate and applicable patent methodology equations applied to Plant C startup event number 2

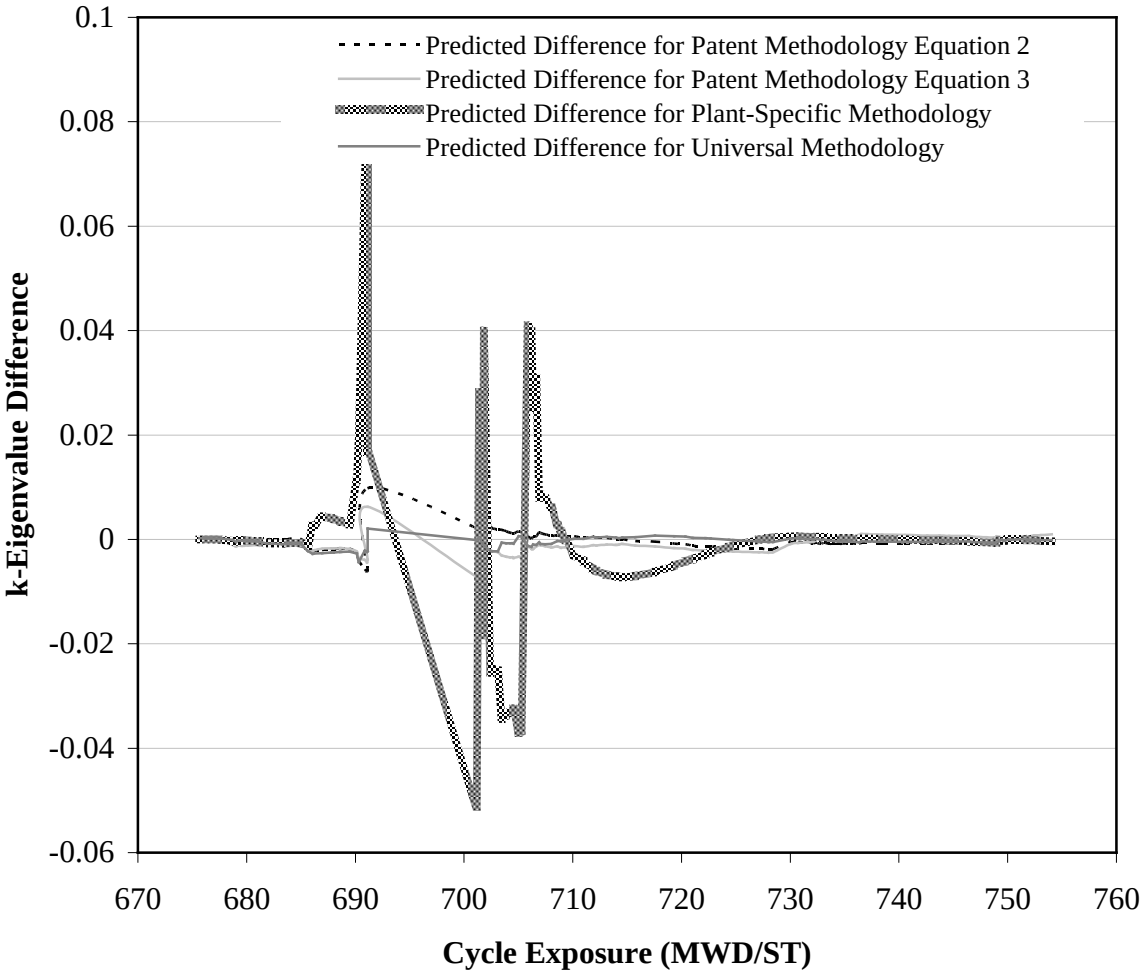

Figure 3-31. The universal methodology normal power maneuver, the plant-specific methodology normal power maneuver, and the most accurate and applicable patent methodology equations applied to Plant C in-cycle startup event number 2

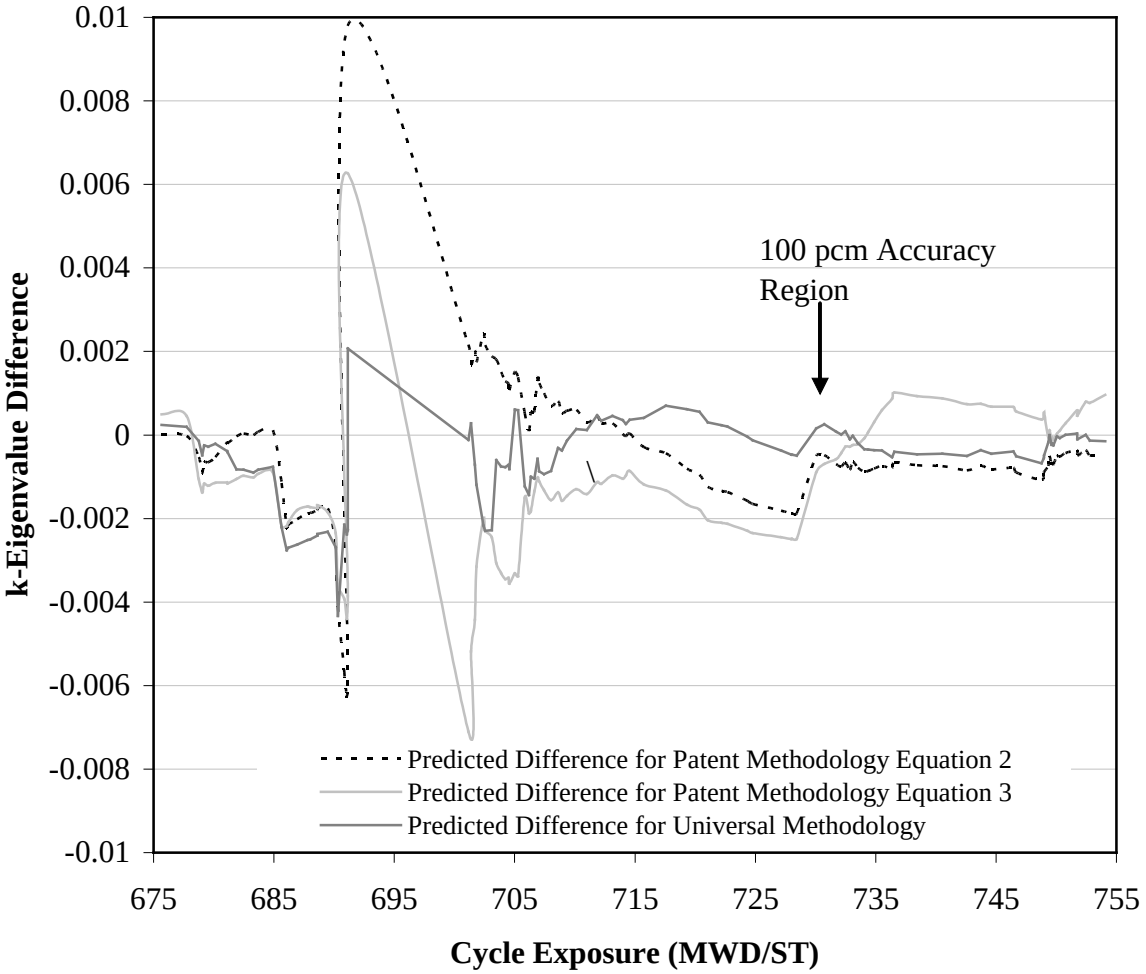

Figure 3-32. A comparison view of the fluctuations in predictions obtained from the universal methodology normal power maneuver equation and the most applicable patent methodology equations applied to Plant C in-cycle startup event number 2

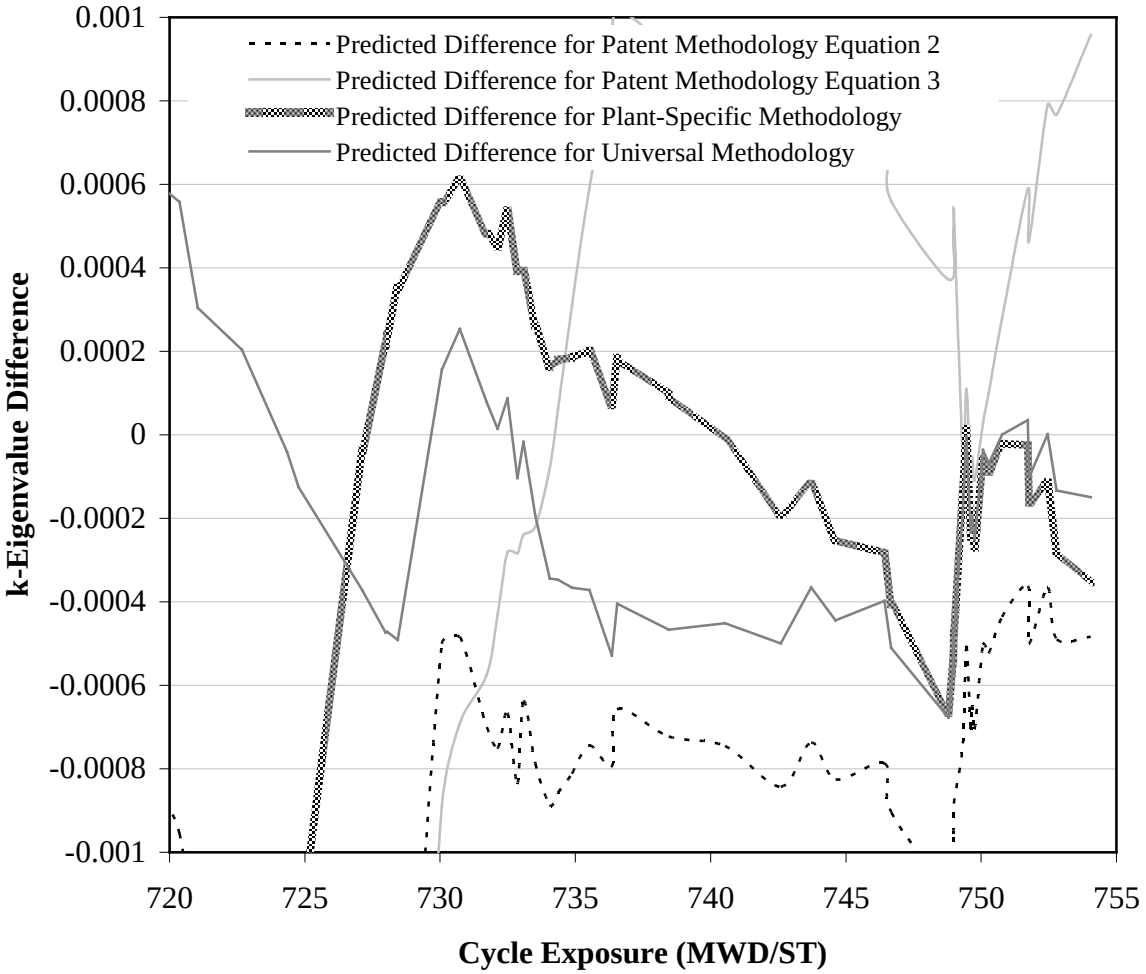

Figure 3-33. A zoomed-in view of the finale predictions obtained from the universal methodology normal power maneuver, the plant-specific methodology normal power maneuver, and the most accurate and applicable patent methodology equations applied to Plant C in-cycle startup event number 2

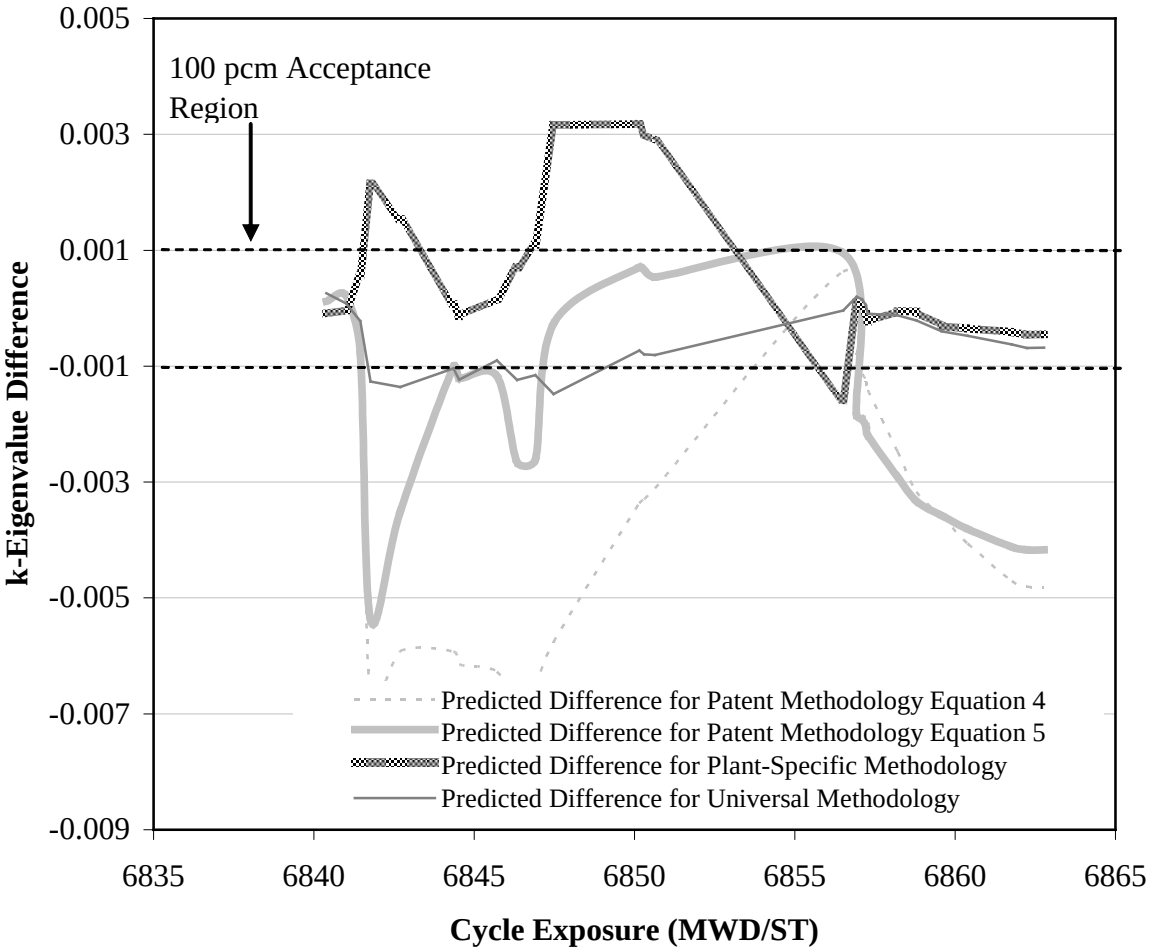

Figure 3-34. The universal methodology normal power maneuver, the plant-specific methodology normal power maneuver, and the most accurate and applicable patent methodology equations applied to Plant C power maneuver event number 2

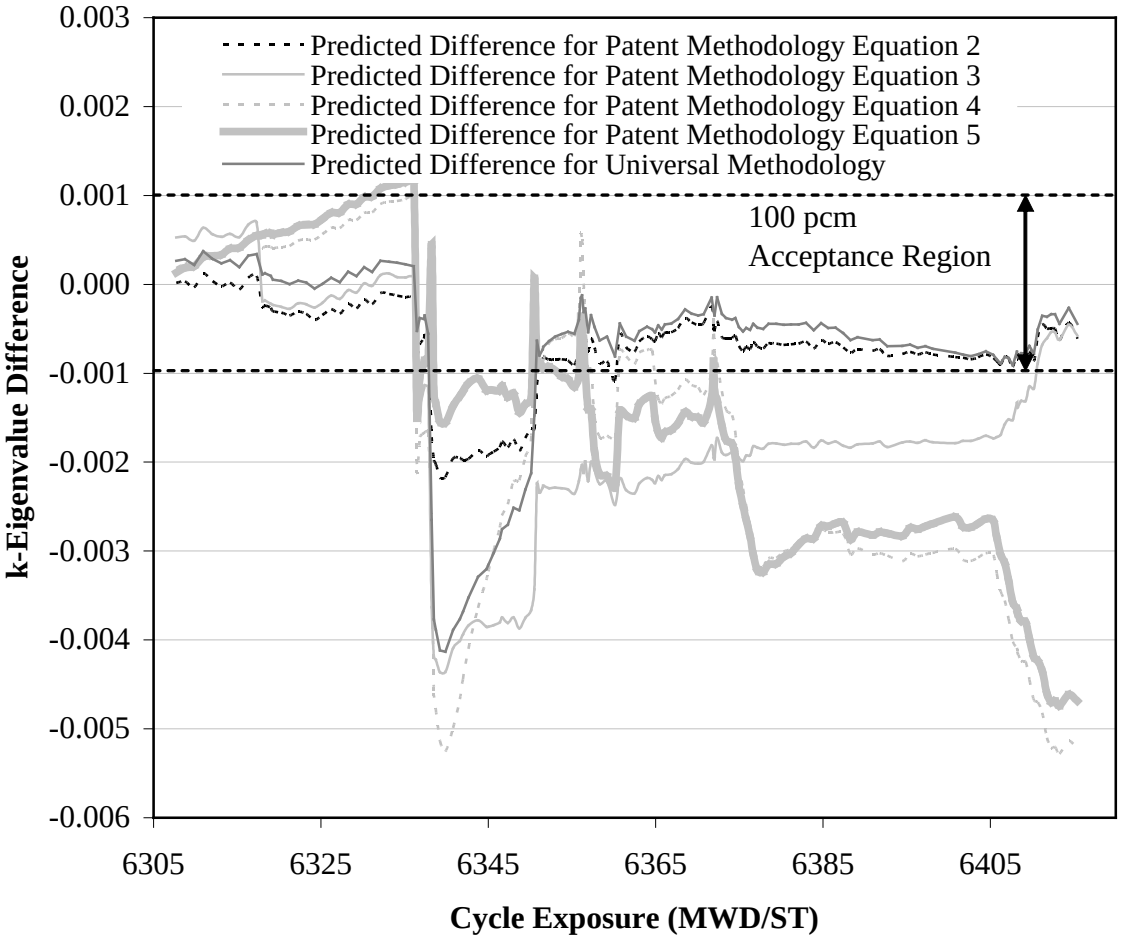

Figure 3-35. The universal methodology normal power maneuver equation and the most applicable patent methodology equations applied to Plant H power maneuver event number 1

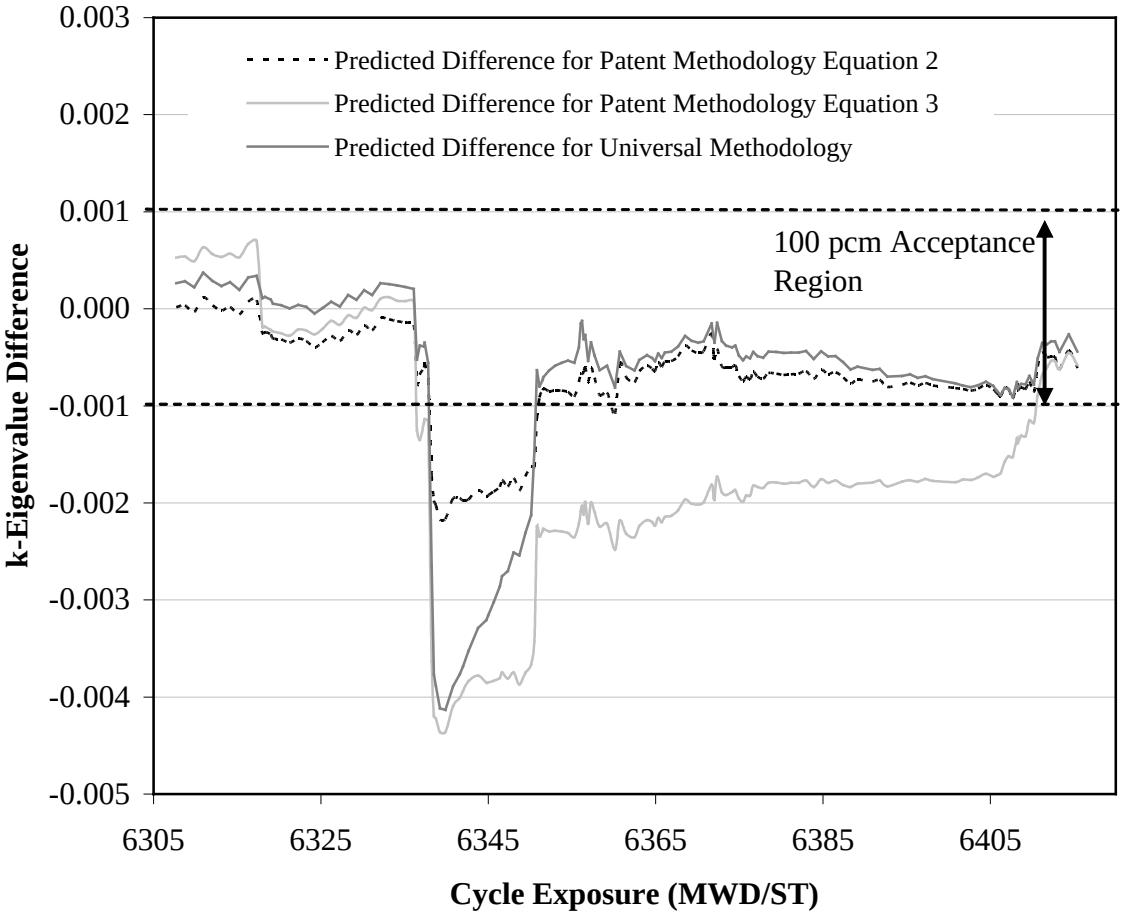

Figure 3-36. The universal methodology normal power maneuver equation and the most applicable patent methodology equations applied to Plant H power maneuver event number 1, with the least accurate patent methodology equations omitted.

CHAPTER 4
CONCLUSION

Over the course of this examination, the many different prediction methodology were applied to similar events in order to judge overall versatility and applicability. Generally, the patent methodology introduced too many opportunities for error as well as achieving some of the poorest results across the board. The plant-specific approach achieved significantly better results in many cases as compared to the patent methodology; however, it introduced difficulty in the fact that large amounts of data from each individual plant prior to the current cycle would be needed. Additionally, the work performed on one plant would have no meaning on another and the amount of analysis necessary would grow at an alarming rate as more and more plants request and require better predictions. On the other hand, the universal approach achieved some of the best results of all three methodologies while incorporating reduced opportunity for error versus the patent methodology and more versatility versus the plant-specific approach.

The inability to determine which prediction equation should be utilized prior to the commencement of a power event remains the major obstacle and stumbling point for the patent methodology approach. Even though certain equations would sometimes achieve accurate results, an engineer or operator utilizing the procedures outlined in Figure 2-2 would most often select the wrong equation. During the course of this analysis, it was found that startup equations might be more useful for certain regular power maneuvers and vice versa. The desire of the creators of the patent methodology to generate as simple a prediction equation as possible is the main reason why what is thought to be an applicable equation fails to function properly. Designers of the patent methodology removed certain regression coefficients and separated more robust and broad equations into multiple individual equations in order to reduce the complexity of each final prediction equation. The removal of coefficients reduced the goodness of fit and

statistical accuracy, while the desire to omit long, robust, and broad equations ensured the current difficulty in determining the applicable equation for a certain event. The one notable exception to the reduction in goodness of fit by desiring simpler equations would be the patent methodology BOC startup equation. When compared to the other BOC startup equations created for this analysis, the patent methodology BOC startup equation does not achieve the desired level of accuracy, but is more regular and consistent in its trending. Further refinement of Equation 1 from the patent methodology could well result in accurate prediction of the desired events; however, its usage in its current form is in question. Overall, this analysis considers the patent methodology the first initial step in the right directions, but questions its applicability across the BWR fleet and structure.

The plant-specific approach represented the aim to solve the prediction issues for reactors locally versus on a global, or fleet-wide, scale as was the purpose of the patent methodology and universal approach. The major impediment for determining the merits of the plant-specific approach stems from the proprietary information concerns that nuclear power plants have in releasing their plant data. The plant-specific approach stipulates that large amounts of past data for a single plant could be used to describe future behavior and the lack of a preponderance of such data challenges its usage. However, the investigation performed on Plant C indicates just how well such a plant-specific approach may function. Compared to the patent methodology, the results from the plant-specific approach are consistently more accurate with the notable exception of BOC startups. Again, the plant-specific approach fails in the area of BOC startups due to a lack of more of such events from previous cycles. The 100 pcm accuracy regime sought by this analysis seemed to be less of an issue for the plant-specific approach then for the patent methodology and it is hoped that that trend would continue in final implementation of a

prediction methodology. However, before the plant-specific approach could be utilized in a real world scenario, data from multiple cycles from multiple plants would be required in order to validate the methodology.

Of the three methods examined in this analysis, the universal approach achieved what should be considered the best possible results. While BWRs could be from different generations, or utilize different reactivity loading, the universal approach seems to indicate that enough similarities exist between the plants to approach the problem on a fleet-wide basis. The ability to apply a single equation to similar events from multiple reactors reduces variability across the fleet as well as reducing the workload for creating such a prediction when compared to the plant-specific approach. Unfortunately, BOC startups again were the major obstacle for the universal approach even though the universal methodology obtained better results for such an event than the two other methodologies. Most significantly, when compared to the other prediction regimes, the universal approach falls most consistently within the desired 100 pcm accuracy region and many times achieves accuracy on the order of 50 pcm in the final prediction value. The consistency of the universal approach ensures that implementation concerns would not arise from operators and engineers obtaining prediction values mid-event, rather than waiting for a return to rated power. On the other hand, this analysis only examined eight BWRs, while 3D MONICORE, the device for final implementation, supports over 30 BWRs across the world. Future usage of the universal methodology should incorporate more BWRs as sources of prediction data in order to ensure applicability across the fleet. However, even though the variability across all 30 BWRs has not been fully investigated, the universal approach seems to be the best method when compared to the other two analyzed herein.

Overall, more data is needed for BWRs across the world in order to best characterize which methodology best predicts off-rated power changes to the critical k-eigenvalue. Furthermore, the incorporation of more data should serve to improve the goodness of fit of a prediction equation generated by the universal approach while ensuring applicability to more varied and different BWRs. This analysis clearly indicates that the universal approach represents the best of the current means for predicting critical k-eigenvalue changes at off-rated power conditions for BWRs and it is hoped that final implementation and usage of any technique will incorporate aspects of and lessons learned from the universal approach investigation performed in this analysis.

LIST OF REFERENCES

3D MONICORE User's Manual. 2004. Global Nuclear Fuel.

BWR Power Plant Training. 1971. NEDO-10260, General Electric.

BWR/6 General Description of a Boiling Water Reactor. 1980. Proposal Engineering, Nuclear Power Systems Engineering Department, General Electric, San Jose, California.

Chopelas, A., Karv, A., Moore, B., Mouney, X., 2007. PANAC11A User's Manual. Global Nuclear Fuel.

Cochran, R., Tsoulfanidis, N., 1999. The Nuclear Fuel Cycle: Analysis and Management. 2nd Edition. American Nuclear Society. La Grange Park, Illinois.

Duderstadt, J., Hamilton, L., 1976. Nuclear Reactor Analysis. John Wiley & Sons, New York, New York.

ESBWR Plant General Description. 2006. General Electric, Wilmington, North Carolina.

Lahey, R., Moody, F., 1993. The Thermal Hydraulics of a Boiling Water Nuclear Reactor. American Nuclear Society. La Grange Park, Illinois.

Lamarsh, J., Baratta, A., 2001. Introduction to Nuclear Engineering. 3rd Edition. Prentice Hall, Upper Saddle River, New Jersey.

Lish, K. 1972. Nuclear Power Plant Systems and Equipment. Industrial Press Inc., New York, New York.

Longnecker, M., Ott, R., 2004. A First Course in Statistical Methods. Duxbury Press, Belmont, California.

Mertyurek, U., Kropaczek, D., Karve, A., Chopelas, A., 2008. Systems and Methods of Predicting a Critical Effective K for a Nuclear Reactor. Global Nuclear Fuels-America, LLC, assignee. Patent US 2008/0123794 A1.

Stacy, S., 2000. Proving the Principle: A History of the Idaho National Engineering and Enivornmental Laboratory. Idaho Operations Office of the Department of Energy, Idaho Falls, Idaho.

BIOGRAPHICAL SKETCH

Brett David Rampal was born in Florida and spent the majority of his young life in the state of Florida. Brett was active in mathematics-based clubs and the national honor society, prior to his high school graduation, in 2003, from Marjory Stoneman Douglas High School. Brett attended the University of Florida following high school graduation and obtained a bachelor's degree in nuclear engineering in December 2007 and completed his graduate studies in May 2009. While enrolled in the University of Florida, Brett engaged in two rotations as an intern with the nuclear division of General Electric, first General Electric Nuclear Energy, and now General Electric-Hitachi. Brett's first rotation with General Electric was in the summer of 2007, while his second rotation began in the summer of 2008 and will end in the spring of 2009. Brett intends to use the knowledge obtained from the University of Florida and his work experience with General Electric in order to obtain fruitful and professional employment in a nuclear energy related field.